TRANSPORTATION RESEARCH RECORD
517

Formerly issued as Highway Research Record

Performance of Earth Retaining Structures and Pile Foundations

7 reports prepared for the 53rd Annual Meeting of the Highway Research Board

TRB
TRANSPORTATION RESEARCH BOARD
NATIONAL RESEARCH COUNCIL
Washington, D. C., 1974

Transportation Research Record 517
Price $4.00

subject areas
27 bridge design
62 foundations (soils)
63 mechanics (earth mass)

These papers report research work of the authors that was done at institutions named by the authors. The papers were offered to the Transportation Research Board of the National Research Council for publication and are published here in the interest of the dissemination of information from research, one of the major functions of the Transportation Research Board.

Before publication, each paper was reviewed by members of the TRB committee named as its sponsor and accepted as objective, useful, and suitable for publication by the National Research Council. The members of the review committee were chosen for recognized scholarly competence and with due consideration for the balance of disciplines appropriate to the subject concerned.

Responsibility for the publication of these reports rests with the sponsoring committee. However, the opinions and conclusions expressed in the reports are those of the individual authors and not necessarily those of the sponsoring committee, the Transportation Research Board, or the National Research Council.

Each report is reviewed and processed according to the procedures established and monitored by the Report Review Committee of the National Academy of Sciences. Distribution of the report is approved by the President of the Academy upon satisfactory completion of the review process.

The National Research Council is the principal operating agency of the National Academy of Sciences and the National Academy of Engineering, serving government and other organizations. The Transportation Research Board evolved from the 54-year-old Highway Research Board. The TRB incorporates all former HRB activities but also performs additional functions under a broader scope involving all modes of transportation and the interactions of transportation with society.

LIBRARY OF CONGRESS CATALOGING IN PUBLICATION DATA

National Research Council. Highway Research Board
Performance of earth retaining structures and pile foundations.

(Transportation research record; 517)

1. Piling (Civil engineering)—Congresses. 2. Earth pressure—Measurement—Congresses. 3. Bridges—Design—Congresses. I. Title. II. Series.
TE7.H5 no. 517 [TA780] 380.5'08s [624'.154] 75-1367
ISBN 0-309-02361-0

CONTENTS

FOREWORD

A persistent problem in the field of design is that of evaluating the performance of a retaining structure on pile foundations. In order to develop more effective design methods and also to evaluate construction procedures, it is necessary that realistic measurements of performance be obtained.

To this end a symposium was held to attempt to gain additional exposure for measurement systems now being used and to delineate the abilities and limitations of each. The papers in this RECORD are from that symposium. They cover earth pressure measurements, end bearing of piles, downdrag on piles, enlarged-tip piles, lateral load tests, displacements in deep excavations, and field performance. Each paper adds significantly to the state of knowledge concerning performance measurements.

This RECORD should be of interest to all soil engineers as well as all structural engineers who deal with tolerable movements and performance evaluation.

HISTORY OF LOADS AND DISPLACEMENTS FOR A DEEP EXCAVATION IN A MIXED SOIL PROFILE

T. D. O'Rourke and E. J. Cording, Department of Civil Engineering,
University of Illinois at Urbana-Champaign

A history of the behavior of an 82-ft-deep excavation for the Washington, D.C., subway is presented. Improvements in the methods for limiting and forecasting soil movements should result in reduced construction costs and damage claims. It was found that the largest volume of soil displacement takes place beneath the advancing excavation and accounts for approximately 60 percent of the total lateral displacement. Maximum apparent earth pressure for this excavation can be predicted by a trapezoidal earth pressure envelope of width $0.25\gamma H$.

•DETAILED investigation of an 82-ft-deep excavation for the Washington (D.C.) Metropolitan Area Transit Authority (Metro) subway system was performed by the University of Illinois in coordination with DeLeuw, Cather and Co., the general engineering consultant to Metro. The excavation was opened at the intersection of 7th and G Streets N. W. as part of construction for the Gallery Place Station. The excavation was extended through a soil profile of interbedded sand, gravel, and stiff clay.

This was the first 80-ft-deep excavation for the Metro system; thus, even though no structures were immediately adjacent to the cut, it was considered worthwhile to evaluate the effect of open cutting on soil movement around the excavation. Because soil displacement determines the need for underpinning or restricted excavation techniques to protect adjacent structures, this study would aid in the planning and design of future deep, braced excavations in similar soil profiles for Metro.

An extensive measurement program was implemented to monitor lateral displacements of the excavation wall and the displacements of the soil surrounding the excavation. A special effort was made to evaluate soil displacement in relation to excavation procedure.

Lateral displacements were measured using the more accurate accelerometer-type inclinometers developed in the last 4 years. With these instruments it was possible to observe in detail the lateral displacements at depth resulting from excavation and bracing procedures. The results presented in this paper show that the magnitude and distribution of lateral displacements were controlled primarily by strut spacing, the depth the excavation was carried below a strut level before the next level of struts was installed, and characteristics of berms near the bottom of the excavation.

Observations in similar soil profiles (interbedded granular and stiff cohesive soils) at other sites in Washington, Boston, and San Francisco (2, 3, 8, 13) indicate that the same parameters controlled the magnitude and distribution of movements, even though a variety of bracing schemes was used. The bracing schemes included soldier beams and timber lagging with tiebacks, soldier beams and timber lagging with struts, and slurry walls with struts.

Strut loads were measured at regular intervals throughout construction at the 7th and G Street excavation. Apparent earth pressure diagrams were computed from the strut loads for the full depth of excavation and compared with various design criteria in general use. The design earth pressure envelope computed from the strut loads was generally within the expected range, although significant variations of load in individual struts or strut levels were observed due to details of the construction procedure such as preloading and the depth of excavation below the previously installed braces. Similar variations have been observed in other excavations in sands or mixed soil profiles (1, 3, 5, 6, 7, 9, 10, 11, 13).

SOIL CONDITIONS

The excavation was deepened through the so-called 50-ft terrace deposit of Washington. This deposit is one of four terraces in the capital city that were formed by changes in sea level and stream gradients during the Pleistocene epoch. At the excavation the Pleistocene terrace soils range from elevation +46, at the street surface, to a depth of 78 ft at elevation -32. The soils are composed primarily of sand and gravel; however, a significant stratum of stiff clay exists between elevation +20 and elevation +6. Immediately underlying the terrace deposits are soils of Cretaceous age that extend from elevation -33 to elevation -84, where they adjoin bedrock. Only the upper 4 to 6 ft of the Cretaceous soils were excavated. This soil is a hard, brown clay with slickensided fissures. The Cretaceous soil below the hard brown clay, between elevation -69 and elevation -84, is composed of sand and gravel. This stratum was significant because it contained artesian pressure, which was relieved during construction by means of deep submersible pumps.

A typical soil profile is shown in Figure 1. Basically, five layers of soil are displayed in sequence from the street surface. They are the upper brown sand, middle gray clay, gray sands and interbedded stiff clay, lower orange sand, and hard Cretaceous clay. The standard penetration resistance and description of the strata are provided in the Figure. The unconfined compressive strength of the middle gray clay is approximately 1.5 tsf and of the hard Cretaceous clay is 3.5 tsf.

INSTRUMENTATION

The measuring equipment chosen was such that its accuracy and repeatability allowed for consistent, detailed observation of the excavation behavior. Essentially, four methods of measurement were employed to monitor soil movement and brace loads. They included inclinometers, heave-point extensometers, vibrating wire strain gauges, and precise settlement surveys. The instruments were concentrated in the test section shown in Figure 2. The test section was approximately 78 ft long and 130 ft wide.

CONSTRUCTION SEQUENCE

The pervious nature of the Pleistocene terrace deposits required dewatering as a prelude to deep open cutting. Wells 12 in. in diameter containing submersible pumps were established along the line of intended excavation. In the vicinity of the test section the wells were installed to tip depths at elevation -35.

The excavation walls were constructed of soldier piles and oak lagging. The excavation was deepened to 56 ft, and four levels of cross-lot braces were installed. With the exception of the first-level braces, which were not preloaded, each strut was jacked to one-half its design load and wedged. Because of the large width of excavation (130 ft), the braces were supported in their central portion by two rows of 1-ft-diameter pipe piles, which were located 51 ft from the north and south walls of the cut. The excavation was deepened in its central portion to 82 ft. Berms were left in place against the lower 26 ft of the north and south walls of the cut. The berms were established on a $\frac{3}{4}$ H:1 V slope and were 8 ft wide at the top. Significant sloughing was observed at the south berm. Water flowed into the cut at the base of the berm along a sand and gravel layer just above the Cretaceous clay at a depth of approximately 78 ft. High-capacity sump pumps were operated continuously within the cut for the remainder of excavation to discharge water. The central portion of the 12-ft-thick concrete invert was constructed in three separate sections. The fourth-level braces were then removed as, simultaneously, rakers were installed between the central portion of the invert and the fourth-level wales. The top 16 ft of both the north and south berms was excavated, and the fifth-level braces were installed between the central portion of the invert and the walls of the excavation. Both the rakers and the fifth-level braces were preloaded to one-half the design load. After the fifth-level braces were installed, the base of the berms remaining between the central portion of the invert and the walls of the cut was removed and the extreme north and south sections of the invert were built. The walls and arch sections of the subway were constructed, after which the third-level cross-lot braces were removed.

Figure 1. Observed soil profile.

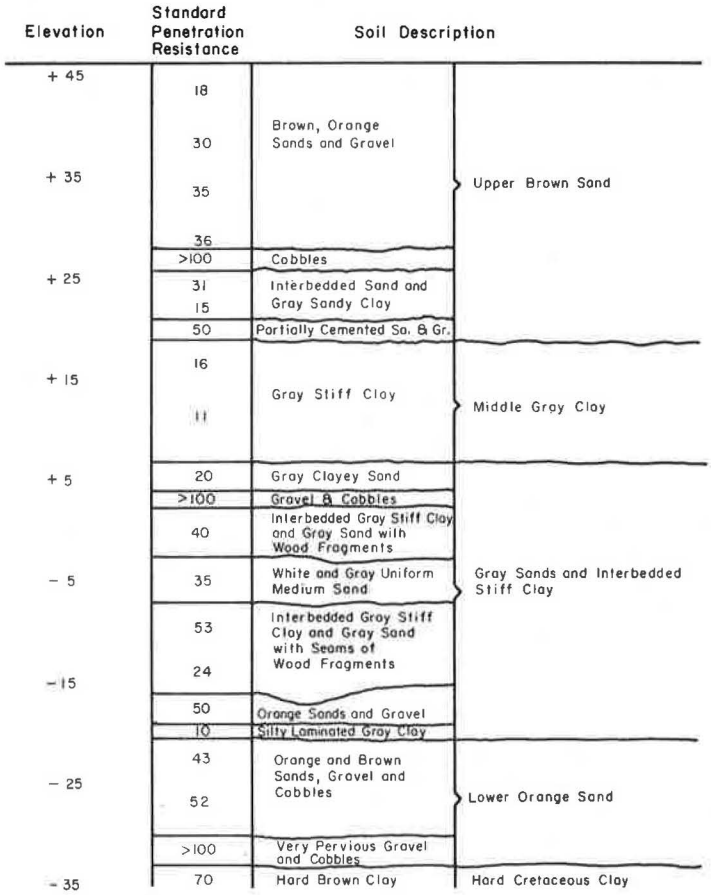

Figure 2. Instrument location.

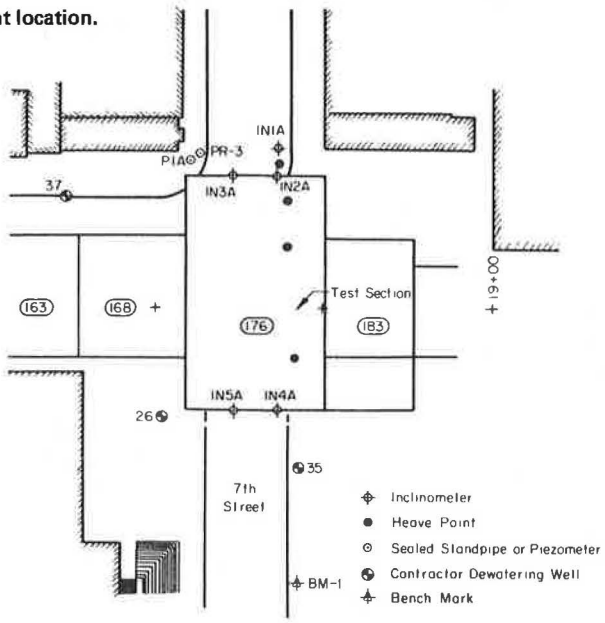

For all levels of braces the horizontal spacing was 13 ft with the exception of the second and third levels, where the struts were concentrated toward the center of the excavation wall. A graphical representation of construction as a function of time for the test section is shown in Figure 3. Day 0 corresponds to July 31, 1971, at which time soil excavation was initiated. Although not indicated in the figure, the third-level braces were removed from the cut on approximately day 690.

OBSERVED SOIL DISPLACEMENT

A history of the braced excavation is summarized in six diagrams (Figures 4 through 9) that show lateral and vertical displacement corresponding to the successive stages of construction at one cross section. Additional movements are delineated in Figures 10 and 11, which show soil behavior at a different location along the south wall of the excavation.

Displacements at Depth of Cut of 38 ft

Figure 4 shows the observed behavior of the test section just prior to and after preloading the second-level braces. Measurable displacement was recorded as deep as 30 ft below the bottom of the cut, with most of the inward movement concentrated near the top of the soldier piles; 17 ft north of the excavation, lateral movement was recorded throughout a depth of 60 ft. At this location the peculiar distribution of movement near the street surface was caused by trench excavation adjacent to the inclinometer casing. Surface settlement both north and south of the excavation was limited to a maximum of 0.3 in.; $\frac{1}{8}$-in. cracks in the street were observed within 10 ft of the cut. Heave-point extensometers indicated an upward movement ranging from 0.08 to 0.18 in. in the gray sands and interbedded stiff clay immediately below the bottom of the cut.

Displacements at Depth of Cut of 60 ft

Figure 5 shows the observed behavior of the test section after the fourth-level braces were installed. Lateral movement of the north wall of the cut was recorded throughout the full depth of the soldier piles. Inward bulging of the excavation walls developed at and below the fourth-level braces; 17 ft north of the excavation, the lateral displacement increased from a maximum of 0.2 in. to 0.3 in. and extended throughout a depth of 75 ft. Adjacent to the cut, surface settlement was a maximum of 0.6 in., whereas deep-seated settlement at 50 ft below the street surface was 0.16 in. Upward movement in the gray sands and interbedded stiff clay increased from a total of 0.15 in. to 0.45 in. Total upward movement in the hard Cretaceous clay was measured by two heave-point extensometers at 0.05 in. and 0.09 in.

Displacement When South Portion of Cut at 82 ft

Figure 6 shows the observed behavior of the test section just prior to construction of the invert. The inclinometers in this cross section showed movement away from the cut in the upper portion of the soldier piles. At the south wall, this outward movement apparently resulted from a small clockwise rotation about the bottom of the soldier pile. Such rotation did not occur at the other instrumented section on the south wall and therefore represents behavior associated only with the soldier pile shown in Figure 6. Possibly, the gradual increase in steel temperature during this time caused the braces to expand. Their interaction with the walls of the cut found expression in the inclinometer measurements as a movement away from the excavation. The outward displacement of the excavation wall resulted in lateral movement 17 ft north of the cut. At this distance, a nearly uniform 0.1-in. movement away from the excavation occurred throughout the upper 40 ft of soil. This resulted in a reduction of the maximum inward displacement from 0.3 in. to 0.2 in. Inward movement of all the instrumented soldier piles occurred below the fourth-level braces. Deep-seated settlement north of the cut increased from 0.16 to 0.20 in., and surface settlement south of the cut increased from a maximum of 0.6 to 0.7 in. Heave-point extensometers indicated that the cumulative upward movement in the hard Cretaceous clay was approximately 0.38 in.

Figure 3. Construction as a function of time.

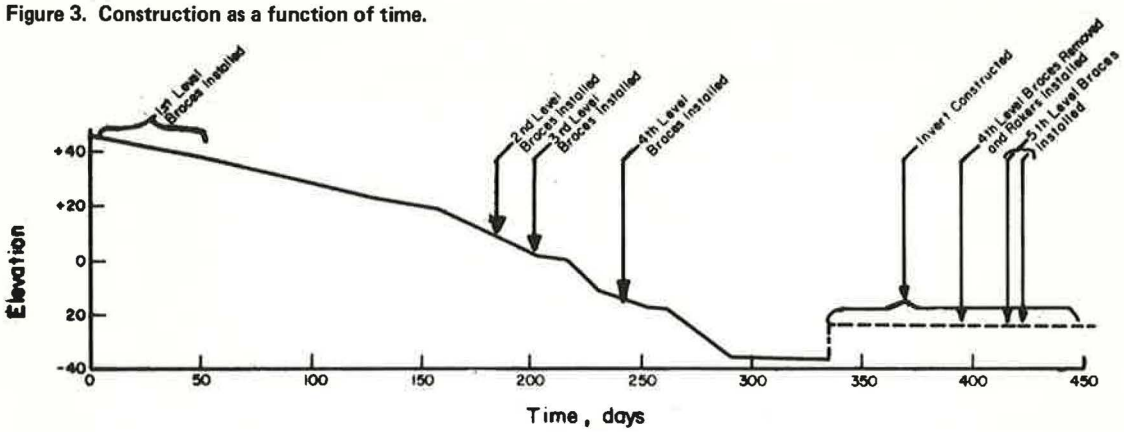

Figure 4. Displacements at depth of cut of 38 ft.

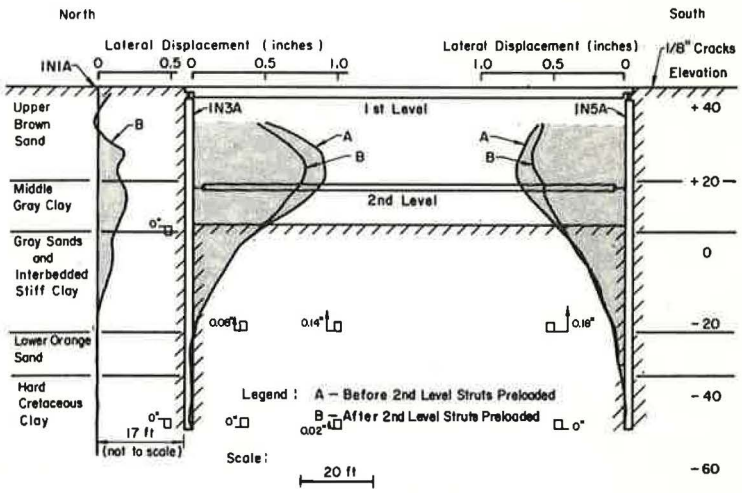

Figure 5. Displacements at depth of cut of 60 ft.

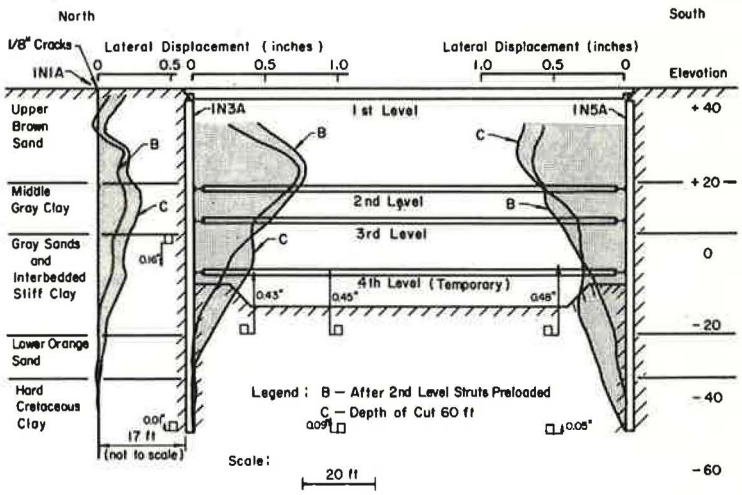

Figure 6. Displacements for south portion of cut at 82 ft.

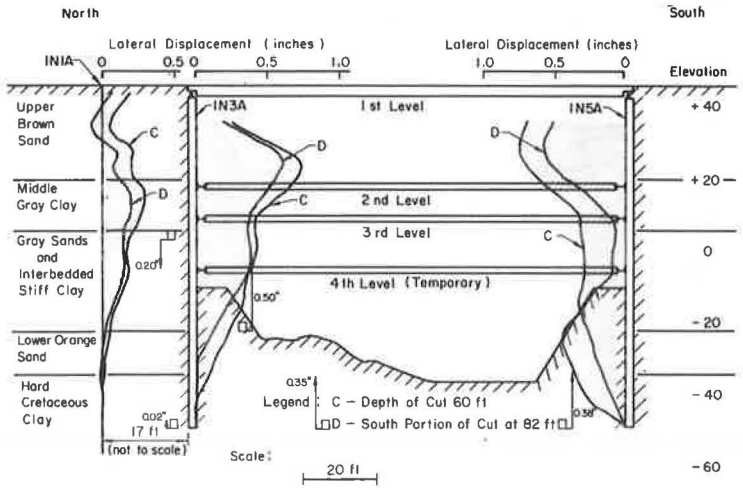

Figure 7. Displacements when central portion of invert constructed.

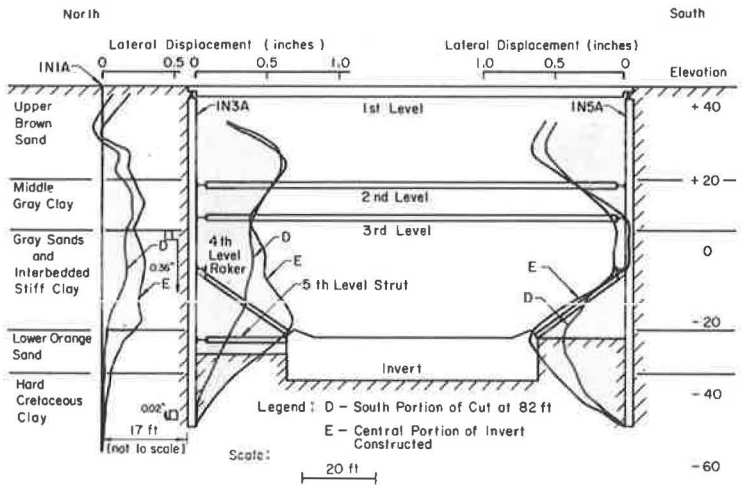

Figure 8. Displacements when excavation and bracing completed.

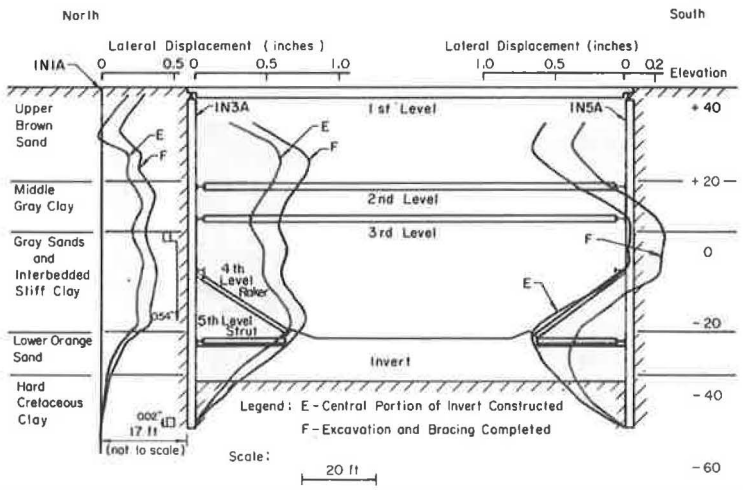

Displacement When Central Portion of Invert Constructed

Figure 7 shows the observed behavior of the test section just after the fifth-level braces were installed on the north side of the cut. A significant increase in deep-seated lateral displacement was measured at all instrumented soldier piles. The additional displacement occurred primarily in response to excavation of the berms adjoining the north and south walls. The deep movement resulted in lateral displacement 17 ft north of the cut where, at a depth of 65 ft, horizontal movement of the soil toward the cut increased from 0.05 in. to 0.25 in. Deep-seated settlement north of the cut increased from 0.20 to 0.36 in., and surface settlement south of the cut increased from a maximum of 0.70 to 0.85 in.

Displacement When Excavation and Bracing Completed

Figure 8 shows the observed behavior of the test section just after the final portions of the invert were constructed. An outward displacement of approximately 0.2 in. occurred at the south side of the cut for the soldier pile shown. This movement coincides with a corresponding 0.2-in. inward displacement at the north wall of the excavation and apparently relates to a temporary unloading of the fifth-level braces at the north side of the cut; 17 ft north of the excavation a nearly 0.1-in. increase in lateral displacement toward the cut occurred throughout a depth of 65 ft. Deep-seated settlement north of the excavation increased from a maximum of 0.36 to 0.54 in., and surface settlement south of the cut increased from a maximum of 0.85 to 1.2 in.

Displacement After Excavation and Bracing Completed

Figure 9 shows the observed behavior of the test section for a period of 2 to 3 months after the excavation was finished. Almost no additional movement occurred at the soldier piles; 17 ft north of the cut, lateral displacement showed a nearly uniform 0.2-in. increase in southward movement. This additional displacement resulted in a maximum, cumulative movement of 0.5 in. between elevation 20 and elevation -20. Deep-seated settlement increased from 0.54 to 0.62 in. The increased displacement partially may have resulted from voids (as large as 1 cu yd) that existed at a depth of 70 ft behind the lagging on the excavation's north side. The voids later were filled, and additional movement was negligible. The heave-point extensometer north of the cut indicated an upward movement of 0.08 in. in the hard Cretaceous clay. The upward movement corresponds to a temporary 8-ft increase of the water level in the lower orange sand. Maximum street settlement south of the excavation increased to cumulative displacements of approximately 1.5 in.

Additional profiles of lateral displacement at the south wall corresponding to the completion of excavation and at a time 2 months afterward are shown in Figures 10 and 11 respectively. Although the location of these displacement profiles is only 26 ft east of those shown in Figures 4 through 9, the magnitude of movement is appreciably different. The maximum accumulated displacement of the south wall at this section was 1.3 in., compared with the 0.5 in. shown in Figure 9. The deep-seated movement, shown by the conspicuous "bulge" between elevation 0 and elevation -50, developed steadily as the excavation was deepened and never showed the shift in displacement away from the cut that characterizes the movement of the south wall in previous cross sections.

It is believed that the movements shown in Figures 10 and 11 are more representative of displacement at the south wall than movements shown in Figures 4 through 9. The deep lateral displacements that were observed in other nearby excavations correspond more closely with the movements shown in Figures 10 and 11. In addition, the measurements of lateral movement in Figures 10 and 11 were referenced to a point 15 ft below the bottom of the soldier pile. Consequently, lateral displacement of the pile bottom was precisely known.

In summary, Figures 4 through 11 provide a history of excavation movement that shows the close relationship between displacement, the depth of cut, bracing scheme, and excavation sequence. A most important feature of the observations is the development of deep-seated, inward movement at depths in excess of 40 ft. Displacement at

Figure 9. Displacements after excavation and bracing completed.

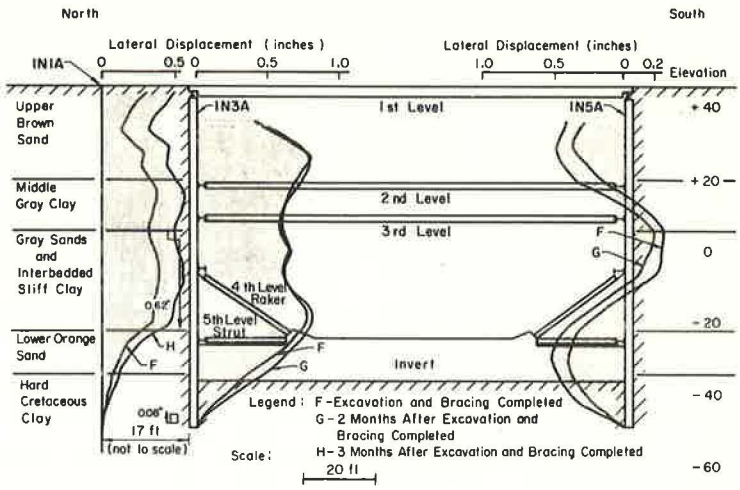

Figure 10. Displacements at south wall when excavation and bracing completed.

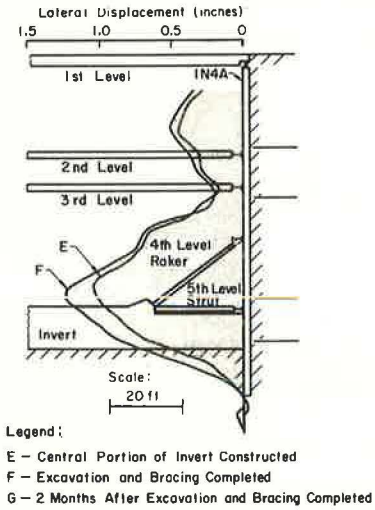

Figure 11. Displacements at south wall after excavation and bracing completed.

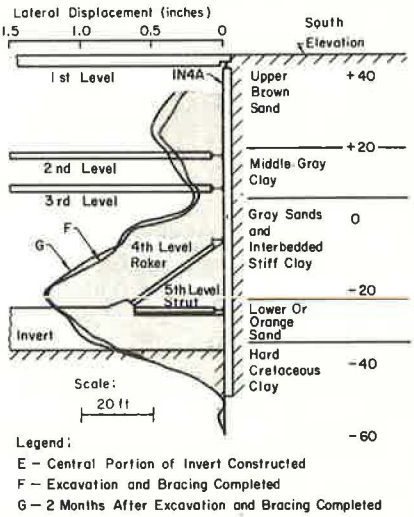

Figure 12. Soldier pile movements below excavation level.

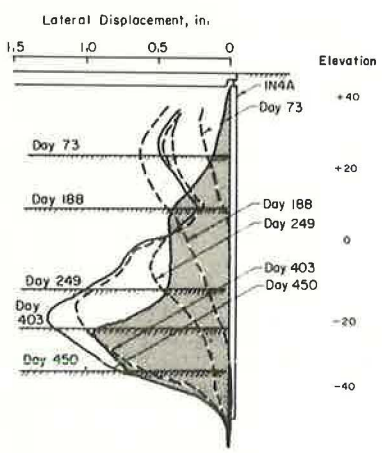

Figure 13. Lateral displacement at base of a soldier pile.

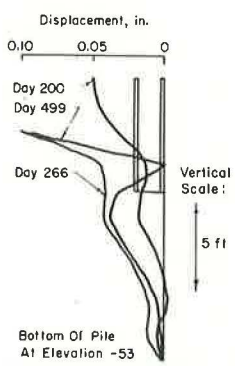

depth leads to loss of ground throughout a greater portion of the surrounding soil, thereby extending the influence area of settlement and deepening the required penetration of underpinning. The magnitude and approximate volumes of the deep-seated displacement are consistent with movement for similar soil profiles published in the literature. Thon and Harlan (13) and Armento (2) show movement profiles for strutted slurry walls that are in close agreement with these diagrams. Liu and Dugan (8) show similar development of displacement for a 55-ft tied-back soldier pile and timber lagging wall in Boston.

Displacement Below the Bottom of Excavation

The greater portion of accumulated displacement occurred below the bottom of the cut. When excavation depths reached 40 ft, lateral movement had developed to the base of the 90-ft-long soldier piles. A comparison of the displacement area that developed below the bottom of excavation at each excavation level and the total displacement area for the full depth of the cut is shown in Figure 12. The cumulative movement that developed below each successive level is shown by the shaded portion of the movement profile. Displacement generated beneath the excavation bottom amounted to over 60 percent of the total lateral displacement. These observations agree with other published data. D'Appolonia (4) has demonstrated a similar accumulation of movement for subway excavation in Boston.

MOVEMENT AT THE BASE OF THE SOLDIER PILES

Special inclinometer casings were extended below the base of selected soldier piles to measure displacement at the pile bottoms. Figure 13 shows the lateral movement that occurred below the base of a soldier pile at the test section. The inclinometer had a repeatability of 0.04 in. over the bottom 15 ft of casing, and thus the measured displacements of 0.05 in. were close to the precision of the instrument. The observations indicate that only a small amount of lateral displacement occurred at and below the base of the soldier pile. Apparently, soil movements caused rotation of the piles about their tips but almost no translation of the tips.

EFFECT OF BERMS ON LATERAL DISPLACEMENT AND STRUT LOADS

The consistent manner in which earth movement developed emphasizes the close relationship between excavation procedure, soil displacements, and strut loads. A good example of this interrelationship is illustrated by the movements and loads associated with excavation below the fourth-level struts where berms were left in place on the north and south walls. The central section of the cut was excavated to subgrade at a depth of 31 ft below the fourth-level struts. Figure 14 shows the development of inward lateral displacement as the cut was deepened and also shows the continuing lateral movement with time after excavation had ceased and berms were in place. These movements are a measure of the berm's behavior and the nature of the soil. As the central portion of the excavation was deepened below the fourth-level struts, the volume of lateral displacement of the south wall increased by 25 percent. Sloughing, seepage at the toe, and construction activity gradually loosened the slightly cemented sands in the berm and allowed additional straining of the wall. After the excavation had ceased with berms in place, the volume of lateral displacement increased an additional 15 percent with time (based on cumulative movement before the central portion of the cut was excavated to subgrade).

The load in all brace levels showed a pattern of development that was consistent with deepening the central portion of the cut and subsequent movement of the berm with time. Figure 15 shows the increase in average strut load at each brace level as a function of time. (The figure shows only the change in load taking place after the fourth-level struts were installed and preloaded.) The loads increased steadily as the central portion of excavation was deepened and continued to increase with time as the berm adjoining the south wall was left in place. The load in the fourth-level braces changed by a maximum of 171 kips, an increase from 91 to 262 kips. The third-level braces

Figure 14. Lateral displacement in response to excavation with berm.

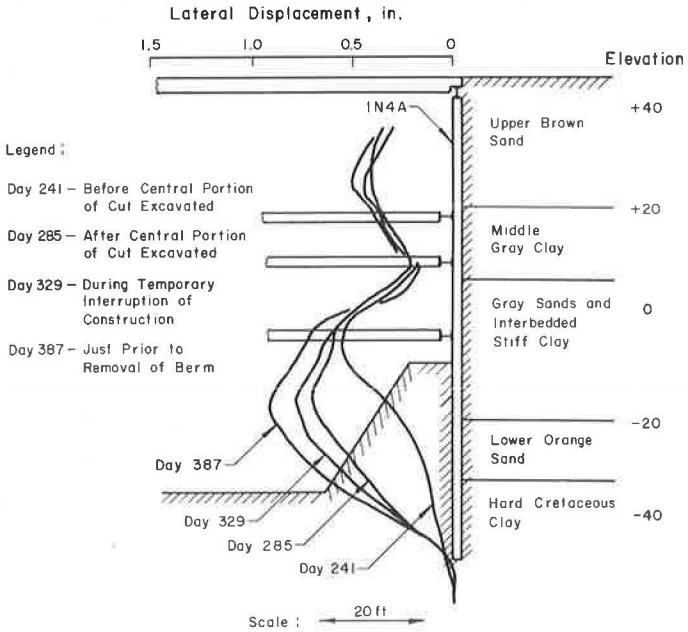

Figure 15. Increase of brace loads in response to excavation with berm.

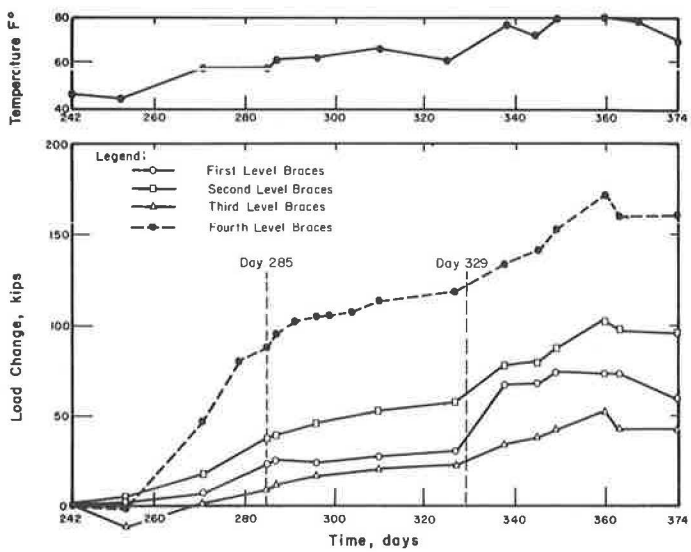

indicated a load increase that was markedly smaller than all other brace levels. Although this behavior may have been related partially to the smaller wall area against which the struts were positioned, it is believed that the smaller load change resulted primarily from the way in which the soldier piles deformed. The load increase in the third-level braces was limited because the bottom struts acted as a pivot point for the soldier pile. Consequently, movement below the fourth-level braces acted to restrain movement at the third-level braces. The first and second brace levels increased in axial load by a maximum of 74 and 101 kips respectively. It appears that temperature changes affected the development of loads in all levels, but its contribution in terms of load increase is difficult to evaluate.

In summary, the berm appears to have been only partially effective in restraining lateral displacement. The use of the berm at depth resulted in both the relatively large lateral movements beneath the fourth-level braces and the correspondingly high load carried by the fourth-level braces.

SETTLEMENT

As a result of pumping from the deep artesian sand and gravel, local subsidence averaging 0.012 ft was measured south of the excavation. The subsidence was small and its magnitude was close to the precision of the optical survey. The subsidence has been subtracted from the total settlements, and thus the data represent only soil movement that occurred in response to excavation.

Settlement profiles south of the test section are shown in Figure 16. The settlement developed incrementally in response to deepening and broadening the excavation. Time-dependent movement is indicated by a comparison of settlement at 1 and 5 months after the completion of excavation. During this period no further removal of soil was undertaken and the bracing system essentially was unchanged. At all stages of construction the slope of the settlement profile is steeper near the excavation.

Figure 17 shows settlement contours south of the excavation. These diagrams indicate the increase of soil movement that occurred between the time the excavation was 45 ft deep and the time of its completion. The diagrams illustrate the spatial relationship of settlement with regard to the excavation and surrounding structures. For the 45-ft depth of excavation, settlement contours parallel the edge of the cut, whereas, upon completion of open cutting, they indicate a slightly greater displacement behind the central and western portions of the excavation wall.

The final settlement expressed as a percentage of the maximum excavation depth is approximately 0.1 percent. In comparison with the settlements summarized by Peck for sand and soft to hard clay (9), this displacement is small. The relatively low magnitude is a reflection of the number of brace levels used, groundwater control, preloading, and other aspects of the construction procedure.

APPARENT EARTH PRESSURE

The apparent earth pressures for the full depth of excavation are shown in Figure 18. Both the average and maximum pressures are shown. The average apparent earth pressure has been computed from the average of all brace loads in each strut level and the maximum apparent earth pressure from the maximum load in an individual strut at each level. The diagrams have been constructed on the assumption that the struts carry a uniform earth pressure halfway between strut levels and that the bottom of the excavation acts as a brace. Load measurements have been corrected for temperature effects and drift of the strain gauges. The apparent earth pressure shows both the influence of construction technique and the nature of the supported soil. The salient features of load distribution are summarized in the following paragraphs.

1. The maximum apparent earth pressure occurred at the third-level braces. The high load measured in these braces is a function of the relatively large preload and pressure redistribution that occurred during preloading. The proximity of the third- and second-level braces allowed mutual interaction. When the third-level braces were preloaded, the load in the second-level struts decreased by an average of 55 kips. This

Figure 16. Settlement profiles associated with excavation.

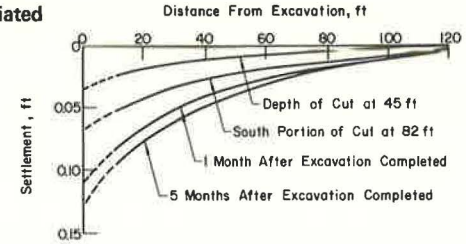

Figure 17. Settlement contours associated with excavation.

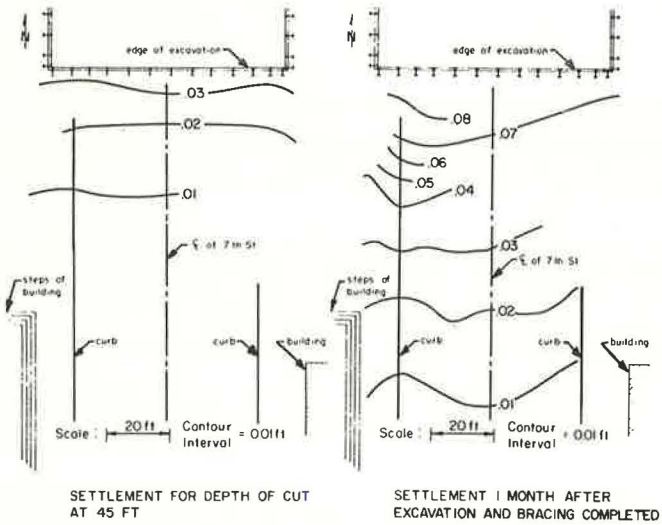

Figure 18. Measured earth pressures.

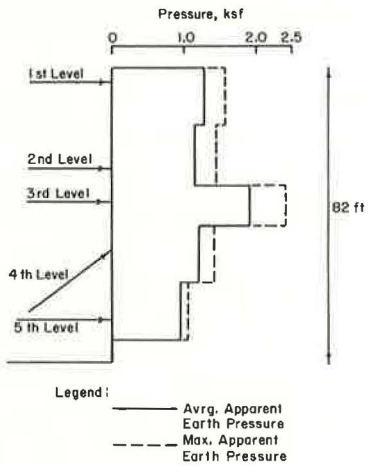

Figure 19. Comparison of earth pressures.

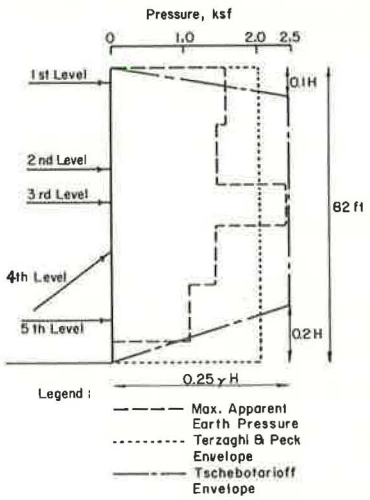

redistribution of load finds expression in the relative magnitude of each pressure. As the excavation was deepened, load in the third-level braces remained proportionately higher than load in other brace levels. Because the design envelope is predicted on the maximum measured load, it often includes a single strut pressure that is anomalously high. Consequently, the design envelope overcompensates for anticipated load. The conservative nature of the earth pressure envelope should be acknowledged and, correspondingly, a limited factor of safety chosen for structural design of the struts.

2. The loads measured in the first-level braces varied through a wide range of values. The variation of load from one strut to another was a function of the construction technique. Initially, the excavation was opened in four separate sections, and a portion of the bracing was installed in each section. As a consequence, the braces were wedged during different times at different depths of cut. The resulting loads show the variable nature of brace installation and early excavation. For the final excavation depth, loads in the first-level braces ranged from a maximum of 243 kips to a minimum of 134 kips.

3. The loads in the bottom-level braces were relatively low with respect to loads in other brace levels. It would be expected that loads would be lower in braces placed very near the bottom of the excavation, particularly when stiffer soils are encountered near and beneath the excavation that allow relatively high lateral stresses to be carried at the base of the excavation. Figure 19 shows the earth pressure envelopes for a braced cut in sand as proposed by Terzaghi and Peck (12) and by Tschebotarioff (14). An angle of shearing resistance, ϕ, equal to 30 deg, and a unit soil weight, γ, equal to 120 pcf, have been chosen as representative of the soil at the instrumented cut. Although both design envelopes approximate the measured load, the trapezoidal distribution provides a better estimate of the reduced load at the base of the cut.

4. All the apparent earth pressures fell within an envelope whose width was equal to $0.25\gamma H$ (Figure 19). Such a value is approximately equal to the maximum apparent earth pressures in a nearby 60-ft-deep cut in the same soil types. Maximum earth pressures in similar soils in Washington have been observed to increase from approximately $0.15\gamma H$ to $0.23\gamma H$ for depths of cut ranging from 28 to 60 ft respectively (3).

CONCLUSIONS

The history of the excavation behavior provides a detailed account of both the magnitude and distribution of movement associated with open cutting in the District of Columbia terrace soils. The records of successive displacement show the relationship between soil movement and various aspects of open cutting, including the bracing scheme, depth of excavation, and construction technique. On the basis of observations and analysis, the following conclusions are offered:

1. It is well known that the protection of structures from ground movements is one of the most important considerations in the design of braced excavations in urban areas. There is a large potential for reduction in construction costs and claims with improvements in the methods for limiting and forecasting soil movements. Thus, primary emphasis in the observation and instrumentation program should be directed toward measuring the significant soil and wall displacements, correlating displacements with construction conditions, and observing their effect on the adjacent structures.

2. Lateral measurements at the line of the excavation wall are most useful in that they can be directly related both to construction conditions and to the surrounding soil displacements. Since the largest volume of lateral displacement takes place beneath the bottom of the advancing excavation, the measurements of lateral displacements must be made with instruments that record the displacements beneath the base of excavation, such as inclinometers.

3. Displacements generated below the bottom of the deepening excavation accounted for over 60 percent of the total lateral displacement.

4. The development of lateral movement was most intense at depths greater than 40 ft. Maximum lateral displacement measured was 1.3 in. at a depth of 60 ft. Since deep-seated displacement leads to loss of ground throughout a greater portion of the surrounding soil and thereby increases the area of damaging movement, the most im-

portant concern should be the method of support and excavation at depth.

5. Construction technique has a significant influence on the amount of lateral soil movement that develops. In particular, the depth of excavation level beneath the lowest previously installed braces is the most influential factor controlling soil displacement.

6. Apparently, steep berms are only partially effective in restraining lateral displacement. Measurements in the instrumented cut show that the volume of lateral movement increased by 25 percent as the central portion of the excavation was deepened and berms were left on the sides of the cut. A further increase of 15 percent in the displacement volume occurred with time after excavation had ceased.

7. As measured by buried heave-point extensometers, total heave of the excavation bottoms was small, being typically 0.4 to 0.5 in.

8. The volume of surface settlement increased 10 percent from the time the excavation was completed to a time 5 months afterward. The final distribution of surface settlement was roughly curvilinear, extending from a maximum 1.5 in. near the edge of the cut to 0.5 in. at a distance of 50 ft and to 0.1 in. at a distance of 120 ft.

9. Inclinometers installed to a depth of 15 ft below the soldier piles indicate that the piles rotated about their tips. Lateral movement of the pile bottoms was limited to 0.05 in.

10. Brace loads are affected by the construction procedure. Large preloads and a large depth of excavation level below the last strut can lead to high strut loads.

11. The maximum apparent earth pressures for the 82-ft-deep excavation can be predicted adequately by a trapezoidal earth pressure envelope of width $0.25\gamma H$ (where γ is the soil unit weight of 120 pcf and H is the full depth of excavation) such as the one shown in Figure 19.

ACKNOWLEDGMENTS

We wish to thank R. B. Peck for his suggestions throughout the instrumentation program. Special credit belongs to William Hansmire for his supervision of instrument installation. The coordinated efforts of Hobart H. MacPherson, who was the soil engineer for DeLeuw, Cather and Co., are appreciated, as are F. Scotland's for his help during field monitoring. Others who lent their efforts include F. L. Gau, J. Mahar, P. Dwiggins, and B. Forde.

REFERENCES

1. Armento, W. J. Criteria for Lateral Pressures for Braced Cuts. Proc. Specialty Conf. on Performance of Earth and Earth-Supported Structures, ASCE, Vol. 1, Part 2, 1972, pp. 1283-1302.
2. Armento, W. J. Cofferdam for BARTD Embarcadero Subway Station. Jour. Soil Mech. and Found. Div., ASCE, Vol. 99, No. SM10, Oct. 1973, pp. 727-744.
3. Chapman, K. R., Cording, E. J., and Schnabel, H., Jr. Performance of a Braced Excavation in Granular and Cohesive Soils. Proc. Specialty Conf. on Performance of Earth and Earth-Supported Structures, ASCE, Vol. 3, 1972, pp. 271-293.
4. D'Appolonia, D. J. Effects of Foundation Construction on Nearby Structures. 4th Panamerican Conf. on Soil Mech. and Found. Engr., Vol. 1, 1971, pp. 189-236.
5. Endo, M. Discussion in Technical Session, Main Section No. 4. Proc. 7th Int. Conf. on Soil Mech. and Found. Engr., Mexico City, Vol. 3, 1969, pp. 335-349.
6. Golder, H. Q., Gould, J. P., Lambe, T. W., Tschebotarioff, G. P., and Wilson, S. D. Predicted Performance of Braced Excavation. Jour. Soil Mech. and Found. Div., ASCE, Vol. 96, No. SM3, May 1970, pp. 801-815.
7. Lambe, T. W., Wolfskill, L. A., and Wong, I. H. Measured Performance of Braced Excavation. Jour. Soil Mech. and Found. Div., ASCE, Vol. 96, No. SM3, May 1970, pp. 817-836.
8. Liu, T. K., and Dugan, J. P. An Instrumented Tied-Back Deep Excavation. Proc. Specialty Conf. on Performance of Earth and Earth-Supported Structures, ASCE, Vol. 1, Part 2, 1972, pp. 1323-1339.
9. Peck, R. B. Deep Excavations and Tunneling in Soft Ground. Proc. 7th Int. Conf. on Soil Mech. and Found. Engr., Mexico City, 1969, State-of-the-Art Vol., pp. 225-290.

10. Scott, J. D., Wilson, N. E., and Bauer, G. E. Analysis and Performance of a Braced Cut in Sand With Large Deformations. Can. Geot. Jour., Vol. 9, No. 4, Nov. 1972, pp. 384-406.
11. Sverdrup and Parcel and Associates, Inc. Cut-and-Cover Tunneling Techniques. Publication No. PB 222 997, National Technical Information Service, Springfield, Va.
12. Terzaghi, K., and Peck, R. B. Soil Mechanics in Engineering Practice. John Wiley and Sons, Inc., 1967, pp. 394-413.
13. Thon, J. G., and Harlan, R. C. Slurry Walls for BART Civic Center Subway Station. Jour. Soil Mech. and Found. Div., ASCE, Vol. 97, No. SM9, Sept. 1971, pp. 1317-1334.
14. Tschebotarioff, G. P. Foundations, Retaining and Earth Structures: The Art of Design Construction and Its Scientific Basis in Soil Mechanics. McGraw-Hill, Inc., 1973, pp. 415-457.

FIELD MEASUREMENTS OF LATERAL EARTH PRESSURES ON A CANTILEVER RETAINING WALL

H. M. Coyle, R. E. Bartoskewitz, and L. J. Milberger, Texas Transportation Institute, Texas A&M University; and
H. D. Butler, Texas Highway Department

This paper presents results from a research study on determination of lateral earth pressure for use in retaining wall design. The broad objective of the study is to develop improved design procedures for retaining walls. The limited objective of the phase of the study covered in this paper is to measure the pressure acting on a typical cantilever retaining wall and to compare the measured pressures with theoretical pressures determined by Rankine and Coulomb theories. Terra Tec pneumatic and Geonor vibrating wire pressure cells were used to measure lateral earth pressures. Procedures used to calibrate the pressure cells are presented. Measurements of the lateral movement of the wall were made during and after backfilling. Data covering a period of 14 months are presented. These data include graphs of earth pressure and wall movement versus time and graphs of pressure distribution versus depth. Engineering properties of the backfill materials are presented. Computed earth pressures based on the Rankine and Coulomb active case are compared with measured pressures. A significant finding is that the measured pressures near the base of the wall are higher than the active pressures. They are nearly equal to the at-rest pressures that are possible as a result of the small movements that occurred at the base of the wall.

•THE findings presented in this paper were obtained during the second year of a 5-year study on determining lateral earth pressure for use in retaining wall design. During the first year of this study an effort was made to evaluate commercially available earth pressure cells. Two promising earth pressure cells were selected for use during the second year. The two cells selected were the Terra Tec pneumatic cell and the Geonor vibrating wire cell. The main effort during the second year involved measurement of the distribution of pressure on a cantilever retaining wall and improvement of calibration procedures for the pressure cells.

The test site for this study is located along highway US-59 near the intersection with Interstate 45 in Houston. Seven cantilever retaining walls were constructed at this site. The Texas Highway Department designated these as retaining walls A through G. One panel in retaining wall G was selected for use during the second year of this study, and this panel is designated here as test wall G. Four Terra Tec and two Geonor cells were installed in test wall G in March 1972. Backfilling operations began in early April 1972, and periodic measurements of earth pressures have been made since that time. The data obtained during the period from April 1972 through May 1973 are presented in this paper. Additional measurements of earth pressures on test wall G are being made during the third year of this research program.

The ultimate objective of the 5-year research study is to develop a more economical design procedure for retaining walls. The specific objectives of the work initiated during the second year of the study were as follows:

1. To measure lateral earth pressures on a cantilever retaining wall using the Terra Tec pneumatic and Geonor vibrating wire pressure cells;

2. To improve the procedures used for calibrating these cells and investigate the effects of grouting, temperature, and drift or change in zero gauge reading on cell response;
3. To measure the lateral displacement of the retaining wall in conjunction with pressure measurements so that wall movements can be correlated with measured pressures;
4. To sample and test the soil used for backfill material; and
5. To compute lateral earth pressures using existing theories (Rankine and Coulomb) so that a comparison can be made between the theoretical pressures and the measured field pressures.

PRESSURE CELLS

The reasons for selecting the Terra Tec and Geonor cells for use in the second year of this research study have been presented in some detail elsewhere (1). The Terra Tec cell is relatively new and has not been proved reliable for long-term performance. However, the ability to backflush the Terra Tec cell and purge the system of entrapped moisture indicates that these cells can be kept operative for long periods of time if mechanical difficulties do not develop. The Geonor cell has been used successfully for long-term pressure measurements, particularly in Canada and Europe (3, 4). The principle of operation of the Terra Tec and Geonor cells is covered elsewhere (1) and will not be discussed in this paper. The Terra Tec cell with readout device is shown in Figure 1. The Geonor cell with readout device is shown in Figure 2.

Before the Terra Tec and Geonor pressure cells could be installed in test wall G it was necessary to conduct calibration tests to determine the response of the cells in terms of pressure sensitivity and temperature variations. Pressure sensitivity of the cells as used in this paper means the output of the pressure cell in response to an applied pressure, or change in pressure, as made manifest by the readout unit to which the cell is connected. In the case of the Terra Tec cells, this response is indicated by a pressure reading in pounds per square inch on the readout unit. The pressure sensitivity of the Terra Tec cell is therefore the pressure change required on the face of the cell to produce a change of 1 psi in the reading of the pressure gauge on the readout unit.

For the Geonor cell the situation is somewhat more complex. During a typical calibration test, known pressures are applied incrementally on the face of the cell. At each pressure increment the frequency of vibration in hertz of the wire inside the cell is displayed on the readout unit. The output of the vibrating wire cell is intrinsically nonlinear, and a graph of applied pressure versus frequency of vibration does not plot as a straight line. Based on the fundamental mathematical theory of the cell, the manufacturer suggests (2) that the data be transformed so that a linear plot will be obtained. If f_0 is the frequency at zero pressure and f is the frequency with a known pressure applied, the squared-frequency difference is then $\Delta f^2 = f^2 - f_0^2$. For example, the cells installed in test wall G have a nominal zero pressure frequency of $f_0 = 1100$ Hz. At 12 psi (83 kPa) applied pressure (the maximum pressure applied during calibration tests) the nominal frequency is f = 1385 Hz; Δf^2 is then $1385^2 - 1100^2$ or $\Delta f^2 = 708\ 225$ Hz. With frequency recorded to four significant figures, Δf^2 is divided by a scale factor of 1000 to obtain numbers that do not exceed the precision of the input data. A plot of applied pressure versus $\Delta f^2/1000$ will be linear, and the slope of the straight line is regarded as being the pressure sensitivity of the cell. Thus, the pressure sensitivity of the Geonor cell is defined as the pressure change per unit of squared-frequency difference Δf^2 divided by 1000.

Calibration was accomplished by placing a pressure cell inside a sealed chamber and then increasing the air pressure in the chamber. A typical calibration run consisted of applying 23 increments of pressure beginning with 0, increasing to 12 psi (83 kPa), and returning to 0. Each increment of pressure was nominally 1 psi (6.9 kPa). A typical calibration curve for the Terra Tec cells is shown in Figure 3. Figure 4 is a typical applied pressure versus frequency plot for the Geonor cells and illustrates the nonlinear response of the cell. Figure 5 shows the linear plot of pressure versus squared-frequency difference.

Figure 1. Terra Tec cell and readout device.

Figure 2. Geonor cell and readout device.

Figure 3. Typical calibration curve for Terra Tec cell (1 psi = 6.9 kPa).

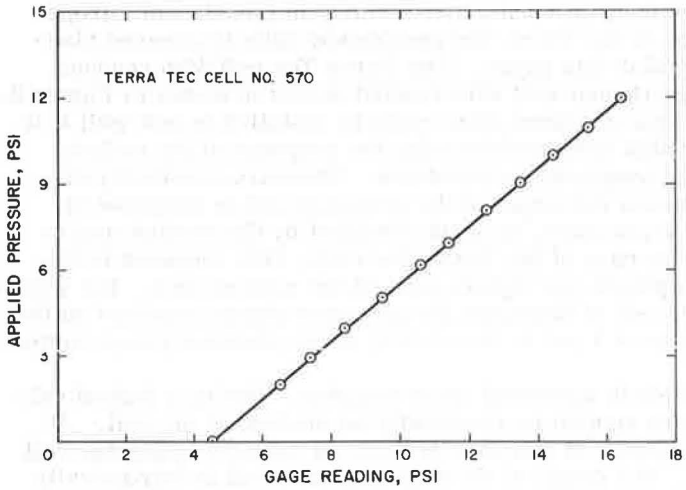

Figure 4. Typical pressure versus frequency curve for Geonor cell.

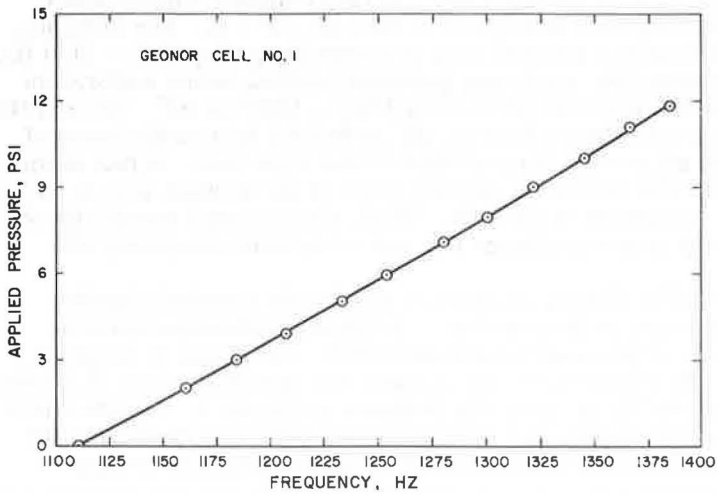

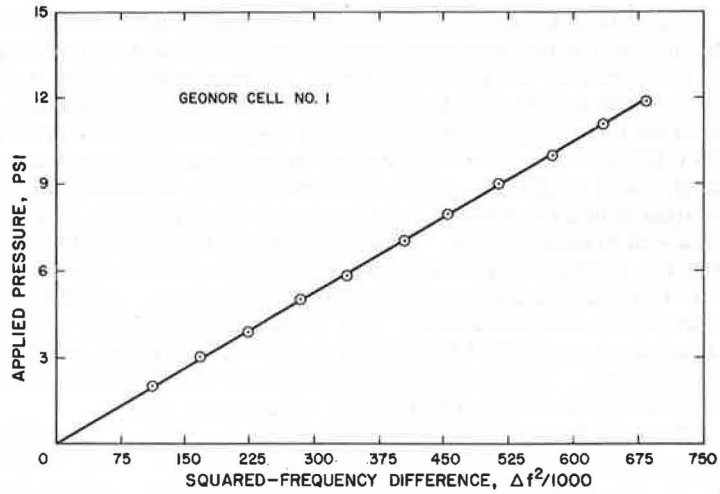

Figure 5. Typical calibration curve for Geonor cell.

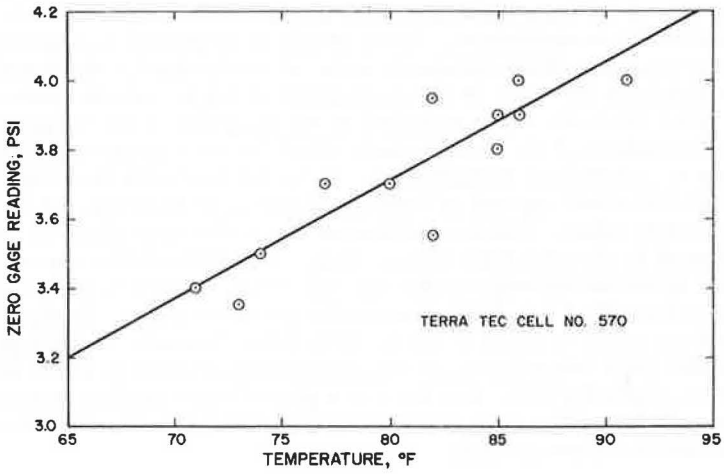

Figure 6. Typical field relationship between zero gauge reading and temperature.

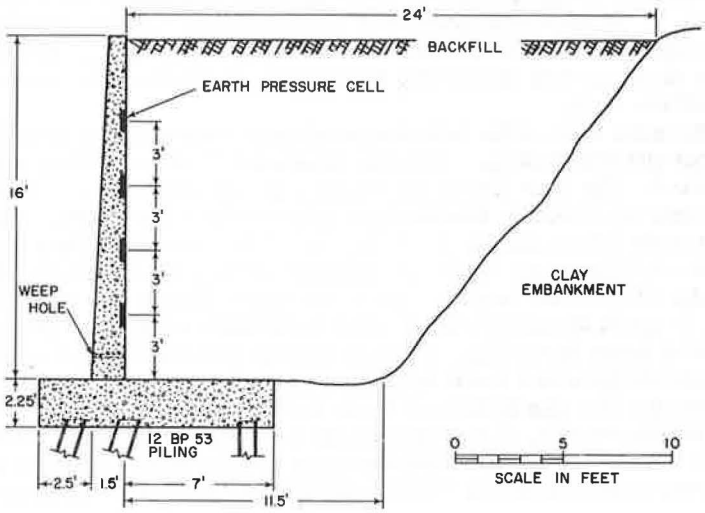

Figure 7. Cross section of test wall G (1 ft = 0.305 m).

After the calibration tests were completed, an investigation was made to determine whether or not the pressure sensitivity is affected or altered when the pressure cells are grouted into the retaining wall. To accomplish this, a Terra Tec cell was grouted into a 4-in.-thick (102-mm), 16-in.-diameter (406-mm) block of concrete. To simulate field installation as closely as possible, the concrete block was cast and allowed to harden. A cavity was cut in the face of the concrete and the pressure cell was grouted in place. Three coats of flexible weatherproof coating containing a high-strength synthetic rubber base material were applied over the entire surface of the block and pressure cell. This was done to isolate the back face of the pressure cell from the pneumatic pressure being applied on the front face. The cell was then calibrated in the exact manner described previously. A total of six calibration tests were made on the embedded cell. The pressure sensitivities computed from the test data ranged from 0.972 to 1.013 psi/psi, the median being 1.006 and the average being 1.001 psi/psi. These data indicate that there is no effect on pressure cell response due to installation or grouting into a retaining wall.

After the pneumatic calibrations were conducted, the effect of temperature on the zero reading was investigated in the laboratory. Five temperatures were used: 52, 62, 74, 84, and 104 F (11, 17, 23, 29, and 40 C). All the cells were placed inside a room where the temperature was maintained constant at one of the given test temperatures. A 24-hour waiting period was allowed for the cells to reach equilibrium with the ambient temperature. A second 24-hour period was allowed during which the zero gauge readings of the pressure cells were checked periodically. All cells were found to exhibit an increase in the zero gauge reading with an increase in temperature.

After the cells were installed in the retaining wall, additional data were obtained for evaluation of the temperature effect on zero reading. In this case it was impossible to control the temperature. In order to obtain the widest range of temperature within the short amount of time available to acquire the data, both day and night readings were taken. The temperatures recorded were those of the concrete immediately adjacent to the pressure cells. They were obtained by means of thermocouples that were mounted directly on the surface of the concrete, a thermocouple being mounted approximately 1 in. from each of the pressure cells. In this manner, a range of temperature from 71 to 91 F (22 to 33 C) was obtained. Readings were not begun until several days after the cells were installed in order to allow the epoxy grout sufficient time to fully harden. Figure 6 is a plot of zero reading versus temperature for Terra Tec cell No. 570. It is representative of the data obtained from the other three Terra Tec and two Geonor cells.

INSTALLATION OF CELLS

A typical cross section of the cantilever retaining wall (test wall G) is shown in Figure 7. It should be noted that the cantilever retaining wall is resting on H piles. The water table is located below the footing of the wall. Weep holes are provided to allow drainage and thus to try to prevent any hydrostatic pressure from building up behind the wall.

The back face of the retaining wall was instrumented with four Terra Tec and two Geonor pressure cells. The cell locations on the retaining wall panel are shown in Figure 8. The four Terra Tec cells were arranged in a vertical row so that measured pressure distribution behind the wall could be established. The upper and lower Geonor cells were located at the same depths as the top and bottom Terra Tec cells so that a check could be made of the magnitudes of the measured pressures at the 4-ft (1.2-m) and the 13-ft (4-m) depths. Also, the upper Terra Tec (No. 570) and upper Geonor (No. 1) could be uncovered at some time after backfilling to check the zero gauge readings for these two cells. A thermocouple was installed at each pressure cell location so that temperature could be determined at the time the pressure readings were taken.

Because the construction of test wall G was completed prior to the installation of the pressure cells, it was necessary to cut a cavity in the wall and grout the cells in place. After the cavities had been cut, the pressure cells were cemented in place with an epoxy grout known as "Patch All Special". The cells were installed so that the face

of each cell was flush with the back of the wall. Care was taken to ensure that uniform and intimate contact with the seating surface was achieved. The installation procedure for a Terra Tec cell is shown in Figures 9, 10, and 11.

A thermocouple was installed at each pressure cell location. Each thermocouple was covered with a waterproofing compound. All connector cables and wires were secured to the retaining wall with a strip of raw tread rubber. The completed installation of the cells for test wall G is shown in Figure 12.

The backfill operation for test wall G took place over a period of 6 days. The backfill material was dumped and roughly spread by heavy scrapers. The completed spreading and compaction were done with a bulldozer. The backfill material was spread in approximately 8-in. (200-mm) lifts, and the bulldozer made approximately three passes on each lift. Care was taken to ensure that none of the instrumentation on the test wall panel was damaged by the earthmoving equipment. Earth pressure measurements were made during the backfilling operation.

Samples of the backfill material were taken during the backfilling operation in order to determine in-place moisture content and wet unit weight (density). The wet (total) unit weight next to the test panel averaged 91.6 pcf (1463 kg/m^3), and at the center of the backfill the wet unit weight averaged 101.3 pcf (1618 kg/m^3). The average moisture content was 20.4 percent, and the specific gravity of the soil was 2.68.

The observed unit weights may be somewhat lower than the unit weights achieved. This is due to the high placement moisture content of the backfill and the method of sampling. Unit weight determinations were made with a Soiltest balloon volumeter. The apparatus is used to determine the volume of soil removed from a test hole by measuring the amount of water required to completely fill the hole. Due to the high moisture content of the soil it is possible that the water balloon pressing against the side of the hole may have increased the volume of the hole. Using the larger volume to compute the unit weights would have the effect of giving lower unit weights than those actually achieved. Because of this problem, a wet unit weight of 110 pcf (1760 kg/m^3) was used in the theoretical computations presented in this paper. An average wet unit weight of 110 pcf was obtained in the backfill of the test panel during the first year of this research study using essentially the same backfill material.

The backfill material was a tan fine sand containing a small percentage of silt. The soil was classified as SP-SM according to the Unified Classification System. Undrained direct-shear tests were conducted on representative samples of the backfill material, and the angle of internal friction was determined to be 32 deg.

DATA COLLECTION

The lateral earth pressures measured on test wall G from April 1972 through May 1973 are given in Table 1. Also, the measured pressures are plotted versus time in Figures 13 through 15. In general, it may be stated that the performance of the pressure cells has been reasonably consistent. The plotted data in Figures 13 through 15 indicate either a simultaneous increase or decrease in pressure during a given period of time. Maximum pressures were achieved at the completion of the backfilling operation, and, except for minor variations, the pressures remained relatively constant until October 1972. The reason for the drop in measured pressures during the winter months is not known. It is possible that temperature corrections were not accurate because the temperature calibration curves were established for a range of 70 to 90 F (21 to 32 C) and the temperatures dropped to 40 to 50 F (4 to 10 C) during the winter months. Consequently, extrapolation was required in order to establish a temperature correction for these lower temperatures.

In October 1972 the upper pressure cells were uncovered (Terra Tec No. 570 and Geonor No. 1) by removing approximately 5 ft (1.5 m) of the backfill material. This was done to establish whether the zero pressure reading for each cell had changed during this 6-month period. As shown in Table 1, the zero pressure readings did not change significantly. However, after the backfill material was replaced, the pressure readings for these two cells never returned to the prior reading of approximately 2 psi (14 kPa). It should be noted that Geonor No. 2 became inoperative in February

Figure 8. Location of earth pressure cells, test wall G.

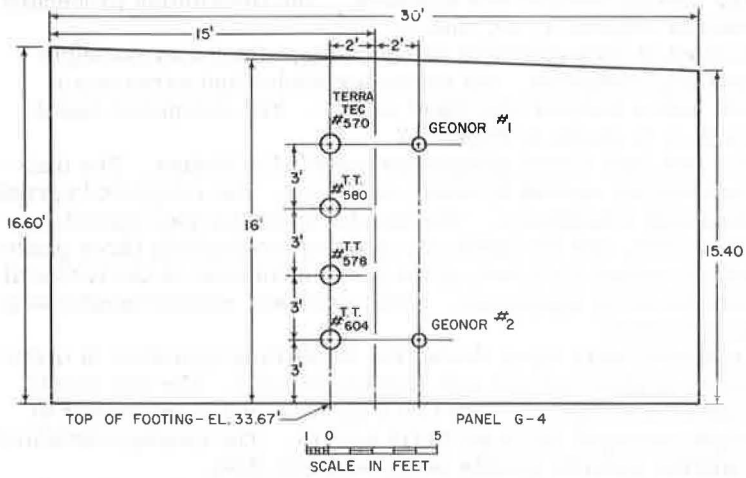

Figure 9. Cell cavity.

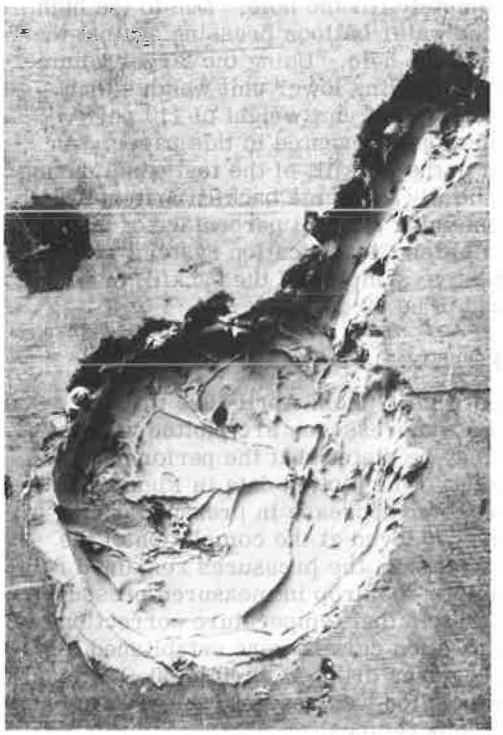

Figure 10. Installed cell.

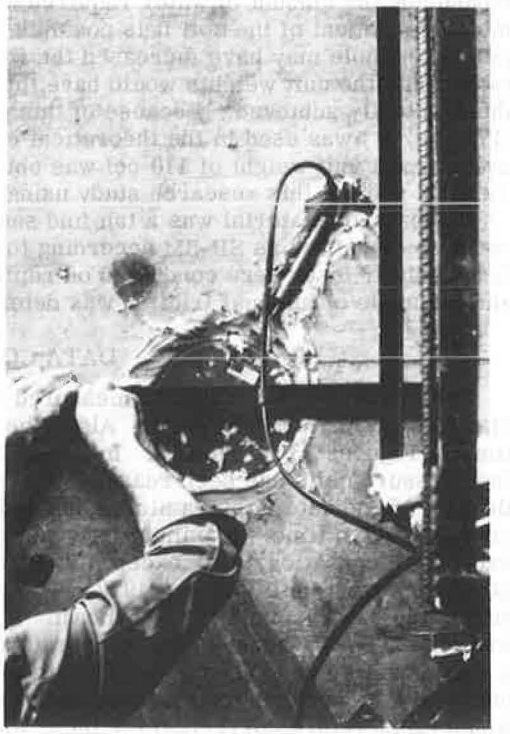

Figure 11. Final grouting.

Figure 12. Completed installation.

Table 1. Measured lateral earth pressures (in psi) for test wall G.

Date	Elasped Time in Days	Terra Tec 9				Geonor 6	
		570	580	578	604	1	2
12 April 1972	1	0	0	0	0.64	0	0.46
13 April 1972	2	0	0	0	1.97	0	1.79
14 April 1972	3	0	0	0	1.20	0	1.19
17 April 1972	6	0	1.65	4.00	4.55	0	4.23
18 April 1972	7	1.74	2.93	6.35	8.05	2.92	7.89
Backfilling operation completed							
20 April 1972	9	1.66	2.87	6.65	8.59	2.40	8.27
25 April 1972	14	1.10	2.48	6.20	8.49	1.80	8.64
2 May 1972	21	1.24	2.54	5.97	8.30	2.64	8.23
10 May 1972	29	1.70	2.98	6.78	8.97	2.89	8.71
17 May 1972	36	0.40	2.60	6.03	8.20	2.31	8.34
1 June 1972	51	1.08	2.27	6.27	8.40	2.40	8.35
15 June 1972	65	2.18	2.68	6.56	9.13	3.22	8.35
18 July 1972	98	1.42	2.24	6.00	8.35	2.40	8.07
6 Sept. 1972	148	2.16	2.51	6.43	9.24	2.30	8.52
10 Oct. 1972	182	1.70	1.76	6.06	8.60	2.38	8.45
5 ft of backfill removed							
10 Oct. 1972	182	0.05	1.96	5.86	8.40	-0.20	8.13
19 Oct. 1972	191	-0.07	2.56	6.52	9.05	-0.08	8.73
Backfill replaced							
19 Oct. 1972	191	0.33	2.46	6.42	8.95	0.31	8.69
19 Dec. 1972	252	-0.05	1.20	4.50	6.35	0.74	7.70
8 Jan. 1973	272	-0.65	0.40	4.30	6.20	0.63	8.12
26 Feb. 1973	321	-0.45	2.00	5.40	7.95	0.35	—[a]
5 April 1973	359	-0.15	1.65	5.10	8.05	0.43	—[a]
9 May 1973	393	-0.10	2.20	6.00	9.40	—[a]	—[a]
31 May 1973	415	0.35	1.75	5.80	9.30	—[a]	—[a]

Note: 1 psi = 6.9 kPa.

[a]Gauge inoperative.

Figure 13. Measured pressure versus time, Terra Tec No. 570 and 580 and Geonor No. 1.

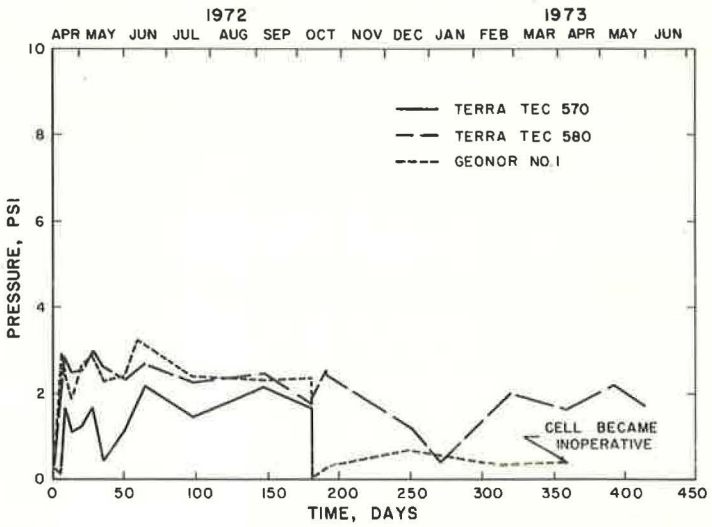

Figure 14. Measured pressure versus time, Terra Tec No. 604 and Geonor No. 2.

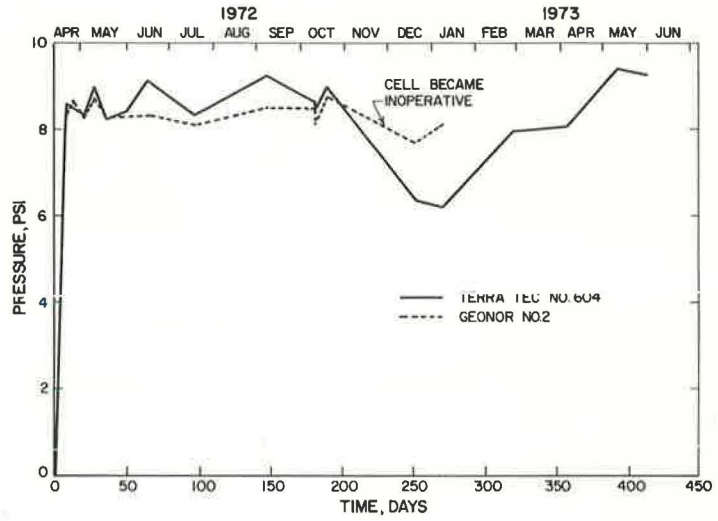

Figure 15. Measured pressure versus time, Terra Tec No. 578, 580, and 604.

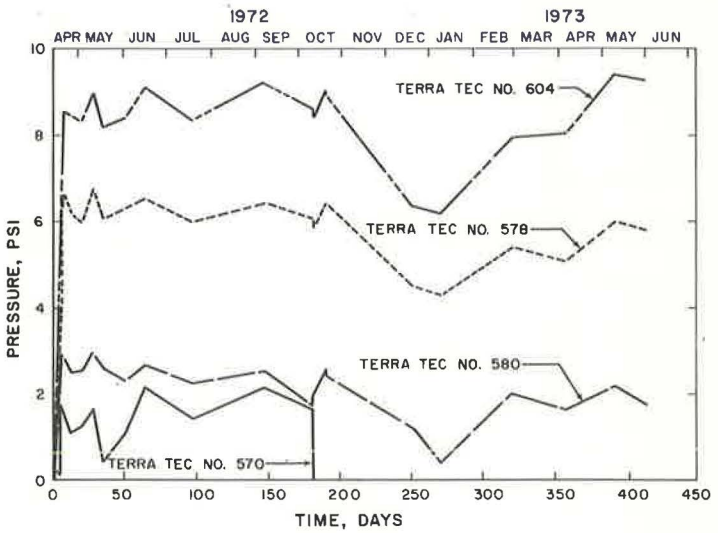

1973 and Geonor No. 1 became inoperative in May 1973. Efforts have been made to restore these cells to an operating condition but have not been successful. All Terra Tec cells are still operating.

Pressure measurements were made periodically during the backfilling operation in an attempt to measure dynamic pressures caused by the hauling and compacting equipment. Neither the Geonor nor the Terra Tec is well adapted for this kind of measurement. Either system requires a certain time period during which the readout unit senses the signal being sent by the pressure cell. The pressure acting on the cell cannot be displayed on the readout unit before the time period is complete. Of the two cells, the Geonor has the shorter period; it is approximately 3 to 4 seconds. For this reason the majority of dynamic measurements were made with the Geonor cell. Check measurements attempted with the Terra Tec cell yielded dynamic pressures that were in general agreement with the Geonor indications. Throughout the course of the dynamic measurements it was observed that the maximum observed dynamic pressure at any time did not exceed the maximum recorded static pressure after the backfill was completely in place. Moreover, as one would expect, at a given point on the wall the influence of the compaction equipment on the pressure at that point decreased as the height of backfill increased.

Measurements of wall movements are needed to establish the expected type of earth pressure distribution. In order to determine the lateral movement of the wall a point was established on the top of the wall. The distance to this point from a fixed point was recorded each time a set of measurements was made. The fixed point was located on a 36-in.-diameter (910 mm) reinforced concrete drilled shaft. The nominal distance from the fixed point to the top of the wall was 67 ft (20.4 m). The distance was measured with an engineer's 100-ft steel tape supported at the 0 and 67-ft marks. The fixed point was located on the drilled shaft at the same elevation as the top of the retaining wall to eliminate the need for slope corrections. Each time a distance was measured the tape temperature was recorded so that observed distances could be corrected for temperature. Tape tension handles were used to ensure a constant 25-lb (111-N) tension when measurements were made.

Displacements due to tilting or rotation were determined by measuring the horizontal offset distance from a vertical line fixed with respect to the top of the wall to several fixed points on the front face of the wall. The vertical reference line was established by suspending a 25-lb (11.3-kg) plumb bob from a frame that was rigidly attached to the top of the wall. With respect to the top of the wall the fixed points were located at heights of 1, 4, 7, 10, 13, and 14½ ft (0.305, 1.2, 2.1, 3.1, 4, and 4.4 m) on a vertical row. The vertical row of points was positioned laterally on the wall so that the four interior points were directly behind the four Terra Tec pressure cells on the back face.

An initial set of measurements was made immediately before the placement of backfill began. The displacements of points on the front side of the wall relative to the top of the wall and to each other during and after backfilling were desired, rather than the exact and true shape of the wall at any time. It was therefore assumed that the front face of the wall was perfectly vertical at the time of the initial measurement. Figure 16 shows the measured translational and rotational displacements at the end of 1 day, 1 week, 1 month, 1 year, and on May 31, 1972. The data shown in Figure 16 indicate that a considerable amount of displacement occurred during the backfilling operation, and very little occurred after 1 month.

THEORETICAL VERSUS MEASURED PRESSURES

The ultimate objective of the research study is to develop a more economical retaining wall design. To accomplish this, it is necessary to determine whether the computed lateral earth pressure on a retaining wall compares favorably with the measured pressure on the real structure. The computed pressure is usually obtained from an equation derived from a theoretical analysis, as opposed to an equation resulting from empirical correlations. There are two earth pressure theories that have attained almost universal acceptance throughout the literature and can be found in nearly all textbooks on soil mechanics. These theories were postulated by Coulomb in the year

1776 and by Rankine in 1857. To arrive at a solution using their theoretical formulation of the problem, Coulomb and Rankine made various assumptions regarding the physical behavior of the soil and the interaction between the soil and the retaining wall. These assumptions and the equations used to compute the coefficient of active earth pressure, K_a, have been presented in detail elsewhere (1). The active earth pressure is the minimum pressure exerted on a structure by a mass of soil. It is the result of an outward movement of the structure with respect to the soil. The parameters used to compute K_a for the conditions at test wall G are α = angle of back of retaining wall with respect to horizontal = 90 deg; β = slope of backfill with respect to horizontal = 0 deg; ϕ = angle of shearing resistance of soil = 32 deg; and δ = friction angle between wall and soil.

The wall friction angle δ is a difficult parameter to evaluate. Approximate values of δ for various types of wall surfaces and finishes may be found in some texts on soil mechanics and foundations. Sowers and Sowers (5) state that, for smooth concrete, δ is often $\frac{1}{2}$ to $\frac{2}{3}\,\phi$. Tomlinson (8) lists $\delta/\phi = 0.88$ for grained concrete (made in timber formwork) in contact with dense dry sand. Terzaghi and Peck (7) suggest that the coefficient of wall friction, tan δ, can be assumed as equal to $\frac{2}{3}$ tan ϕ for fairly permeable soils. Without a doubt this is a very wide range of values for wall friction. However, it is fortunate that δ exerts little influence on Coulomb's value of K_a for the conditions given above by α, β, and ϕ. For $\delta = \frac{1}{2}\,\phi$, K_a equals 0.278, and for $\delta = \frac{2}{3}\,\phi$, K_a equals 0.275. The Rankine theory assumes no wall friction, and for the conditions stated K_a is equal to 0.307.

The theoretical totally active pressures computed by the Coulomb and Rankine theories for test wall G are given in Table 2. The value of $\delta = \frac{2}{3}\,\phi$ was used to compute the Coulomb value of K_a, the unit weight of the backfill was taken to be 110 pcf (1760 kg/m^3), and the depths correspond to the locations of the pressure cells.

Figure 17 shows the measured earth pressures at each depth on a given day. The earth pressure distributions have been plotted for 7, 182, 321, and 415 days after the start of backfilling. The data indicate that, in general, the lateral earth pressure distribution behind test wall G is triangular, i.e., the pressure increases more or less linearly with increased depth. However, the slope of the pressure versus depth curve changes at a depth of 7 ft (2.1 m). From the surface down to 7 ft the lateral pressure increases at an average rate of about 0.4 psi per ft (9 kPa per m). From 7 to 13 ft (2.1 to 4 m) the average rate of pressure increase is approximately 1 psi per ft (22.6 kPa per m). A possible explanation for this increase in pressure gradient can be obtained from a consideration of the displacements that occurred in the upper and lower portions of the retaining wall. It is apparent from the retaining wall displacement curves shown in Figure 16 that the wall tended to rotate about some point near the top of the footing. According to Taylor (6), the pressure distribution on a retaining wall will be triangular if the wall rotates away from the backfill about a point near the base of the wall. Furthermore, from Figure 16 it is evident that some bending occurred in the upper 7 ft (approximately) of the wall. Apparently, the upper portion of the wall experienced a greater movement (yield) per unit depth with respect to the backfill than did the lower portion. If the gross movement of the wall were such that the totally active pressure distribution were approached but not completely achieved at all points along the wall, one would expect the greater movement in the upper portion of the wall to cause a greater reduction in pressure below the at-rest level than the smaller yielding that occurred near the base. In this context the at-rest pressure is the pressure that would be exerted on the wall after the backfill is placed provided that no wall movement occurs.

Figure 16 also shows that the base of the retaining wall experienced approximately 0.2 in. (5 mm) lateral displacement, or two-thirds of the total, at the end of the first day. [Backfill level was only 2 ft (0.6 m) above the footing.] This seemingly large displacement can be attributed to the ground conditions at the site. The footing, although supported by H-piles, was built on top of clay. It is believed that the heavily loaded earthmoving equipment compacted the soil on the back side of the footing and pushed the wall outward. Taylor (6) states, "If the top of the wall moves outward an amount roughly equal to $\frac{1}{2}$ of 1 percent of the wall height, the totally active case is

Figure 16. Displacement of test wall G (1 in. = 25.4 mm).

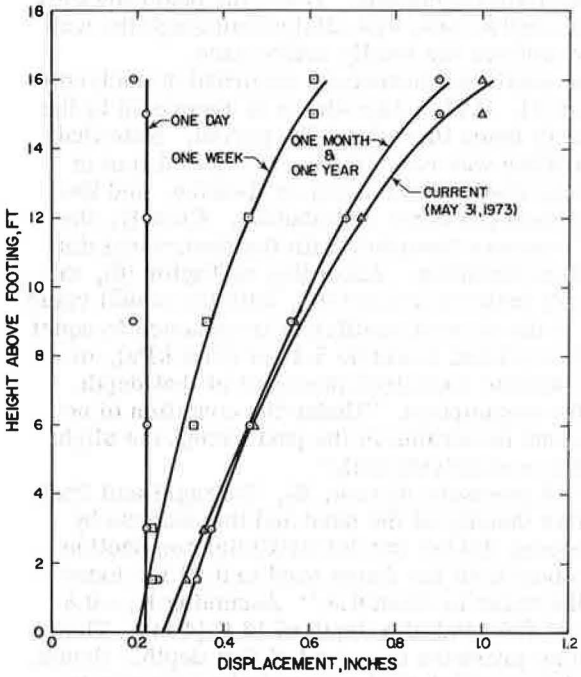

Table 2. Theoretical earth pressures based on Coulomb and Rankine theories.

	Pressure, psi	
Depth, ft	Coulomb	Rankine
4	0.92	1.02
7	1.60	1.79
10	2.29	2.56
13	3.00	3.32

Note: 1 ft = 0.305 m; 1 psi = 6.9 kPa.

Figure 17. Pressure distribution curves.

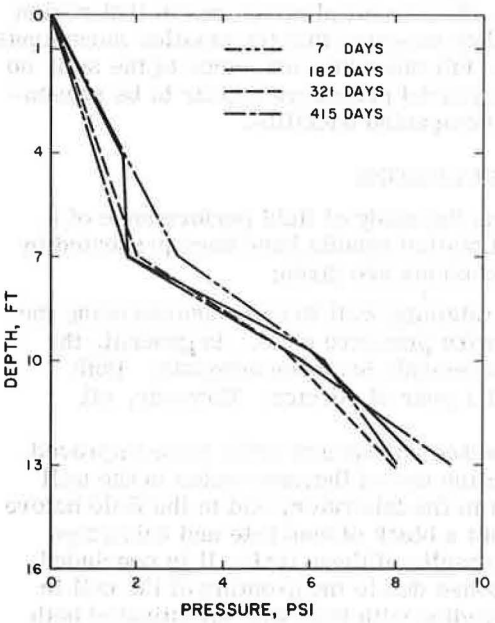

Figure 18. Theoretical versus measured pressure.

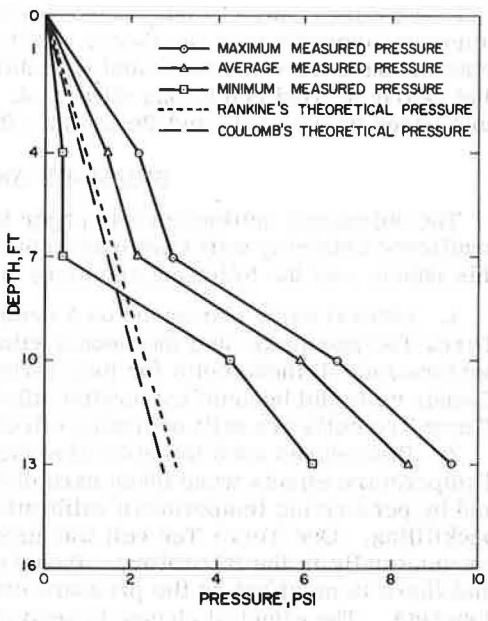

attained. This criterion holds if the base of the wall either remains fixed or moves outward slightly." In this case, ½ of 1 percent of the wall height equals 0.96 in. (24.4 mm). Figure 16 shows a movement of approximately 0.7 in. (18 mm) at the top of the wall after the initial lateral translation occurred. Thus, the observed wall movements would seem to indicate that the active case was attained although the wall movement may not have been sufficient to achieve the totally active case.

Figure 18 is a plot of the minimum and maximum pressures recorded at each cell location from April 18, 1972, through May 31, 1973. Also shown in Figure 18 is the average of all earth pressure measurements made throughout the period. Note that April 18, 1972, is the date on which backfilling was completed. The dotted line in Figure 18 indicates the theoretical pressure distribution based on Rankine, and the broken line illustrates the Coulomb theoretical pressure distribution. Clearly, the measured pressure distribution does not compare favorably with the theoretical distribution forecast by the Coulomb or Rankine theories. According to Taylor (6), the at-rest earth pressure coefficient may vary between 0.4 and 0.5, with the actual value dependent on the density of the backfill. If the at-rest coefficient is assumed to equal 0.5, the computed pressure at the 13-ft (4-m) level would be 5.4 psi (37.3 kPa), or approximately 35 percent less than the minimum measured pressure at that depth. Taylor's at-rest coefficient is based on the assumption, "Under the condition of no movement of the wall, the soil has undergone no strains in the past except the slight vertical compression caused by the placing of overlying soil."

With reference to the coefficient of earth pressure at rest, K_0, Terzaghi and Peck (7) state, "Its value depends on the relative density of the sand and the process by which the deposit was formed. If this process did not involve artificial compaction by tamping, the value of K_0 ranges from about 0.40 for dense sand to 0.50 for loose sand. Tamping in layers may increase the value to about 0.8." Assuming $K_0 = 0.8$ yields a computed pressure equal to 8.7 psi (60 kPa) at a depth of 13 ft (4 m). This value is very close to the average maximum pressure observed at that depth. Hence, the earth pressures that are being recorded would at first appear to be contrary to the theoretical pressures. However, it must be remembered that the theoretical equations based on the Coulomb and Rankine theories give the pressure for totally active conditions. If the assumption is made that the larger movements in the upper 7 ft (2.1 m) induced nearly totally active pressures, the measured pressures in that region compare favorably with the theory. If it is further assumed that the smaller movements near the base were not sufficient to mobilize the full shearing resistance of the soil, so that nearly at-rest conditions still exist, the measured pressures appear to be reasonable based on Terzaghi and Peck's $K_0 = 0.8$ for compacted backfills.

SUMMARY AND CONCLUSIONS

The objectives outlined in this paper involving the study of field performance of a cantilever retaining wall have been achieved. Detailed results have been presented in this paper, and the following summary and conclusions are given:

1. Lateral earth pressures on a cantilever retaining wall were measured using the Terra Tec pneumatic and the Geonor vibrating wire pressure cells. In general, the performance of these cells for long-term measurements has been adequate. Both Geonor cells did become inoperative after about 1 year of service. However, all Terra Tec cells are still operating effectively.
2. Procedures used in calibrating the Terra Tec and Geonor cells were improved. Temperature effects were taken care of through the use of thermocouples in the wall and by performing temperature calibration both in the laboratory and in the field before backfilling. One Terra Tec cell was grouted into a block of concrete and calibrated pneumatically in the laboratory. Based on the results of these tests, it is concluded that there is no effect on the pressure cell response due to the grouting of the cell in concrete. The effect of change in zero gauge reading with time was investigated both in the laboratory and in the field before and after backfilling. It was found that the zero gauge reading did not change significantly when the backfill material was removed after 6 months.

3. Lateral displacement of the test wall was measured accurately. Measurements of the wall movement were made each time that pressure readings were taken, starting at the time of the backfilling operation. This was done so that wall movements could be correlated with measured pressures.
4. Samples of the backfill material were taken and tested to determine the physical and engineering properties of the soil. These properties were used to make theoretical determinations of lateral earth pressure.
5. Computed lateral earth pressures based on Rankine and Coulomb theories were computed with measured lateral earth pressures. It was found that measured pressures agreed with the theoretical pressures to a depth of about 7 ft (2.1 m) on the test wall. Wall movements were large enough above the 7-ft depth to indicate the totally active case. Below the 7-ft depth, the measured earth pressures were larger than the theoretical pressures. Wall movements between the 7-ft and the 13-ft (4-m) depth indicated that the state of the soil in the backfill was somewhere between the totally active and the at-rest case. At the 13-ft depth the movements were small enough to indicate the at-rest condition.

The most recent data given in this paper were taken in May 1973. Pressure readings and wall movements have been made once a month since that time. Readings will be taken continually during the third and fourth years of the study. Surcharge loads in the form of highway pavements were to be applied to the test wall in the fall of 1973. Therefore, it will be possible to study the effects of these surcharge loads on the test wall.

ACKNOWLEDGMENTS

This investigation was conducted as a part of Research Study 2-5-70-169, entitled "Determination of Lateral Earth Pressure for Use in Retaining Wall Design". The cooperative research study is sponsored jointly by the Texas Highway Department and the Federal Highway Administration of the U.S. Department of Transportation. Receipt of this research support is gratefully acknowledged.

The contents of this paper reflect the views of the authors, who are responsible for the facts and the accuracy of the data presented. The contents do not necessarily reflect the official views or policies of the Federal Highway Administration.

REFERENCES

1. Corbett, D. A., Coyle, H. M., Bartoskewitz, R. E., and Milberger, L. J. Evaluation of Pressure Cells Used for Field Measurements of Lateral Earth Pressures on Retaining Walls. Texas Transportation Institute Research Report No. 169-1, Texas A&M University, Sept. 1971.
2. Calibration of Earth Pressure Cell P-100. Geonor A/S, Calibration Report 71442, Oslo, Norway, unpublished.
3. Hamilton, J. J. Earth Pressure Cells: Design, Calibration, and Performance. Technical Paper No. 109, Division of Building Research, National Research Council, Canada, Nov. 1960.
4. Scott, J. D. Experience With Some Vibrating Wire Instruments. Canadian Geotechnical Journal, Vol. 4, No. 1, Feb. 1967, pp. 100-123.
5. Sowers, G. B., and Sowers, G. F. Introductory Soil Mechanics and Foundations, Second Ed. Macmillan Company, Toronto, Ontario, 1961.
6. Taylor, D. W. Fundamentals of Soil Mechanics. John Wiley and Sons, Inc., New York, 1948.
7. Terzaghi, K., and Peck, R. B. Soil Mechanics in Engineering Practice, Second Ed. John Wiley and Sons, Inc., New York, 1967.
8. Tomlinson, M. J. Foundation Design and Construction. John Wiley and Sons, Inc., New York, 1963.

FIELD PERFORMANCE OF REINFORCED CONCRETE PIPE

Raymond J. Krizek and Ross B. Corotis, The Technological Institute, Northwestern University; and
M. Hassan Farzin, Stone and Webster Engineering Corporation, Boston

The field performance of a full-scale reinforced concrete pipe in an embankment installation is described. Normal stresses were measured by specially designed stress cells placed in the soil and at the soil-pipe interface. Displacements in the soil were obtained by settlement plates, and the resulting data were used to calculate a settlement ratio that is in agreement with that anticipated for such an installation. In the pipe itself, diameter changes and strains in the concrete and reinforcing steel were monitored. Data were taken to investigate the response of the soil-pipe system to incremental increases in the height of cover and to the application of a live load under conditions of shallow cover. In general, the experimental measurements are mutually consistent, but they exhibit some differences from results predicted by a plane strain finite element model that utilizes soil parameters obtained primarily from uniaxial strain tests.

•DESPITE the availability of high-speed digital computers to provide essentially exact numerical solutions to idealized problems, the practicing engineer is often unable to use this information to evaluate with any degree of assurance the anticipated response of a given soil-structure system; this is due in large part to incorrect modeling of the physical phenomenon and inadequate determination of the proper values for the input parameters (particularly the stress-strain behavior of the soil). This unfortunate situation exists because, as a consequence of the costs involved, the profession has seldom been provided with the opportunity to adequately instrument and monitor the field performance of a full-scale installation. In recent years, however, the importance of measuring field performance and comparing it with results predicted from a mathematical model has been increasingly recognized, and several significant contributions have emanated from such investigations.

The field performance of a full-scale reinforced concrete pipe buried in an embankment installation is described here. Instrumentation was provided to measure the stresses at the soil-pipe interface and in the adjacent soil, the displacements in the soil above and below the pipe and in the free field, shape changes of the pipe, and strains along the inner and outer faces of the pipe and in the reinforcing cages. Experimental measurements are shown to be mutually compatible and in qualitative agreement with intuitive expectations based on engineering judgment. Typical values at discrete points in the soil-pipe system are compared quantitatively with results calculated by use of a plane strain finite element model, and soil parameters are determined from uniaxial strain tests and triaxial tests on the actual soils from the field installation. Although not yet fully realized, the goals of this study are to develop reliable procedures for predicting the field response of coupled soil-pipe systems.

FIELD EXPERIMENT

As shown in Figure 1, the experimental installation is located on the grounds of the Ohio Highway Transportation Research Center in East Liberty. A 60-in. inside diameter, Class IV, B wall concrete pipe (manufactured by the wet cast method) was installed in a positive projecting embankment condition with a cover of 25 ft. The required strength of the pipe was determined by means of the Marston-Spangler theory, and the pipe was installed in accordance with the specifications of the Ohio Department of Highways. The selected pipe size is the result of a compromise between the

Figure 1. Location of field site.

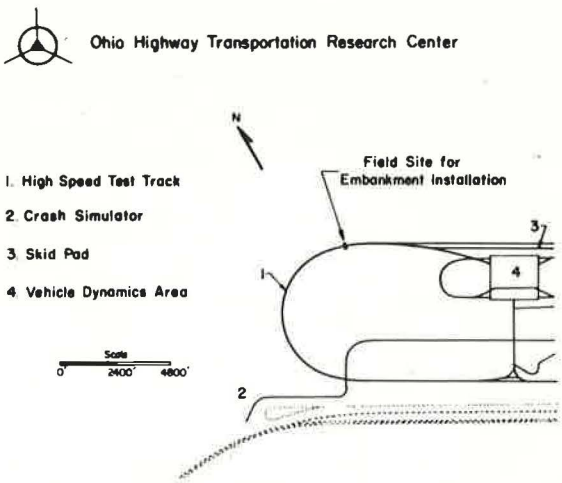

Figure 2. Log of soil boring at field site.

State of Ohio
Department of Highways
Testing Laboratory

Log of Boring

Date Started 4-5-71 Sampler Type Truck Auger Water Elev Immediate None Project Identification Logan-Union
Date Completed 4-5-71 After ___ Hours ___ Log: Uni-Ohio Hwy. Trans. Res. Center
Boring No ___ Station & Offset 360-00 50' Rt. Large Loop Surface Elev. ___ Concrete Pipe Res. Installation Site

Location of Pipe	Depth	Description	Fld. No.	Lab No.	Physical Characteristics % Agg	% C.S.	% F.S.	% Silt	% Clay	L.L.	P.I.	W.C.	SHTL Class.
	0												
	2												
	4	Brownish-Gray Silty Clay	1	28794	2	1	5	31	61	53	27	29	A-7-6
	6												
	8												
	10	Brown Silty Clay	2	28795	3	2	5	27	63	42	19	23	A-7-6
	12												
	14	Gray Silty Clay	3	28796	4	4	7	33	52	38	16	21	A-6b
	16												
	18	Gray Silty Clay	4	28797	2	4	8	32	54	39	20	21	A-6b
	20												
	22	Bottom of Boring											
	24												
	26												
	28												
	30												
	32												
	34												
	36												

Figure 3. Cross section of field installation.

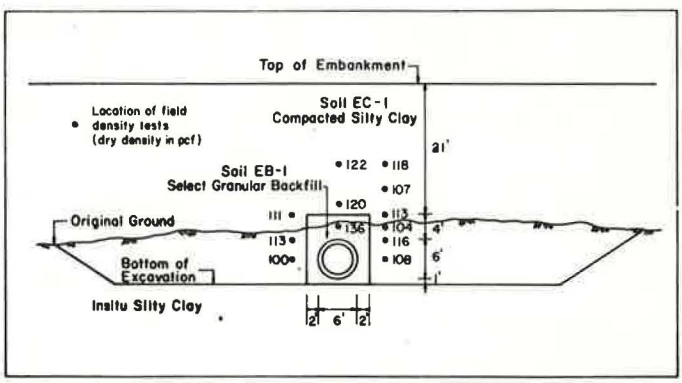

smallest pipe for reasonable access of personnel and instruments and the largest pipe consistent with available height of cover, which was dictated by topography and economics. The installation consists of five 8-ft-long instrumented pipe sections (the middle one of which is most heavily instrumented) and several buffer sections at either side. It is located under a section of the 7.5-mile high-speed test loop at the Research Center and forms part of an access tunnel through the embankment. To achieve a 25-ft height of cover, it was necessary to excavate the existing ground prior to installation of the pipe; the width of this excavation at the base was more than 70 ft, thereby giving reasonable assurance that true embankment conditions were achieved. Figure 2 shows the log of one nearby soil boring, which indicates that (a) the soil conditions beneath the pipe were reasonably uniform and consisted essentially of silty clay and (b) the existing water table was below the proposed elevation of the pipe.

The field instrumentation was designed to measure stresses and displacements in the soil and in the pipe as well as at the soil-pipe interface. Total stress cells were employed to measure the normal stresses acting on the soil-pipe interface, at certain discrete points in the soil adjacent to the pipe, and in the free field; a detailed description of these cells and an assessment of their performance are given by Krizek et al. (2). In the pipe itself, horizontal and vertical diameter changes as well as variations in a number of chords were measured to an accuracy of 0.002 in. by mechanical extensometers, and an extensive set of strain readings was collected. Total displacements of the pipe and the soil and relative displacements between the soil and the pipe were monitored by means of settlement plates and the use of ordinary surveying methods. In-place unit weights of the soil were determined to provide information regarding the magnitude of the load increments and the density condition that controls the stiffness of the soil.

The installation of the test pipe was undertaken in June 1971 and was completed about 4 months later. The existing ground surface in the vicinity of the installation was excavated to a depth of about 1½ ft below the designated elevation of the pipe invert, as shown in Figure 3. Then, a select granular bedding material, designated as EB-1 and described in Figure 4, was placed under the pipe with an average thickness of about 1 ft and compacted by use of a small vibratory compactor. Instrumentation to measure stresses and displacements under the pipe was installed before the pipe sections were laid, and every effort was made to ensure that intimate contact was achieved between the pipe and the bedding. The backfilling operation started after all pipe sections were positioned, and, with occasional delays at various stages to install instrumentation, it continued up to a height of 4 ft above the top of the pipe. The same soil used for the bedding was used for the sidefill (about 1½ or 2 ft to either side of the pipe) and the fill above the pipe; each lift was about 1 ft thick before being compacted.

After this stage of the backfilling was completed, the embankment was constructed of the natural excavated soil, a silty clay designated as EC-1 and described in Figure 5. Heavy construction equipment was used to move and compact the soil in approximately 1-ft lifts until a cover of 25 ft was obtained. Densities of the compacted fill were measured frequently during the construction period, and typical data are shown in Figure 3. The operation was stopped every 4 ft to allow readings to be taken from the various types of instrumentation. In addition, the effect of a live load was studied when the pipe was under 4 ft of cover. During the first part of the installation, including most of the instrumentation and backfilling operations up to a height of cover of 12 ft, the weather was generally fair. A cover height of 16 ft was attained after a few weeks, but the remaining 9 ft of cover was not placed until about 4 months thereafter. This delay, although unanticipated, provided the opportunity to evaluate time effects to a limited extent.

STRESS DISTRIBUTIONS DUE TO EARTH LOADS

Ten 6-in.-diameter and eleven 10-in.-diameter total stress cells were installed at discrete points within the soil adjacent to the pipe and at the soil-pipe interface to obtain direct measurements of the average normal total stress (effective stress plus pore water pressure) acting at these points. Nine 6-in.-diameter cells were placed in the

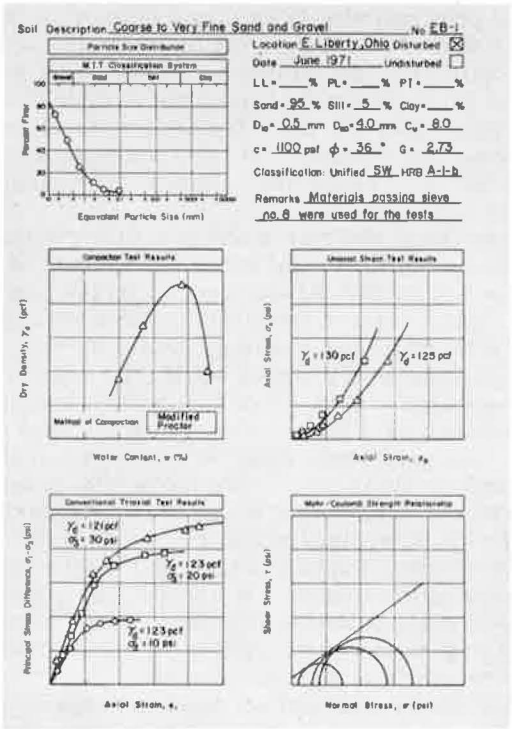

Figure 4. Summary of test data for soil EB-1.

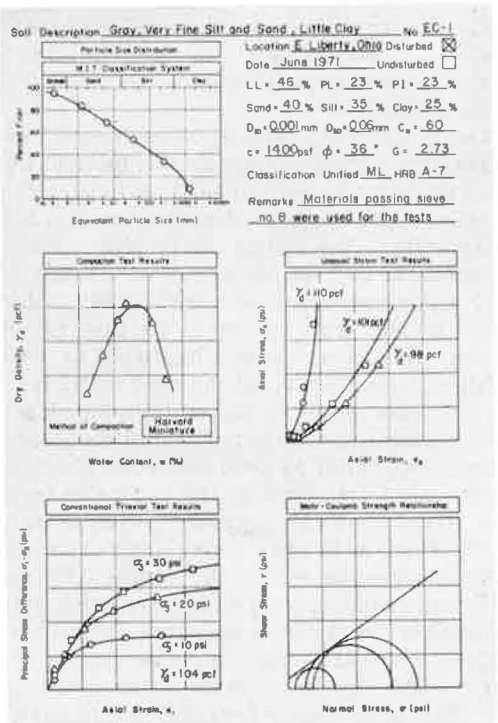

Figure 5. Summary of test data for soil EC-1.

wall of the principal pipe (E3); single cells were installed every 45 deg (alternately in two planes spaced at +30 in. from the midplane) around the pipe with two cells at the top. All cells were placed in recesses provided at the time the pipe was cast, and the surfaces of all cells are flush with the surface of the pipe. In addition, one 6-in.-diameter and two 10-in.-diameter cells were placed in the free field at the elevation of the pipe spring line and 15 ft from the pipe, and nine 10-in.-diameter cells were installed in the soil immediately adjacent to (within about 2½ ft of) the top, bottom, and spring line of the pipe.

Data concerning the stress and temperature measurements were obtained from a digital readout voltmeter and converted to units of gauge pressure, and the resulting distributions of normal stresses acting on the pipe for various heights of cover are shown in Figure 6; these distributions have been drawn by fitting curves to the symmetrized data, which were obtained every 45 deg. The narrowness of the peak at the invert represents an attempt to satisfy the observed fact that the template used to shape the bedding was oversize, thereby providing for pipe contact with the compacted bedding over approximately a 10-deg arc. Since the total stress cells measured only normal stresses, no experimental data were obtained on shear stresses along the soil-pipe interface; because these shear stresses would, in general, not be zero, it follows that the complete stress distribution at the soil-pipe interface has not been obtained. Although the readings from symmetrically placed cells are reasonably similar, the resulting stress distributions shown in Figure 6 are different from that suggested in the classical Marston-Spangler approach. In general, the effect of time (4 months at 16 ft of fill) on the stresses at the soil-pipe interface caused increases on the order of 1 to 3 psi; variations in all the other cells ranged from about -5 psi to +3 psi, and there was no apparent pattern to the increases and decreases.

Only 2 of the 21 cells did not function properly. The failure of the cell 6 in. below the pipe was due to a damaged transducer, which was replaced in the field when the fill was about 4 ft above the top of the pipe; although this replacement was accomplished satisfactorily, the reference for this cell was lost, and all subsequent readings represent only a change in stress rather than absolute stress. After approximately 3 weeks (16 ft of cover) of satisfactory performance, one cell (S6) at the spring line ceased to function; the reason is not known.

In the case of the cells (S7 and S9) embedded in the crown of the pipe, there is a serious difference between supposedly identical readings; although no definite reason for this discrepancy can be advanced, it is probably due to the heterogeneity of the fill above the cells. The large readings of the cell (S1) at the bottom of the pipe are probably due primarily to the weight of the pipe acting over a small strip; for example, if the pipe is assumed to rest uniformly on a strip 6 in. wide, the weight of the pipe alone accounts for a normal stress of about 20 psi. Since the actual reading for the situation where the fill is even with the top of the pipe is somewhat greater than 50 psi, it is likely that the cell is resting on a high spot or a hard spot in the bedding material because the fill up to the crown of the pipe could not possibly account for the additional 30 psi. The normal stresses on the pipe increased more or less in proportion to the height of fill. The three cells in the soil directly above the pipe gave stresses that were approximately midway between those given by cells S7 and S9 at the top of the pipe. The stresses recorded by the two cells beneath the pipe attenuate with distance, as expected, and values are consistent with those registered by cell S1 at the bottom of the pipe. The four cells (two measuring vertical stresses and two measuring horizontal stresses) in the adjacent soil at the spring line of the pipe yield stresses that are both qualitatively and quantitatively consistent with those measured at the soil-pipe interface. The horizontal stress at the spring line decreases with distance from the pipe, as expected, and the vertical stress increases with distance from the pipe, probably because the relatively rigid pipe is carrying some of the load that would normally be distributed to the soil. Two of the three free field cells gave stresses that are very close to those calculated by use of the actual overburden of soil, but the third registers somewhat low.

STRESS DISTRIBUTIONS DUE TO LIVE LOADS

The effects of live loads due to heavy equipment passing over the pipe during the

Figure 6. Stress distribution at soil-pipe interface due to earth loads.

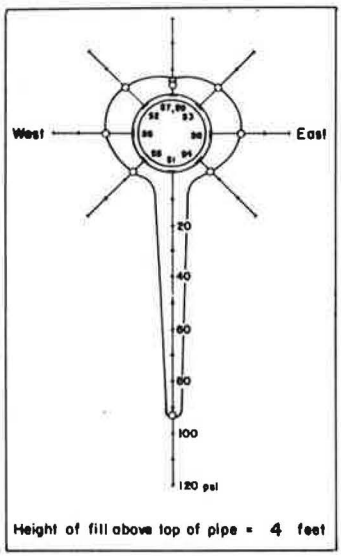

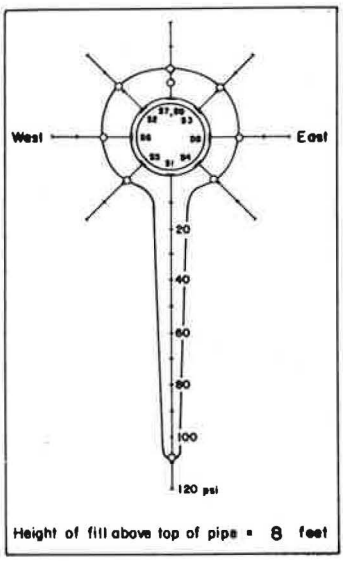

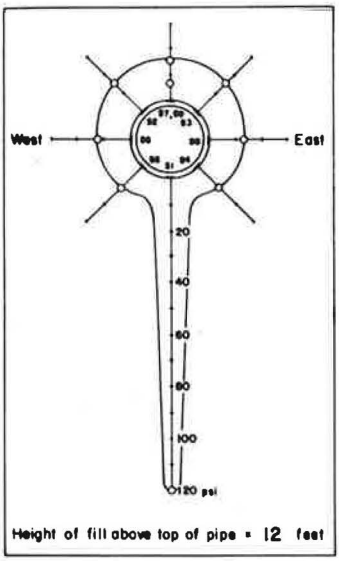

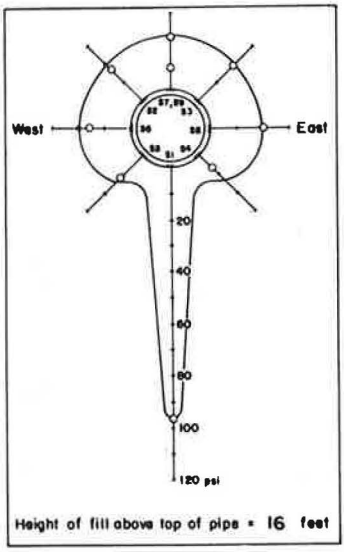

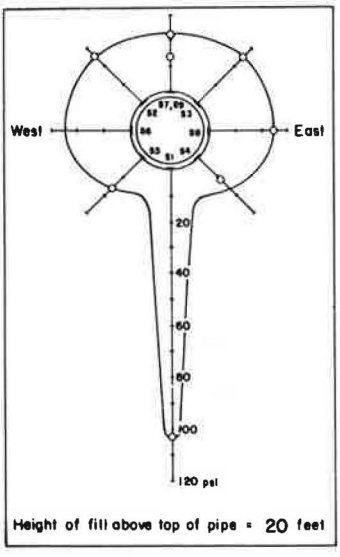

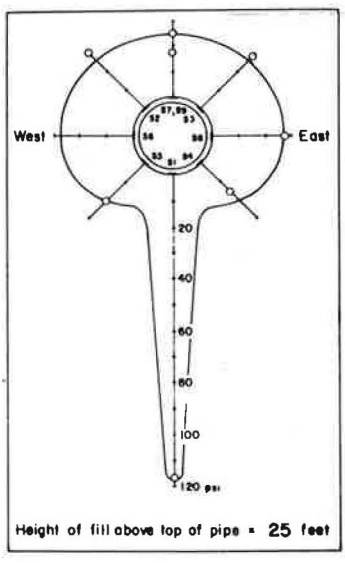

construction phase may be of considerable importance, especially when the depth of cover is relatively shallow; however, the effect of a surface load decreases rapidly with increasing depth. To evaluate the influence of construction loads on a pipe with a relatively shallow cover, a fully loaded (heaped) Caterpillar 631B 30-yd^3, rubber-tired tractor-scraper was used to load the pipe when it was covered with 4 ft of fill. Based on manufacturer's specifications, the load on each front wheel of the tractor-scraper was estimated to be about 39,000 lb; this load, in conjunction with a measured 3.0- by 1.5-ft wheel contact area, yields an assumed uniformly distributed static load of 8,700 psf or about 60 psi. The tractor-scraper was parked over the pipe at the two different locations shown in Figure 7, and stresses and deformations were recorded at four stages. The first measurements were made shortly before application of the load; the second and third recordings correspond to the load positioned directly above and 5 ft to the east of the test pipe; and a fourth reading of stresses and deformations was made after the load was removed from the vicinity of the pipe. The normal stress distributions corresponding to these stages are shown in Figure 8.

These data suggest three important points of interest. First, the surface load has a relatively small effect on the overall distribution of stresses around the pipe; except at the bottom of the pipe, the maximum stress increase due to application of the load is less than 5 psi in the extreme case, and it occurs at the pipe crown when the front wheels of the tractor-scraper are directly above the pipe. In general, the stress changes are almost uniformly distributed around the pipe; this is particularly important because a hydrostatic compression load at the soil-pipe interface is a very desirable type of loading from the viewpoint of minimizing the shear stresses that often cause failure of the pipe. This effect was also observed in the deformation measurements taken during these stages of loading; that is, there were no appreciable differences in the diameter changes in the various directions. The situation is a little different in the case where the load was offset by 5 ft from the axis of the pipe; the change in the distribution of stresses around the pipe is not as uniform as in the previous case, but the magnitudes of the changes are relatively small.

A second interesting point can be observed when the stress increase at the crown of the pipe is examined for those case where the load is directly above the pipe. A simple calculation based on the assumption of a homogeneous, isotropic, linearly elastic half-space subjected to the same surface load indicates that the vertical stress increase at a depth of 4 ft is about 7.3 psi, whereas the average normal stress increase measured by cells S7 and S9 in the crown of the pipe is approximately 4.6 psi. Furthermore, since the pipe is presumably stiffer than the volume of soil it replaces, this difference of 2.7 psi seems to be in the wrong direction—that is, the stress is transferred to the surrounding soil instead of being carried by the pipe. The decrease in the vertical diameter was measured to be about 0.03 in. when the tractor-scraper wheels were above the pipe. On the other hand, when the wheels were offset, the diagonal diameter in line with the tractor wheels decreased by only 0.01 in. In both cases it is difficult to evaluate the load transfer mechanism because the shear stresses at the soil-pipe interface are unknown.

The third relatively important conclusion concerns the apparent elastic behavior of the soil-pipe system. Figures 8a and 8d show that the stress distribution after the removal of the load is very much the same as that existing before the load was applied; that is, there are no residual stresses in the system. Although this behavior does not prove that the soil-pipe system is elastic, since strains were not measured, it does lend some support to the use of elastic theory, at least for short-term applications of static loads.

DISTRIBUTION OF DISPLACEMENTS

Information concerning the vertical displacements at discrete points in the soil-pipe system was obtained by use of settlement plates. A total of 22 settlement plates were installed at points in planes parallel and perpendicular to the longitudinal axis of the pipe, as shown in Figure 9. The extreme three plates to either side of the pipe in the transverse plane were intended to measure the free field response. All plates were

Figure 7. Position of tractor-scraper relative to pipe.

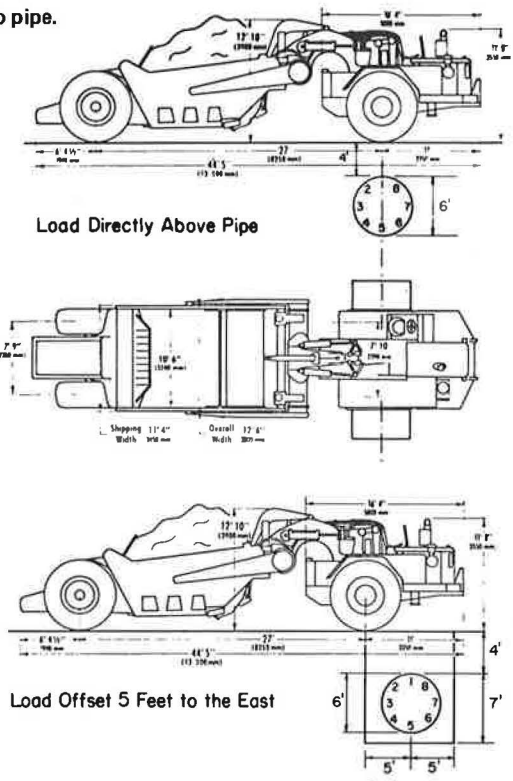

Figure 8. Stress distribution at soil-pipe interface with addition of live load.

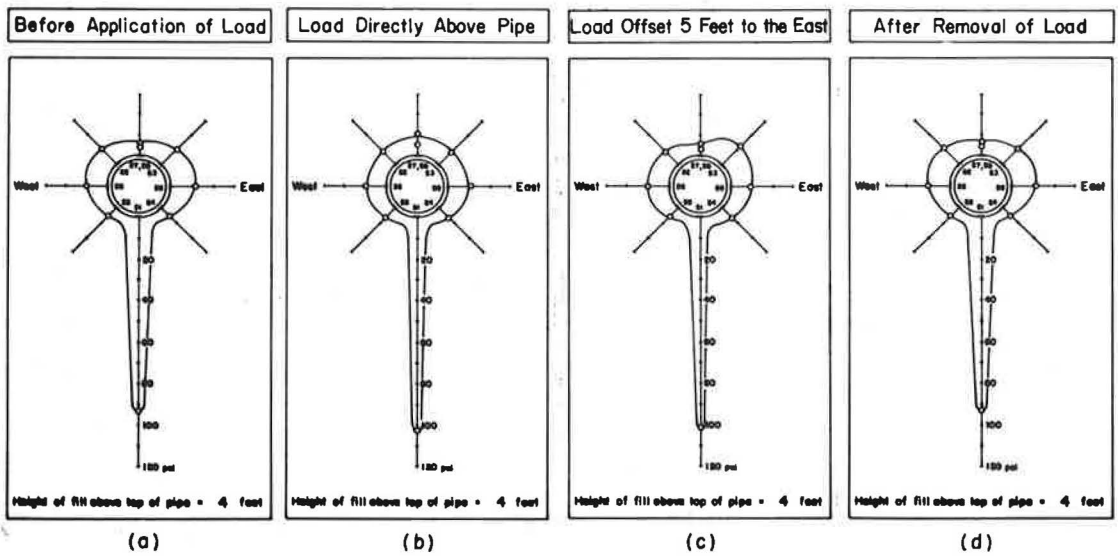

placed in recesses that were excavated and filled with a few inches of a uniform sand to ensure proper seating; then the plates were covered with several inches of soil to hold them in position as the adjacent fill was placed. The vertical rods attached to the plates in the longitudinal plane passed through sleeves in the pipe wall, and these plates gave relative displacements between the plate and the pipe wall. The vertical rods fixed to the plates in the transverse plane passed through a casing to eliminate the frictional resistance of the soil on the rods and extended to the surface; ideally, these plates should measure absolute displacements, but the lack of a suitable long-term benchmark diminished the reliability of these measurements. A short-term benchmark was established by driving a steel pipe a few feet deep and several hundred feet from the installation, and some of the variations in the results are probably due to the use of this type of benchmark. Despite attempts to flag the area, the construction equipment may have caused some disturbances to the exposed extension rods of the settlement plates in the transverse plane; in several cases the extension rods were bent somewhat, and undetermined movements of the plates may have occurred. In one isolated instance, a large tractor-scraper apparently ran over an extension rod (a 1-in.-diameter pipe) and cut through its rubber tire, thereby disturbing the plate by some unknown amount.

Longitudinal Plane

Average relative displacements (taken after 25 ft of cover had been placed) of the settlement plates in the longitudinal plane are shown in Figure 10 as a function of the distance of the plates from the outer wall of the pipe. Overall trends and magnitudes indicate that (a) the relative displacements in the soil below the pipe are considerably higher than those above the pipe and (b) these relative displacements appear to attain essentially their maximum values at small distances from the pipe wall (on the order of a few feet). The former observation is consistent with the measured stresses shown in Figure 6. At 25 ft of cover the vertical stresses at the soil-pipe interface above and below the pipe are about 20 psi and 120 psi respectively; hence, it is logical to anticipate displacements below the pipe that are 5 to 10 times those above the pipe (due to the nonlinear behavior of the soil), and this is generally the order of magnitude shown in Figure 10. The latter observation regarding the rapid attenuation of relative displacements has been suggested by virtually all continuum models of soil-pipe interaction, although there admittedly has been little substantiating experimental evidence.

Transverse Plane

The settlement readings taken in a transverse plane are shown in Figure 11, which has been plotted by assuming that the original position of each individual settlement plate is at the position given by the curve of the preceding settlement plate for the appropriate height of fill; then, the changes in the settlement of each plate are plotted with reference to the established datum for each plate. For example, plate T3 was installed at the crown of the pipe; then, 5 ft of fill was placed over the crown and the plate settled approximately 0.08 ft, at which time plate T5 was installed with the 0.08-ft reading as a datum. Then, for instance, since the total cumulative settlement of plate T5 was measured to be 0.20 ft after 20 ft of fill was placed, the corresponding value plotted in Figure 11 is 0.28 ft (that is, 0.08 + 0.20 ft). Although there is some scatter in these data, they nevertheless give a general appreciation for the overall response of the system of settlement plates. As a consequence of the benchmark problems previously discussed, there is a degree of uncertainty regarding the absolute settlements of these plates; however, the relative displacements between plates T1 and T3 and the other plates in the installation are considered to be quite accurate. The difference between any two curves in Figure 11 represents the relative displacement between the corresponding two plates due to the soil placed above the higher plate.

The settlement ratio, r_{sd}, as defined by Spangler and Handy (3), is given by

$$r_{sd} = \frac{(s_m + s_g) - (s_f + d_c)}{s_m} \qquad (1)$$

Figure 9. Locations of settlement plates.

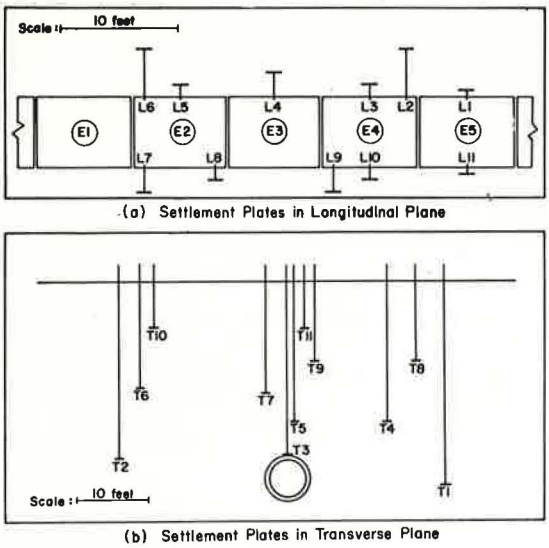

Figure 10. Relative displacements of settlement plates in longitudinal plane.

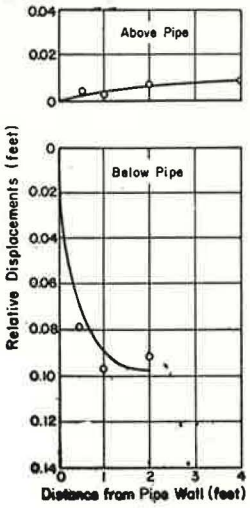

Figure 11. Cumulative displacements of settlement plates in transverse plane.

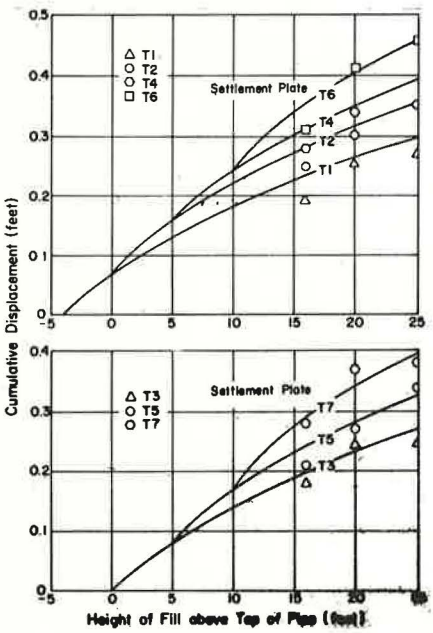

Figure 12. Comparisons between experimental and theoretical results.

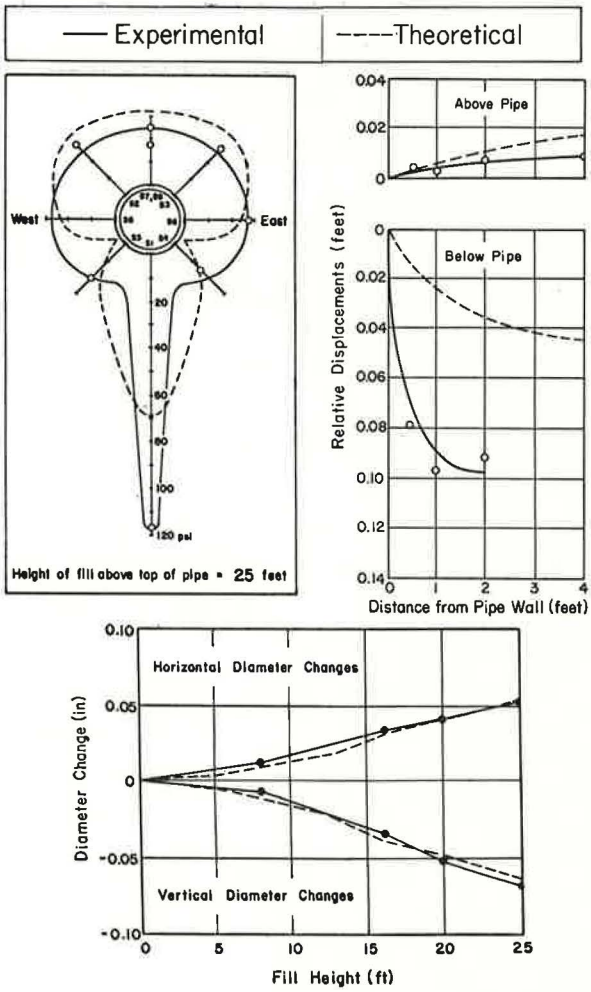

where

s_m = compression of the exterior prisms of soil adjacent to the pipe,
s_g = settlement of the natural ground or compacted fill surface adjacent to the pipe,
s_f = settlement of the pipe into its bedding foundation, and
d_c = change in the vertical diameter of the pipe.

For the curves shown in Figure 11, based on the measurement of all settlements due to the fill above the crown of the pipe only, the magnitudes of the foregoing parameters for the completed installation are $s_m = 0.09$ ft, $s_g = 0.23$ ft, and $(s_f + d_c) = 0.27$ ft. The value of s_m is determined by taking the difference between the settlements of T1 and T2 caused by 25 ft of fill (0.06 ft) and multiplying by 1.5, because T1 is located 4 ft below the crown instead of 6 ft. The value of 0.23 ft for s_g is obtained by assuming that the absolute settlement of T1 caused by 25 ft of fill is approximately the same as it would be if it were located at the elevation of the pipe bottom. Finally, $(s_f + d_c)$ is taken directly from the settlement of T3 under 25 ft of fill. Accordingly, the settlement ratio can be computed as

$$r_{sd} = \frac{(0.23 + 0.09) - 0.27}{0.09} = \frac{0.05}{0.09} = 0.56 \qquad (2)$$

which is reasonably representative and consistent with the soil and pipe conditions at this installation.

ANALYTICAL COMPARISONS

Some appreciation for the ability of a fairly sophisticated mathematical model to describe the field performance of this soil-pipe system can be obtained by comparing the experimental data at certain discrete points with calculated results. For this purpose a plane strain finite element program developed by Anderson (1) was used; the plane strain condition was justified on the basis of experimentally measured longitudinal strains in the pipe wall. The mathematical model of the pipe, including the mechanical properties of the concrete and reinforcing steel and an appropriate cracking mechanism, consists of 320 elements, and its ability to characterize the response of the pipe was validated by means of a series of load tests on pipes of different diameter, wall thickness, and reinforcement. This validated pipe model was then incorporated into a soil-pipe model, which consists of up to 257 additional soil elements, depending on the height of cover above the pipe, and requires the specification of appropriate mechanical properties for each element of soil. Idealized boundary conditions (no shear and no normal displacement) were used at the external boundaries (about 1 diameter below the pipe and 3 diameters to the side of the pipe), and the interface condition between the pipe and the soil was assumed to be full bond.

Piece-wise linear values for the modulus and Poisson's ratio of soils EB-1 and EC-1 were determined by a series of uniaxial strain tests and triaxial tests, typical data from which are shown in Figures 4 and 5. Since density was found to exert a significant influence on the stress-strain behavior of these soils, an attempt was made to prepare test specimens at three different densities (the maximum dry density determined from a standard Proctor test, a density 10 percent above this value, and a density 10 percent below this value). The uniaxial strain tests were performed on disc-shaped specimens (2.5 in. in diameter and 1.0 in. thick) in accordance with the standard loading schedule for consolidation tests; all specimens were saturated prior to testing, and each sample susceptible to swelling was subjected to a sufficient load (not included in the stress-strain data) to prevent any swelling. The triaxial tests were conducted by subjecting cylindrical specimens (2.5 in. in diameter and 5.0 in. long) at approximately optimum water content (as determined from a standard Procter compaction test) to a constant confining pressure and increasing the axial load incrementally; radial displacements were measured at seven discrete points on the boundary of each specimen by use of electronic distance-measuring probes. In all tests the stresses were expressed in terms of effective stresses, since specimens were partially saturated in the triaxial tests and pore pressures were allowed to dissipate completely in the uniaxial strain tests.

Although modulus relationships determined from the triaxial tests could have been used in a general case as input information for the mathematical model, results from the simpler uniaxial strain test were incorporated in this study, and the triaxial test data were used only to provide guidance in the selection of appropriate values for Poisson's ratio (as engineering judgment improves, this step can possibly be eliminated). Once the value of Poisson's ratio, ν, corresponding to a given state of stress is chosen, the associated piece-wise linear value of the modulus, E, can be determined from the relationship

$$E = \frac{(1 + \nu)(1 - 2\nu)}{(1 - \nu)} M \tag{3}$$

where the constrained modulus, M, is the slope of the stress-strain curve obtained from a uniaxial strain test at the stress load of interest. Since the soil in the vicinity of the pipe was subjected to different states of compaction (as observed during the field installation), and since the stress-strain behavior of a soil is strongly dependent on its density, the mechanical properties assigned to each soil element of the mathematical model were selected to reflect the estimated or measured initial density of that element; then, as the state of stress in the element changed due to the increase in the height of cover above the pipe, the mechanical properties were varied incrementally to account for this nonlinear behavior.

Typical comparisons between experimentally measured data and results obtained from the mathematical model of the soil-pipe system for a cover height of 25 ft are given in Figure 12. The respective stress distributions exhibit the greatest discrepancy at the bottom of the pipe, where the mathematical model (averaged every 10 deg) predicts a lower normal stress than was measured experimentally; although impossible to determine with certainty, this is probably related directly to the bedding condition of the pipe. Despite attempts in the field to properly seat the pipe in a shaped bed, it appears that this condition was not achieved, and a considerable stress concentration exists at the bottom of the pipe; this high stress is substantiated by experimental data from other stress cells in the soil below the pipe. In general, the predicted stresses across the top of the pipe are slightly higher than the measured ones, but the respective distributions are quite similar. The apparent variation between experimental and theoretical stresses in the haunch region of the pipe may be simply a consequence of insufficient experimental data points in this area of high stress gradient; if the computed stresses were further smoothed over this region, the experimental and theoretical values would be in very good agreement. Considerable reliability is given to the measured stresses at the spring line, because a stress of 27 psi was measured at the soil-pipe interface and stresses of 22 psi and 18 psi were measured at points 6 in. and 12 in. respectively from the pipe wall. Possible improvements in the computed results may stem from a modification of the assumed condition of perfect bond at the soil-pipe interface, improved stress-strain relationships for the soils, better characterization of nonhomogeneities in the field installation, and use of a finer mesh for the finite element grid. The calculated relative displacements in the soil above the pipe are somewhat higher than the measured values, but the opposite is true below the pipe; however, this is consistent with the stress comparisons. This suggests that the experimental data are mutually compatible and probably quite reliable, although they are not in full agreement with the values determined from the mathematical model. The foregoing comparisons between experimental and theoretical stresses and displacements represent rather severe situations, because the values are obtained at discrete points in the system; in contrast, the diameter changes in the pipe reflect to a greater extent the integrated response of the overall soil-pipe system. As seen, the experimental and theoretical diameter changes in the horizontal and vertical directions are in excellent agreement.

CONCLUSIONS

Within the scope and limitations of the results reported here, certain conclusions can be deduced. Of considerable importance is the fact that the experimentally mea-

sured stresses and displacements appear to be mutually consistent, although these values at certain discrete points in the system differ somewhat from values calculated by use of a mathematical model. However, both the experimental and theoretical distributions of stresses around the pipe differ somewhat from those suggested in the Marston-Spangler approach. The experimentally measured and theoretically calculated horizontal and vertical diameter changes due to earth loads only were found to be in excellent agreement. The application of a heavy construction load to the pipe under a depth of cover of 4 ft had little effect on the diameter changes of the pipe or the stress increases and distribution of stresses at the soil-pipe interface, and upon removal of the load the pipe exhibited no residual stresses or displacements.

ACKNOWLEDGMENT

This work was performed as part of an extensive research effort supported by the American Concrete Pipe Association to investigate the soil-structure interaction of buried concrete pipe.

REFERENCES

1. Anderson, J. E. A Model for Evaluating the Response of Buried Circular Concrete Pipe. Doctoral dissertation submitted to Northwestern University, 1974.
2. Krizek, R. J., Farzin, M. H., Wissa, A. E. Z., and Martin, R. T. Evaluation of Stress Cell Performance. Jour. Geotechnical Engineering Division, ASCE (in press, 1974).
3. Spangler, M. G., and Handy, R. L. Soil Engineering, 3rd Edition. Intext Educational Publishers, New York, 1973.

DISCUSSION

M. G. Spangler, Engineering Research Institute, Iowa State University

This paper is a valuable addition to the literature on the structural performance of buried conduits and is of special interest to this writer for two reasons: first, because of the experimental evidence dealing with the technology of soil-structure interaction in this type of structure and, second, because it represents the culmination of a major reversal in policy by the sponsoring agency, the American Concrete Pipe Association.

This fine industrial organization was not always research-minded. The writer well remembers a period about 45 years ago, when the Association did not approve the efforts being made at the Iowa Engineering Experiment Station toward unraveling some of the mysteries of soil-pipe performance. When our bulletin, "The Supporting Strength of Rigid Pipe Culverts" (4), was published in 1933, the managing director at the time was very critical and said, "The mathematics in that bulletin would make any self-respecting concrete pipe blush with shame." This reversal in policy is a welcome development.

On the technical side, this writer has difficulty accepting the normal unit pressure measurements at the spring line of the pipe, as shown in Figure 6. The diagrams indicate a nearly uniform distribution of pressure around the periphery of the structure above the bedding. This quasi-hydrostatic pattern is more typical of the distribution around a flexible pipe in which a relatively large increase in horizontal diameter, as the pipe is loaded, brings into play the passive resistance pressure of the soil at the spring line. In contrast, a reinforced-concrete pipe deflects a negligible amount, and the unit pressure at the spring line would probably be more nearly equal to the active lateral pressure of the soil. According to Figure 12, the horizontal diameter of the pipe increased approximately 0.05 in. under 25 ft of fill. This indicates an outward movement of each side of the pipe of 0.025 in., which is not enough to mobilize any passive resistance pressure of the soil.

The question raised, then, is not concerned with the accuracy of the pressure cells used or the accuracy of observations. Rather, the question is directed toward the

validity of measuring the unit pressure on a relatively small area and extrapolating the measurement to apply to a larger area such as the side of a concrete pipe. The soil that constitutes the fill over and around a pipe may appear to be quite uniform. However, the writer's experience has led to the conclusion that the pressure indicated by a pressure cell may not be representative of the pressure on a larger prototype area because of unapparent heterogeneity of the soil. The authors quite properly suggest this possibility in their discussion of the different results indicated by cells S7 and S9, which were embedded in the crown of the pipe at points of supposedly identical pressure.

In an effort to minimize this possible discrepancy between a pressure cell reading and the actual prototype unit pressure on a larger area, this writer developed a pressure-measuring device that consisted of a stainless steel ribbon, ½ in. wide by 0.008 in. thick. This ribbon was mounted on the outside of a pipe along longitudinal elements of theoretically equal pressure. The ribbon was confined between layers of canvas and passed over stainless steel rollers at the ends of a 4-ft-long section of pipe. Then the ends of the ribbon could be pulled in a radial direction from the inside of the pipe. After calibration and during and after construction of an embankment, the pull required to start the ribbon sliding gave a measure of normal pressure on the pipe wall that was mechanically averaged over an element ½ in. wide and 48 in. long.

The pressure distribution measured in this manner on a 44-in. outside diameter concrete pipe is shown in Figure 13 (4). The 15-ft-high embankment in this case was constructed by teams and wheeled scrapers and was not compacted in a formal manner but only by the team and scraper traffic. The reason for the skewness of the vertical load on the pipe is not known, but may be related to the heterogeneity of the soil as noted earlier. It may or may not be significant to note that the direction of the skewness is toward the direction of approach of the team traffic. Attention is directed to the fact that the lateral pressures on the sides of the pipe are considerably less than the vertical and seem to be more compatible with the normal relationship between active lateral pressure and vertical pressure of soil.

The relatively minor load effect on the authors' experimental pipe caused by a heavy live load applied to the surface of the fill at an elevation 4 ft above the pipe essentially agrees with the findings by the writer in an extensive series of tests performed approximately 50 years ago (5). In these tests, a heavily loaded truck wheel was positioned over a culvert section 2 ft long and 3.5 ft in outside diameter. The load transmitted to the culvert was measured and expressed as a fraction of the truck wheel load when applied at the surface of fills ranging in depth from 6 in. to 6 ft. The transmitted loads were compared with loads calculated by the Boussinesq theory of stress transmission in an elastic, isotropic, homogeneous medium of semi-infinite extent (half space). Although soil is neither elastic, nor isotropic, nor homogeneous, it was found that a reasonably good correlation existed between the measured and theoretical loads. The following conclusion on this matter is quoted from Bulletin 79 (5):

> The theoretical formula (Boussinesq) seems to give a locus showing the maximum percent of load transmitted through any thickness of fill. In the experimental work, however, this maximum load generally was not reached, but when conditions were most favorable... the experimental results came very close to the theoretical.

The correspondence between the theoretical and experimental loads on the culvert is shown in Figure 14.

It is of interest to compare the authors' measurements of vertical unit pressures on cells S7 and S9 with calculated pressures by the Boussinesq equation. Using Newmark's integration, unit pressures along the longitudinal centerline of the experimental pipe have been calculated and are shown in Figure 15. The position of the live loads relative to the pressure cells was furnished to this writer by Krizek. The measured pressures are somewhat greater than the theoretical value, which is contrary to the writer's experience noted above, but the divergence is not significant.

In estimating the effect of surface traffic loads on a buried conduit, the possibility of impact loads must be considered. In the writer's experiments referred to earlier (5), impact loads were measured along with static loads. Impact loads varied widely,

Figure 13. Radial earth pressures on concrete pipe measured by pressure ribbons.

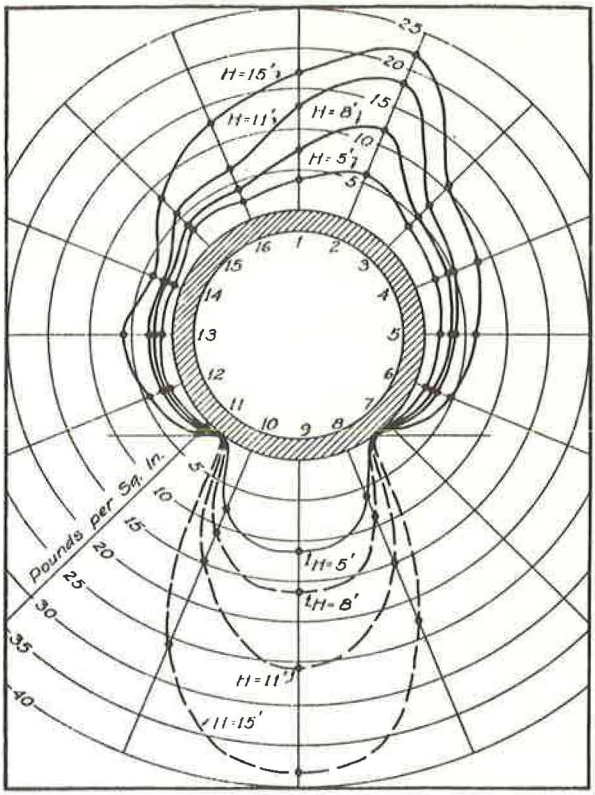

Figure 14. Static wheel loads transmitted to a section of culvert 2 x 3½ ft in outside diameter.

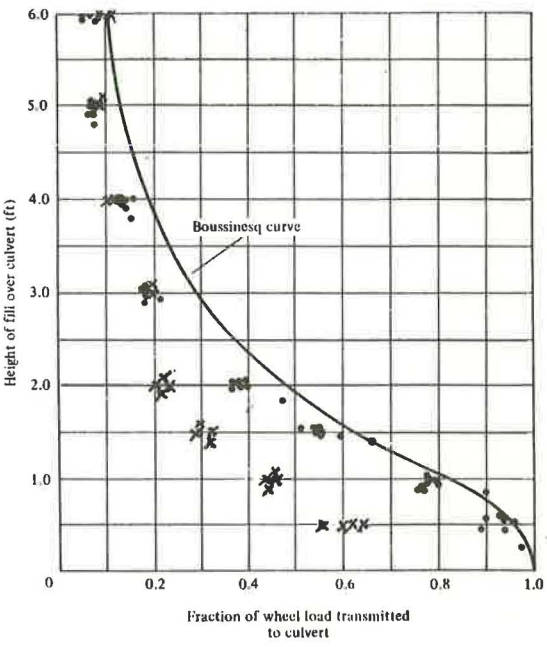

Figure 15. Calculated pressures along centerline of pipe.

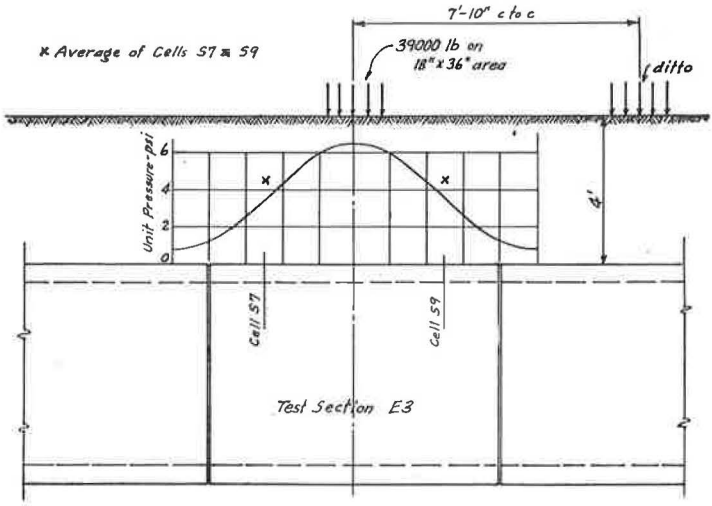

Figure 16. Total load on buried conduit versus height of fill.

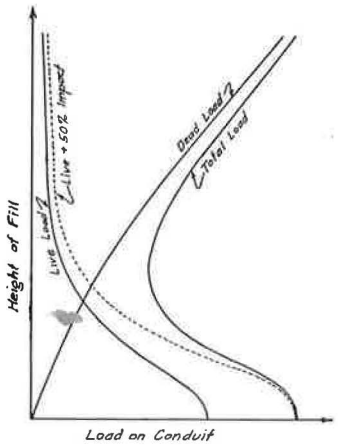

Figure 17. Measured values of settlement ratio for rigid culverts.

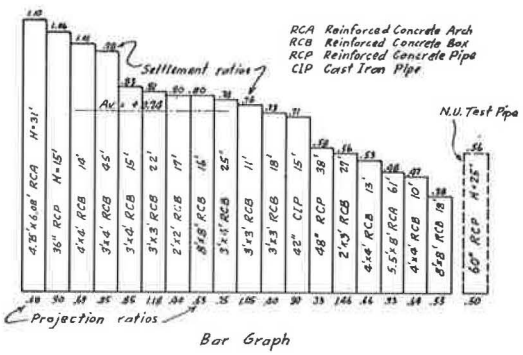

mainly depending on the character of the roadway over the culvert. The type of vehicle used in the authors' experiments probably would exert an impact load on a buried conduit under actual field conditions. Such vehicles operate at fairly high speeds and have been observed to operate in a "bouncing" or "porpoising" manner at times, which undoubtedly would cause considerable impact if the downward cycle of a bounce came directly above the conduit. This writer estimates that an appropriate impact factor of 2.0 probably would suffice, if a design were based on such a vehicle operating on the surface at a shallow depth of cover.

A diagrammatic relationship between earth load, static and impact loads, and total load on a buried conduit at various depths of cover is shown in Figure 16. It is indicated that the total load decreases to a minimum at some relatively shallow height of fill, then increases as the height increases.

Another factor of interest in connection with concentrated surface loads is the matter of the "effective length" of conduit to be considered in connection with such loads. The load produced by a concentrated surface load is of varying intensity on the conduit, being a maximum directly under the center of the applied load and decaying rather rapidly in a longitudinal direction, as indicated in Figure 15. Effective length is defined as the length of conduit over which the transmitted load can be considered to be uniformly distributed to produce the same stresses and deflections in the pipe ring as does the actual varying load. To illustrate, suppose the authors' experiments had been conducted on a pipe only 2 ft long. In all probability the measured stresses in the pipe would have been greater than those observed in the 8-ft-long pipe section.

As far as the writer is aware, no research on this matter of effective length has ever been reported.

The authors measured the settlement ratio that prevailed in the experimental installation and found it to be +0.56. This is of great interest and value, as such measurements are very scarce, and every additional reliable measurement adds a great deal to our knowledge in this area. The writer has measured this ratio in connection with 18 actual field structures consisting of reinforced-concrete arch culverts, reinforced-concrete box culverts, reinforced-concrete pipe culverts, and one cast-iron pipe culvert (6). The average of these measurements was +0.74. The authors' measured value fits very nicely with these values, as shown in Figure 17.

The writer has for many years advocated using a value of +0.7 for this factor in design work on positive projecting conduits, particularly in cases where environmental conditions are not sufficiently well defined to permit a rational estimate, which is usually the case. This measurement by the authors lends support to this design practice.

REFERENCES

4. Spangler, M. G. The Supporting Strength of Rigid Pipe Culverts. Bull. 112, Iowa Engineering Experiment Station, Ames, 1933.
5. Spangler, M. G., Mason, C., and Winfrey, R. Static and Impact Loads Transmitted to Culverts. Bull. 79, Iowa Engineering Experiment Station, Ames, 1926.
6. Spangler, M. G. Long-Time Measurement of Loads on Three Pipe Culverts. Highway Research Record 443, 1973, pp. 1-14.

AUTHORS' CLOSURE

The authors thank Spangler for his interesting and thought-provoking discussion of this work. His vast experience in the area of buried conduits provides the necessary background to place this study in appropriate historical perspective, and his added data and supplemental calculations are most welcome.

The normal pressure measurements at the spring line of the pipe are indeed higher than had been expected from the Marston-Spangler theory, but there are good reasons to believe that these measurements are reasonably accurate. Among these reasons

are the facts that (a) the stress cells employed were evaluated quite thoroughly by a coordinated experimental and theoretical study; (b) their sensing area is relatively large (over 25 $in.^2$ per cell and an equivalent linear sensing area for all nine cells equal to one quadrant of the pipe); (c) the readings from nine stress cells symmetrically distributed in two transverse planes were reasonably symmetric and, with the exception of the cell at the bottom of the pipe and one cell at the top, yielded a relatively smooth and continuous normal pressure distribution around the pipe; (d) the magnitudes of the normal stresses at the soil-pipe interface were consistent with other normal stresses (not reported in this paper) measured in the soil immediately adjacent (within a foot or two) to the pipe; (e) the measured normal stresses are consistent with those calculated by use of the stress-strain properties of the soils and simultaneously measured normal strains; and (f) the measured stresses due to an imposed live load are consistent with those anticipated from an engineering approximation of the problem. In brief, Spangler is certainly correct in his statement that the pressure indicated by any one stress cell may, due to installation conditions and/or local heterogeneity of the soil (as was apparently the case with one of the cells at the top of the pipe), not be representative of the pressure on a larger prototype area, but we feel that the foregoing facts tend to substantiate the reasonable overall validity of the stress measurements reported and the interpretations deduced.

It is agreed that the small horizontal displacements of the pipe at its spring line are, in all likelihood, not sufficient to mobilize the full passive resistance of the adjacent soil. However, by the same token, the outward displacements of the pipe at its spring line do not suggest the presence of an active pressure condition. As described in the paper, the approach advocated is based on the stress-strain properties of the various components of a continuum model, and the active or passive resistance of the soil is not incorporated into the formulation.

The excellent supplemental information regarding the effect of a live load and the favorable position of our measured settlement ratio in the context of 18 case histories accumulated by Spangler are sincerely appreciated. Such agreements tend to illustrate and emphasize the tremendous early contributions made by Marston, Spangler, and their coworkers, and they further serve to demonstrate the compatibility between the present analytical approaches to problems of this type and the engineering approaches taken by the Iowa group.

LONG-TERM LOAD TRANSFER IN END-BEARING PIPE PILES

Donald L. York, Port Authority of New York and New Jersey;
Vincent G. Miller, Dames and Moore, Cranford, New Jersey*; and
Nabil F. Ismael, Ontario Hydro, Toronto*

Load transfer in small groups of concrete-filled steel pipe piles is determined by means of electric resistance stress and strain meters located in the concrete core along the length of the piles. These load-transfer measurements are compared with those obtained on individual instrumented piles that were load-tested. Measurements of dragdown loads are presented and compared with design values. The effects of live load superimposed on piles subjected to dragdown loads are examined.

•CURRENT knowledge of load transfer in piling is derived from short-term load tests on instrumented piles (e.g., 7, 8, 9, 17, 19, 20). Presumably these results are applied to the design of foundation piling, although it is generally recognized that load transfer in short-term tests may differ from long-term behavior.

Investigations of the long-term behavior of load transfer have been limited to measurements of dragdown loading due to negative skin friction (2, 3, 4, 10, 11, 12, 13, 15). Understandably, these investigations have concentrated on situations where the drag forces were large in comparison with the applied loads. Ground settlements accompanying these dragdown loads have generally been quite substantial.

This paper reports the results of long-term measurements of load transfer in small groups of end-bearing pipe piles. The piles, which are approximately 50 ft (15 m) long, were driven to shale bedrock through successive layers of hydraulic sand fill, a tidal marsh deposit of organic silts and peats, and a glacial outwash and lake deposit. The tidal marsh deposit was stabilized by preloading, but the upper 20 to 30 ft (6 to 9 m) of the piles are being subjected to dragdown loads due to secondary compression of these organic soils. All piles are supporting mainly structural loads, and dragdown constitutes a small fraction of the design loading. The present study deals specifically with the following points:

1. Development of dragdown loading resulting from remolding of the cohesive soils because of pile driving and the soils' subsequent reconsolidation;
2. Development of dragdown loading due to secondary compression of the tidal marsh deposit;
3. Comparison of short-term load transfer as measured in an instrumented test pile with long-term load transfer in foundation piles; and
4. The effect of superimposing transient loading on a pile group subjected to dragdown loading.

PROJECT DESCRIPTION

The expansion of Newark International Airport in New Jersey includes many important structures that are supported on piling. Among these structures are three terminal buildings and an adjoining elevated roadway, a central heating and refrigeration plant, and several bridges for the roadway system. The entire project required more than 500,000 linear feet of piling.

Foundation support is provided by steel pipe piles driven to bedrock and filled with concrete. A 12.75-in. (32.4-cm) outside diameter steel pipe of 0.25 in. (0.64 cm) wall

*This paper is based on work performed while the authors were with the Port Authority of New York and New Jersey.

thickness provides an allowable design capacity of 80 tons (712 kN). Allowable pile loads were determined by deducting 75 percent of the computed dragdown load from the design capacity. Piles are closed at the tip with either a flat plate or an angle-fin driving point.

Subsurface Conditions

The airport site has been developed by filling over a tidal marsh deposit consisting of from 2 to 20 ft (0.61 to 6.1 m) of extremely soft and compressible organic silts and peaty soils. The organic soils are generally underlain by fine-grained gray sands. Below the sands are glacial outwash and lake deposits, glacial till, and bedrock.

The glacial lake deposits consist of reddish-brown silts and clays, frequently varved and preconsolidated to pressures of 3 to 4 tsf (287 to 383 kPa), about $1\frac{1}{2}$ tsf (144 kPa) in excess of the existing overburden pressures. The lake deposits are interposed with outwash material eroded from the more highly elevated outwash deposits to the west of the airport.

Bedrock is a red shale and occurs at depths ranging from 40 to 100 ft (12 to 30 m) below sea level. The upper surface of the bedrock is frequently badly weathered to depths ranging from a few inches to several feet. Overlying the bedrock is usually a stratum of glacial till, a very dense clayey silt with gravel, cobbles, and boulders.

The tidal marsh deposit has been surcharged with sand fill to remove primary settlements in paved areas. Sand drains were used under roadway embankments that interconnect the terminal buildings and are about 10 ft (3 m) above the general grade. However, post-construction settlements have occurred due to secondary compression of the tidal marsh and have caused dragdown loading on those structures that are pile-supported.

Pile Installation

Piles were driven to a resistance of 20 blows/in. (8 blows/cm) with air- or steam-operated hammers, producing 24,000 to 26,000 ft-lb (32.5 to 35.3 kJ) of rated energy per blow. Piles drove easily through the overburden and penetrated several inches into the shale bedrock. During driving, measurements of pile heave were taken and individual piles that heaved more than $\frac{3}{16}$ in. (0.48 cm) were redriven. In addition, for pile groups where more than $\frac{3}{8}$ in. (0.95 cm) heave was observed, all vertical piles were redriven.

Pile Instrumentation

Three pile groups were selected for long-term measurements of load transfer. The groups consisted of 5 to 8 piles, and they were located in areas where dragdown loading was expected to vary because of differences in the anticipated magnitude and rate of post-construction settlement. Since a principal objective of the testing was to measure the effect of superimposing a live load on piling subject to dragdown loading, pile groups supporting elevated roadways were selected for load measurement because these groups could be conveniently subjected to live loading by positioning heavy vehicles on the roadway. The locations of the instrumented groups are shown in Figure 1, and a simplified geologic profile is shown in Figure 2.

Electric resistance strain and stress meters (Carlson Elastic Wire Strain and Stress Meter) were used for pile load measurements (18). A string of from 3 to 6 strain meters was placed in each pile during placement of the concrete core. The meters were mounted in positioning brackets that served to align them with the axis of the pile and protect them during the concrete filling operation (Figure 3). This type of instrumentation was selected because previous experiences with these strain meters had shown them to be stable and reliable. In addition to reading strains to an accuracy of a few microinches, the meter is also an accurate thermometer. As a minimum, each pile of the group had strain meters at the pile top, the bottom of the tidal marsh deposit, and the pile tip so that pile loads could be measured at these locations.

To permit determination of the creep strain behavior of the concrete core, a pair of strain and stress meters was positioned at the tops of selected piles. Dummy strain

Figure 1. Location plan.

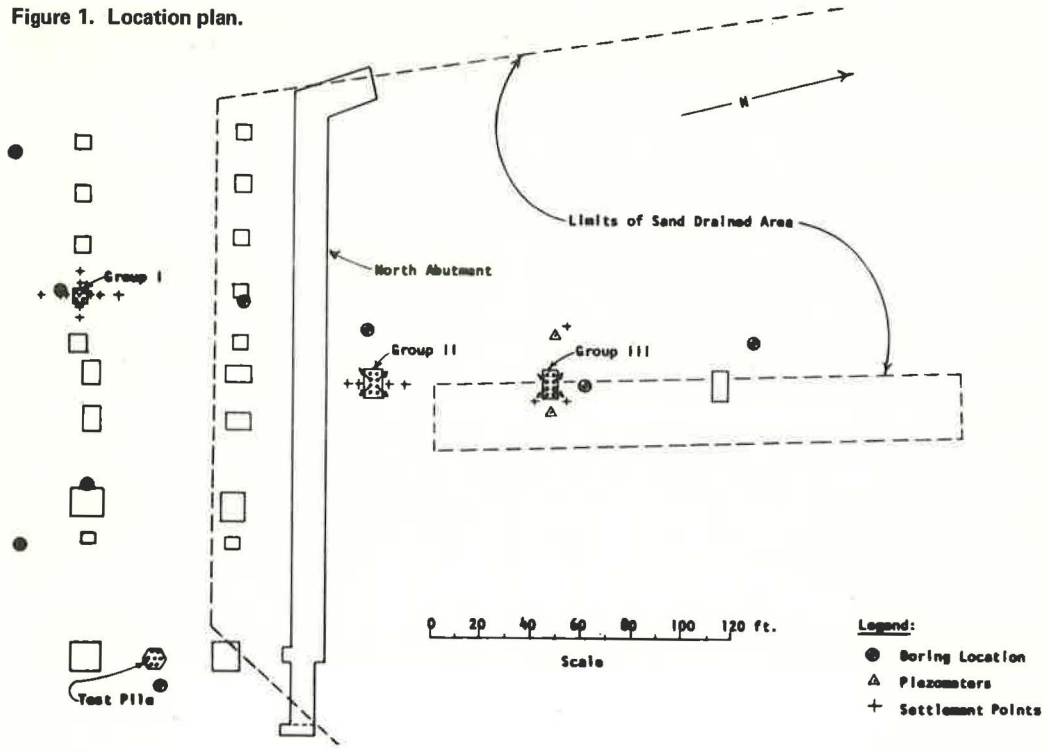

Figure 2. Section through foundations.

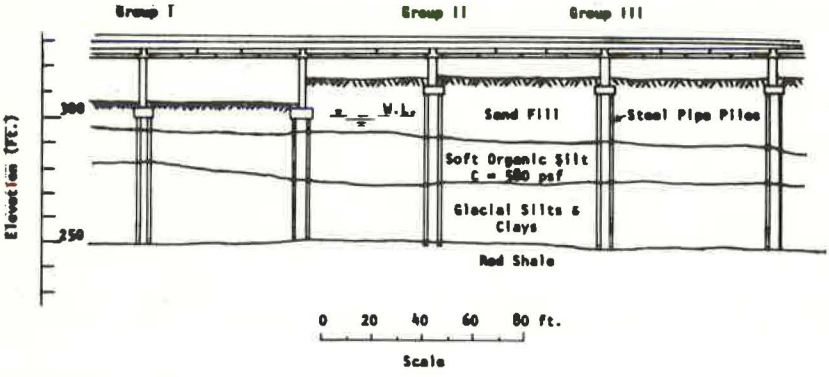

Figure 3. Installing strain meter and positioning bracket.

Figure 4. Plan and section, instrumented groups 2 and 3.

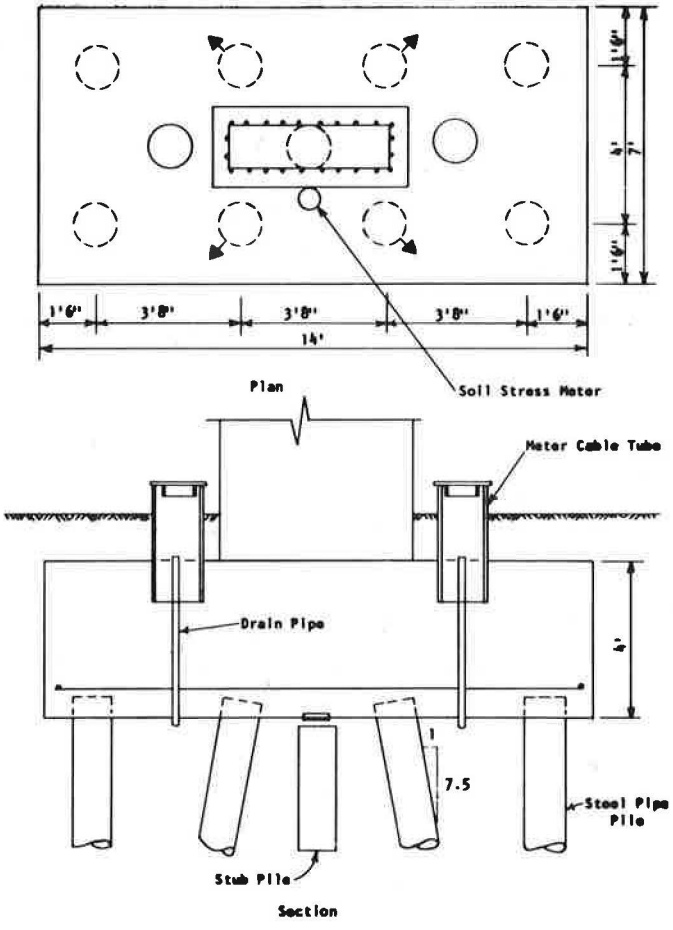

meters were installed in short, unloaded stub piles to record strains due to shrinkage and temperature changes. Soil stress meters were used to measure the contact pressure at the base of pile caps. The arrangement of instruments for pile groups 2 and 3 is shown in Figure 4.

Prior to construction of the foundations, several instrumented piles were load-tested to prove out the proposed design loading and to measure the loads carried by skin friction and point bearing. To provide specific information in the vicinity of the instrumented pile groups, an additional test pile was instrumented and load-tested during foundation construction. This information provides a direct comparison of load transfer in test piles with that measured in the foundation piles. As shown in Figure 1, the test pile was located 150 ft (46 m) east of group 1. The soil profile and driving record are shown in Figure 5, and the load-settlement record is shown in Figure 6. Pile settlements were very small. Under the total test load of 200 tons (1779 kN), the gross settlement was only 0.045 ft (1.37 cm) and net settlement 0.018 ft (0.55 cm).

For the test pile, the fill and organic silt surrounding the pile were removed after pile installation and replaced by a mud slurry. The load at the pile top was measured with an electric resistance load cell. With this arrangement, it was possible to measure the pile stiffness with the upper strain meter when the test load was cycled at the end of each load increment. These data are used to calculate the pile loads at the other meter locations.

Computation of Pile Loads

Axial loads in foundation and test piles were determined from strain measurements by multiplying measured strain by the pile stiffness after correcting for strains due to temperature variations, shrinkage, and creep. The general accuracy of the instrumentation and methods of computation was verified by a number of checks:

1. A comparison of concrete stresses obtained from direct measurements by Carlson stress meters placed in selected piles with the indirect measurements provided by strain meters placed at the same location;
2. A comparison of computed loads from instrumentation measurements with calculated structural loads determined from construction records (Figure 7); and
3. A comparison of computed loads from instrumentation measurements with calculated live loads imposed during the transient load test.

Correction for concrete creep at a sustained high stress level upon construction completion was achieved by adopting a viscoelastic model consisting of a chain of Kelvin models and a Maxwell model (1, 16). Test results with computed pile loads are shown in Figures 5, 7, 8, 10, and 11.

LOAD TRANSFER

Load transfer is defined as the transfer of load between a pile and the surrounding soil. It is considered to be positive when load is being transferred from pile to soil. When the surrounding soil settles relative to the pile and load is transferred from soil to pile, negative load transfer, or dragdown, occurs.

To summarize the results of this study and to compare these results with the findings of other investigators, it is useful to express load transfer in fundamental terms. Load transfer in piles has been expressed in terms of effective stress (6, 14). According to this concept, shaft friction due either to positive skin friction or negative skin friction (dragdown) is related to the effective overburden pressure ($\bar{p}$) by the simple relationship

$$F_s = K \tan \phi' \bar{p} \quad (1)$$

or

$$F_s = \beta \bar{p} \quad (2)$$

where K is the coefficient of lateral earth pressure and ϕ' is the effective angle of friction between the soil and the pile shaft.

Figure 5. Load transfer and soil properties, test pile.

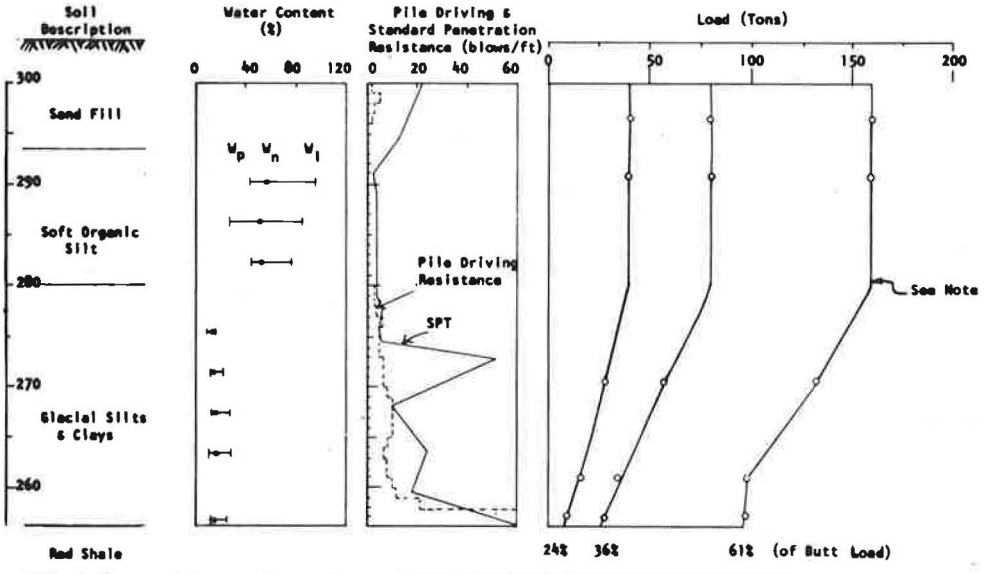

NOTE: Soil removed from annular space around pile and replaced with mud slurry from ground surface to Elevation 280.

Figure 6. Load settlement diagram, test pile.

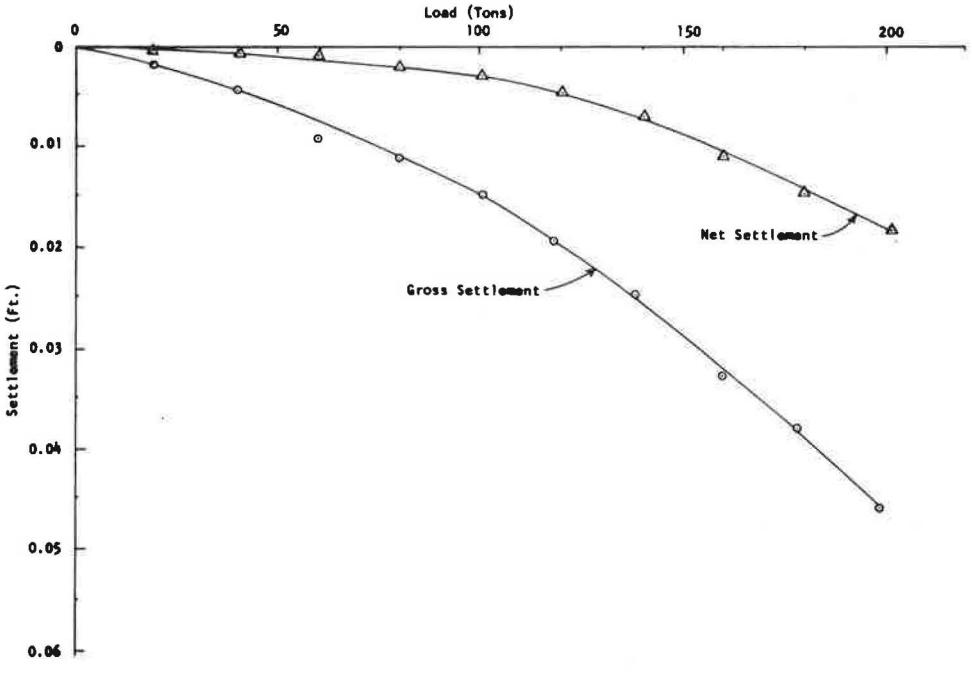

Figure 7. Comparison of calculated loads versus instrumentation.

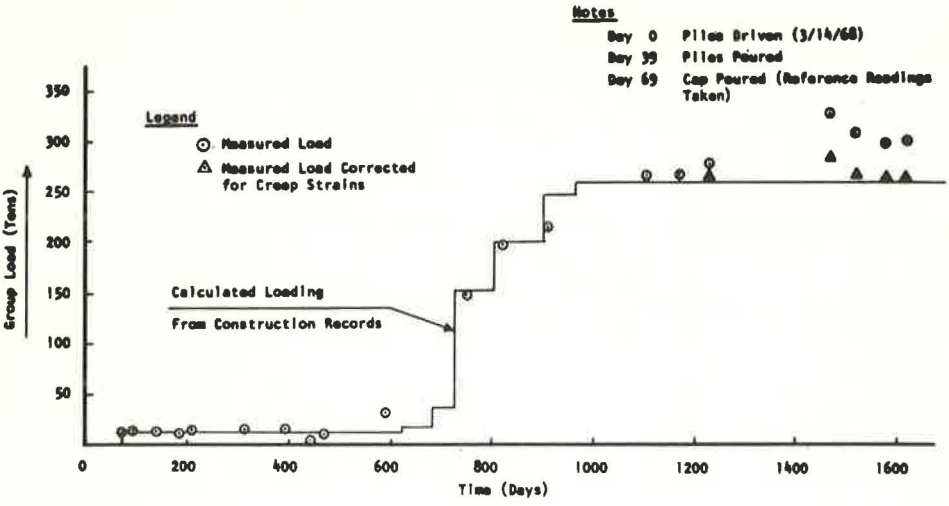

Figure 8. Load transfer, group 1.

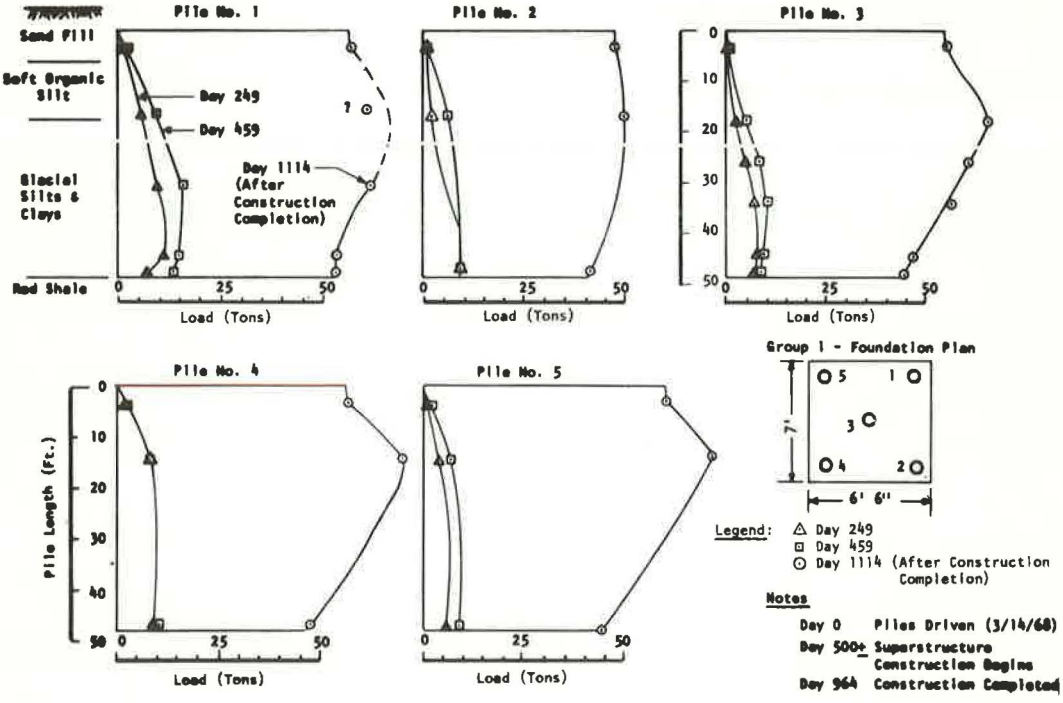

The magnitude of the lateral earth pressure coefficient K depends on the soil type, the stress history of the soil, and the method of pile installation. The value of ϕ' depends on the soil type and the properties of the pile surface. Average values of β can be obtained empirically from measurements of load transfer in instrumented test piles by restating Eq. 2 as

$$\beta = \frac{F_s}{\bar{p}} \tag{3}$$

and taking F_s as the slope of the load transfer curve.

For normally consolidated clays, the results of a large number of pile load tests show that the value of β ranges between the limits of 0.25 to 0.4 (6). Long-term measurements of negative skin friction yield values of β that range from 0.20 to 0.25 for tests where the dragdown loads were fully developed (14).

For overconsolidated clays, the effective stress approach is more complex, mainly because of the effect of remolding resulting from pile driving and because of wide variation in the value of the coefficient of lateral earth pressure (K). For these reasons, there is considerable scatter in the measured values of β; however, β values are larger than for normally consolidated clays.

TEST RESULTS

Settlement and Piezometer Observations

Settlement observations on pile caps show that the application of structural and dragdown loads caused a maximum cap settlement of only $\frac{1}{8}$ in. (0.32 cm). Post-construction observations of ground settlements and piezometric levels indicate that the preload was effective in stabilizing the tidal marsh deposits. Ground settlements over a $2\frac{1}{2}$-year period show settlement rates that are generally equal to or less than the rates of settlement due to secondary compression, as predicted on the basis of laboratory tests. For groups 1 and 2 and the sand-drained portion of group 3 (Figure 1), the maximum rate of ground settlement is 0.1 in./year (0.25 cm/year). Piezometer data in the non-sand-drained area adjacent to group 3 show excess pressures of 2.4 psi (16.5 kPa) at the center of the compressible layer, indicating that the tidal marsh deposit is slightly underconsolidated at this location. The maximum rate of ground settlement in this area is 0.3 in./year (0.76 cm/year).

Dragdown Loads

Test results show that dragdown loading resulted from two distinct phenomena:

1. Remolding of the cohesive soils because of pile driving and the subsequent reconsolidation of the soils, and
2. Secondary compression of the tidal marsh deposit.

The piles for group 1 were driven 19 months prior to the start of construction of the superstructure. This delay in the construction provided an opportunity to study dragdown loading resulting from remolding of the cohesive soils because of pile driving and the soils' subsequent reconsolidation. Dragdown loading due to this phenomenon developed slowly, reaching a maximum about 250 days after pile installation. As shown in Figure 8, a neutral point defining the change from negative to positive skin friction was reached deep in the glacial lake deposit at a depth approximately equal to 90 percent of the pile length. Thereafter, the development of drag load due to secondary compression of the tidal marsh deposit caused a progressive increase in compressive pile strains that gradually reduced the negative skin friction in the underlying glacial lake deposit. With the application of the structural loads, positive load transfer developed in the glacial silts and clays and dragdown occurred entirely within the tidal marsh deposit and the overlying sand fill.

As shown in Figure 9, dragdown loading due to secondary compression of the tidal marsh developed slowly, reaching a magnitude of about 9 tons/pile (80 kN/pile) after 400 days. With the application of the structural loads, there was an abrupt decrease

Figure 9. Development of dragdown with time, group 1.

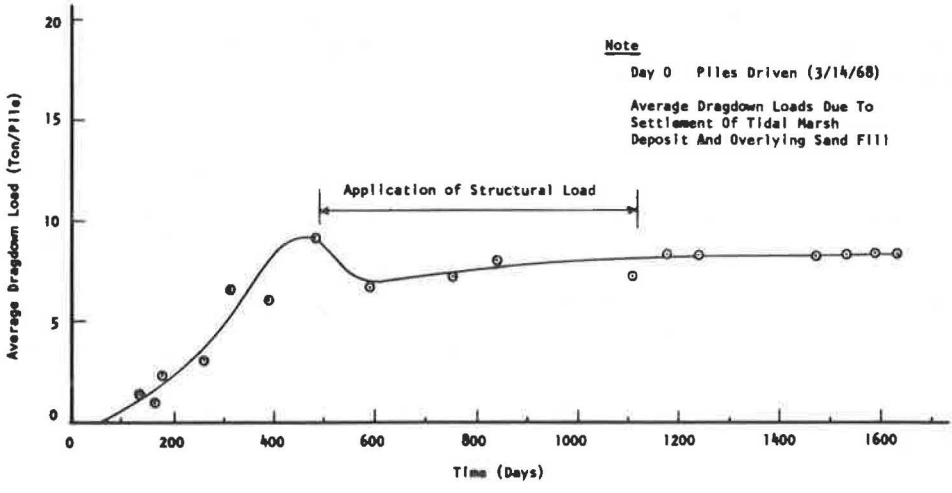

Figure 10(a). Load transfer in vertical and batter piles, group 2.

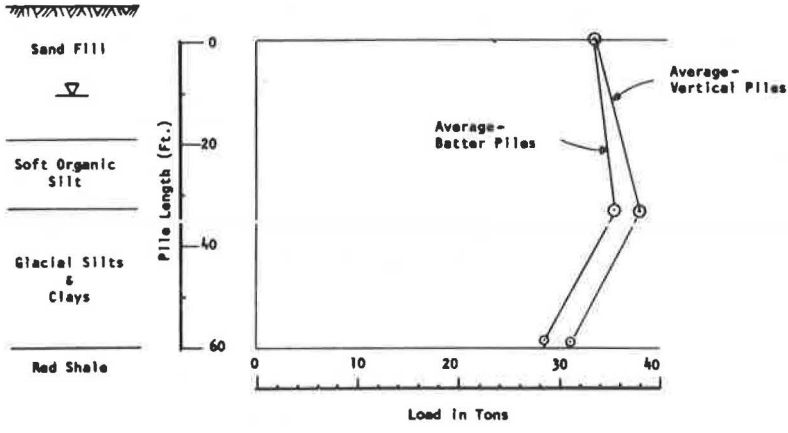

Figure 10(b). Load transfer in sand-drained and non-sand-drained areas, group 3.

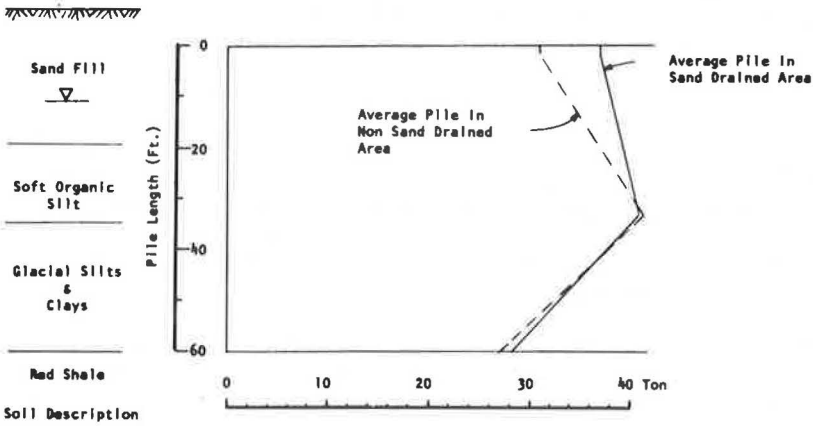

in dragdown loading followed by a very gradual increase; 1,600 days after pile installation the drag load averaged 8.2 tons/pile (73 kN/pile).

For pile groups 2 and 3, the construction of the roadway structure started shortly after installation of the piles, so there was insufficient time to develop drag loading resulting from remolding and subsequent reconsolidation of the cohesive soils. Load transfer for pile groups 2 and 3 is shown in Figure 10.

Very little difference was observed between dragdown loading on vertical piles when compared to batter piles. The design of the foundations had anticipated that batter piles would be subjected to larger dragdown loads due to the weight of overlying soil acting on that portion of the batter pile that is within the zone of soil settlement. However, ground settlements to date have been small and apparently not sufficient to cause additional dragdown loading.

A comparison of the measured post-construction dragdown load with calculated values is given in Table 1. There are two observations of particular significance:

1. There is good agreement between measured and computed values for piles in the non-sand-drained areas, and
2. In areas treated by sand drains, the drag forces were reduced and ranged from only 22 percent to 39 percent of calculated values. This indicates that ground settlements in sand-drained areas were less than the threshold values needed for the full development of dragdown forces.

Positive Load Transfer

It is particularly interesting to note the differences in positive load transfer between foundation piles and the test pile. For foundation piles, the positive load transfer within the glacial soils was far less than that measured in the test pile.

Measurements of load transfer for the test pile are shown in Figure 5. A substantial amount of the applied load is carried by friction. As load was applied, the magnitude of skin friction increased gradually at a decreasing rate. The average value of mobilized skin friction was 810 psf (38.8 kPa) for the 40-ton (356-kN) loading and 1,520 psf (72.8 kPa) for the 160-ton (1423-kN) loading.

As the magnitude of mobilized skin friction approached a constant value, an increasing proportion of each additional increment of load was transferred to the pile tip. In the high load range most of the load applied is supported by point resistance.

Positive skin friction in the foundation piles was relatively constant with depth and much smaller than that observed in the test pile. A comparison of these data is shown in Table 1 and Figure 11. For foundation piles, positive skin friction mobilized within the glacial soils was only 16 to 42 percent of that measured in the test pile at comparable applied loads, and in terms of peak skin friction the range was only 10 to 26 percent of that mobilized by the test pile. Due to reduced positive skin friction and the superimposed dragdown loads, a very high proportion of the applied load reached the tip of the foundation piles. For group 2, which is subjected to only minor dragdown loading, 84 percent of the applied load reached the pile tip.

Transient Load Test

Pile group 1 supporting the arrival roadway was selected to measure changes in load transfer resulting from the superposition of transient loading on piles subjected to dragdown loading. Two trucks were positioned to produce column loads of 20, 35, and 50 tons (178, 311, and 445 kN). All meters were read when the trucks were in a parked position.

As shown in Figure 11, most of the applied load was carried in friction. The distribution of load transfer was similar to that observed in the test pile. The application of the 50-ton (445-kN) transient load reduced the dragdown loading acting on the cap from 38 tons to 15 tons (338 kN to 133 kN), a 60 percent reduction. Figure 12 shows the reduction in dragdown loading as a function of the applied transient load. The total test load of 50 tons (445 kN) was cycled 15 times with no apparent change in the distribution of load transfer.

Table 1. Summary of load transfer characteristictics, test pile and pile groups.

Pile Group	Point Load Percent Butt Load	Average Positive Skin Friction, psf (β-Values)	Measured Post-Constr. Drag/Pile, tons	Calculated Dragdown Load, tons[a]
1	84	265 (β = 0.13)	8.2[b]	6.5
2	84	170 (β = 0.05)	3[c]	13.5
3	87	300 (β = 0.08)	5.5[c]	13.5
			15.5[b]	
Test pile[d]	25	940 (β = 0.31)		
Test pile[e]	61	1,520 (β = 0.50)		

[a]Dragdown loads calculated with β = 0.4 for sand fill, β = 0.3 for organic silt.
[b]Piles located in non-sand-drained area.
[c]Piles located in sand-drained area.
[d]50-ton load.
[e]160-ton load.

Figure 11. Comparison of load transfer, test piles versus foundation piles.

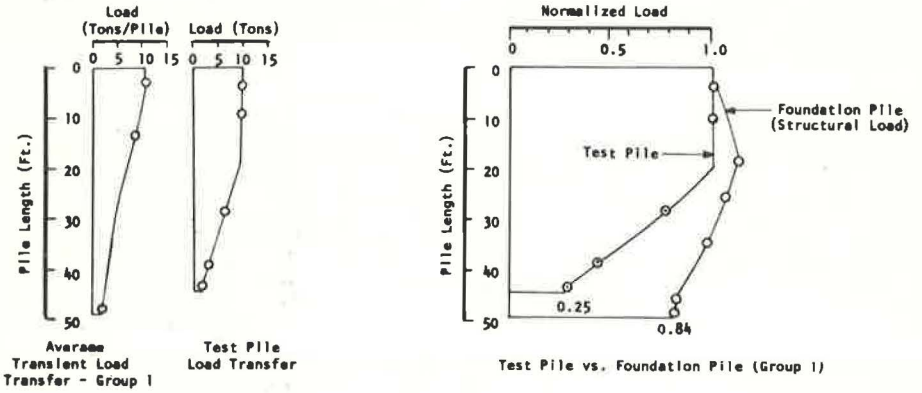

Figure 12. Dragdown load during transient load test, group 1.

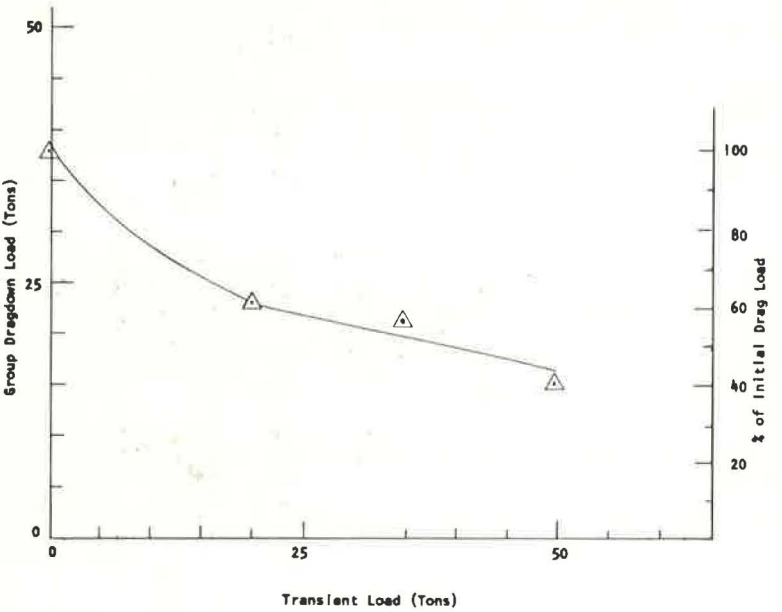

Miscellaneous

Soil stress meters located in the soil beneath pile caps recorded small compressive stresses equivalent only to the weight of the pile cap, verifying that column loads were fully supported by the piling. For pile group 1, soil stresses averaged 3.5 psi (24.2 kPa) in the period of construction (2 years) as compared to 3.6 psi (24.8 kPa) representing the weight of the cap only.

CONCLUSIONS

The conclusions of this testing program are necessarily limited by the particular geologic conditions of the site. Comparisons are difficult because of the lack of previous data concerning long-term behavior of pile groups, and there are only a few examples in the literature of measurements of dragdown loading in areas of small ground settlements. This study is in essence a case history; however, some of the following conclusions may have general application to end-bearing piles driven through cohesive soils:

1. Load transfer in foundation piles differed significantly from that measured in test piles. Values of mobilized positive skin friction in the foundation piles ranged from 16 percent to 42 percent of those measured in the test pile at comparable applied butt loads and were only 10 percent to 26 percent of measured test pile values for peak skin friction. Due to dragdown loading and reduced positive skin friction, most of the load applied to the foundation piles reached the pile tips.
2. Dragdown loading resulted from two causes: (a) remolding of the cohesive soils because of pile driving and the subsequent reconsolidation of the soils, and (b) secondary compression of the tidal marsh deposit.
3. The application of structural loads obliterated the effects of dragdown loading due to remolding, but it appears that this effect contributed to the reduction in positive skin friction developed in the glacial lake deposit.
4. For pile groups located in non-sand-drained areas, the measured dragdown loading agreed closely with computed values for ultimate dragdown. However, for pile groups in sand-drained areas, the measured dragdown loads were considerably less than computed values. Dragdown loads on piles battered 1 on 7.5 were no greater than those on vertical piles; however, ground settlements to date have been very small.
5. The application of transient loading of 50 tons (445 kN) on pile group 1 reduced the dragdown loading due to compression of the tidal marsh deposit from 38 tons to 15 tons (338 kN to 133 kN), a 60 percent reduction. Fifteen applications of load cycling did not alter the load transfer behavior.

REFERENCES

1. Ali, I., and Kesler, C. E. Creep in Concrete With and Without Exchange of Moisture With the Environment. Theoretical and Applied Mechanics Report No. 641, Dept. of Theoretical and Applied Mechanics, Univ. of Illinois, 1963.
2. Bjerrum, L., Johannessen, I. J., and Eide, O. Reduction of Negative Skin Friction on Steel Piles to Rock. Proc. 7th Int. Conf. on Soil Mechanics and Foundation Engineering, Mexico City, 1969, Vol. 2, pp. 27-34.
3. Bozozuk, M., and Labrecque, A. Downdrag Measurements on 270-Ft. Composite Piles. Performance of Deep Foundations, ASTM Spec. Publ. 444, 1966, pp. 15-40.
4. Bozozuk, M. Downdrag Measurements on a 160-Ft. Floating Pipe Test Pile in Marine Clay. Canadian Geotechnical Jour., Vol. 9, 1972, p. 127.
5. Broms, B. B. Design of Pile Groups With Respect to Negative Skin Friction. Swedish Geotechnical Institute, Reprints and Prelim. Repts. 42, 1971, 2 pp.
6. Burland, J. Shaft Friction of Piles in Clay: A Simple Fundamental Approach. Ground Engineering, Vol. 6, No. 3, May 1973, pp. 30-42.
7. Coyle, H. M., and Reese, L. C. Load Transfer for Axially Loaded Piles in Clay. Jour. Soil Mechanics and Foundations Div., ASCE, Vol. 92, No. SM2, March 1966, pp. 1-26.

8. D'Appolonia, E., and Hribar, J. A. Load Transfer in a Step-Taper Pile. Jour. Soil Mechanics and Foundations Div., ASCE, Vol. 89, No. SM6, Nov. 1963, pp. 57-77.
9. D'Appolonia, E., and Romualdi, J. P. Load Transfer in End Bearing Steel H-Piles. Jour. Soil Mechanics and Foundations Div., ASCE, Vol. 89, No. SM2, March 1963, pp. 1-25.
10. Endo, M., Minou, A., Kawasaki, T., and Shibata, T. Negative Skin Friction Acting on Steel Pipe Piles in Clay. Proc. 7th Int. Conf. on Soil Mechanics and Foundation Engineering, Mexico City, 1969, Vol. 2, pp. 85-92.
11. Fellenius, B. H., and Broms, B. B. Negative Skin Friction for Long Piles Driven in Clay. Proc. 7th Int. Conf. on Soil Mechanics and Foundation Engineering, Mexico City, 1969, Vol. 2, pp. 93-98.
12. Fellenius, B. H. Negative Skin Friction on Long Piles Driven in Clay. Swedish Geotechnical Institute, Proc. No. 25, 1971.
13. Fellenius, B. H. Down-Drag on Piles in Clay Due to Negative Skin Friction. Canadian Geotechnical Jour., Vol. 9, 1972, pp. 323-337.
14. Garlanger, J. E., et al. Prediction of the Downdrag Load at Cutler Circle Bridge. Symposium on Downdrag of Piles, M.I.T. Department of Civil Engineering, 1973.
15. Johannessen, I. J., and Bjerrum, L. Measurement of the Compression of a Steel Pile to Rock Due to Settlement of the Surrounding Clay. Proc. 6th Int. Conf. on Soil Mechanics and Foundation Engineering, Montreal, 1965, Vol. 2, pp. 261-264.
16. Kesler, C. E., and Wallo, E. M. Prediction of Creep in Structural Concrete. Engineering Experimental Station Bull. 498, Univ. of Illinois.
17. Mansur, C. J., and Kaufman, R. I. Pile Load Tests, Low Sill Structure, Old River, Louisiana. Trans. ASCE, Vol. 123, 1958, pp. 715-743.
18. Raphael, J. M., and Carlson, R. W. Measurement of Structural Action in Dams. J. J. Gillick and Co., Berkeley, California, 1956.
19. Schlitt, H. G. Group Pile Loads in Plastic Soils. Proc. Highway Research Board, Vol. 31, 1952, pp. 62-81.
20. Sherman, W. C. Instrumented Pile Tests in a Stiff Clay. Proc. 7th Int. Conf. on Soil Mechanics and Foundation Engineering, Mexico City, 1969, Vol. 2, pp. 227-232.

MEASUREMENT OF PILE DOWNDRAG BENEATH A BRIDGE ABUTMENT

John E. Garlanger, Ardaman and Associates, Inc., Orlando, Florida*

Steel H piles for a bridge abutment were driven through 25 ft (7.6 m) of fill, 13 ft (4.0 m) of sand, and 50 ft (15.2 m) of soft clay into a dense glacial till. Seventeen years after the bridge was completed, the differential settlement between the bridge deck and the approach fill had exceeded 18 in. To determine the amount of downdrag loading carried by the piles, which were designed to carry a total loading of 60 tons (530 kN) per pile, measurements of strain and movement were made at the top of one of the piles as the pile was cut free from the abutment and as the skin friction forces were removed through a combination of excavation and electro-osmosis. The measured vertical load and moment at the top of the pile were 114 tons (1015 kN) and 1,140 in.-kips (130 kN-m) respectively. The total vertical load at the top of the glacial till, back-figured from the movement at the top of the pile, was 230 tons (2050 kN), indicating over 100 tons (890 kN) of pile downdrag.

•AS part of a study conducted at the Massachusetts Institute of Technology to develop better methods for predicting downdrag forces on piles, direct and indirect measurements were made of the loads acting on one of the piles supporting an existing bridge abutment. The magnitude of settlement between the approach fill and the abutments indicated that full negative skin friction should have developed along at least 70 ft (21 m) of the piles supporting the abutments. Because none of the piles had been instrumented prior to driving, it was not possible to measure the downdrag loads directly. These loads had to be back-figured from measurements of movement at the top of one of the piles after a section of the pile was cut out and the negative skin friction forces removed.

THE CUTLER CIRCLE BRIDGE

The measurements of pile downdrag were made beneath the west abutment of the Cutler Circle Bridge, a simply supported, 3-span overpass structure carrying the proposed extension of Interstate 95 over State Route 60 near Revere, Massachusetts. A 25-ft-high (7.6 m) approach fill, constructed over 13 ft (4.0 m) of sand and 50 ft (15.2 m) of soft clay, was placed before construction of the abutments began. A cross section through the embankment and soil profile is shown in Figure 1.

The designers of the bridge predicted that the settlement of the approach fill after 50 years would exceed 3 ft (91 cm). However, they did not "... anticipate any damage to the abutment of the bridge since [they had] coped with the tendency of a drag load on the supporting piles by providing extra piles." Some consideration had been given to surcharging the embankment and foundation, but time-settlement calculations indicated that insufficient time was available for the surcharge to be effective. In addition, stability calculations indicated that the factor of safety, even without the surcharge, was only 1.2 to 1.3. Lightweight fill had been ruled out as being too expensive.

*This paper is based on work performed while the author was Assistant Professor of Civil Engineering at Massachusetts Institute of Technology.

The construction proceeded as follows:

August 1956 to November 1957	Fill placed and compacted
February 1957	Piles for abutments driven
March 1957 to June 1957	Abutments formed and poured
June 1957 to July 1957	Beams for bridge superstructure placed
August 1957	Concrete bridge deck poured
January 1958	Level survey along centerline of completed bridge taken

The available evidence indicates that the piles (14BP73 H-sections) were driven to at least 7 blows/in. (3 blows/cm) for the last inch with a Vulcan No. 1 pile hammer. The specified design load was 60 tons (530 kN). Because of the extra piles provided to carry the downdrag load, the average load per pile computed from the weight of the bridge deck and the abutments is 40 tons (350 kN).

Settlement data obtained from the Massachusetts Department of Public Works for a station on the bridge deck and a nearby station on the approach fill are plotted in Figure 2. At the abutment, which has settled less than ½ in. (1.2 cm), the embankment has settled approximately 18 in. (46 cm).

The large differential settlement is apparent both behind and in front of the abutment (Figures 3 and 4). There is also visual evidence that the top of the abutment has rotated about the rear piles toward the fill.

To determine the existing soil and groundwater conditions beneath the abutment, a subsurface investigation was made in May 1972. A summary of the boring logs, the vane shear test results, and the piezometer data is shown in Figure 5 along with the results of unconsolidated-undrained (UU) triaxial tests performed on 5-in. fixed-piston samples. The piezometer data indicate that consolidation of the clay is essentially complete.

INSTRUMENTATION

In late November 1972, a sheeted and braced excavation 5 × 7 ft (1.5 × 2.1 m) in plan was made behind the west abutment of the bridge to expose one of the supporting piles. The excavation also exposed an 18-in. (46-cm) gap between the pile cap and underlying fill into which a person could crawl to examine the remaining piles. During the examination of the piles it was observed that two of the batter piles in the front row had been pulled out of the pile cap (Figure 6), further confirming the suspicion that the piles were subjected to large downdrag loads.

Because none of the piles had been instrumented before driving, it was not possible to measure the downdrag loads directly. The only measurements possible were gross movement and strain at the top of the piles after releasing forces from the pile. The forces acting on the pile are the structural load transmitted by the pile cap, the downdrag forces created by the fill, sand, and clay, and the friction and end bearing resistance in the bearing layer. To isolate each component for separate evaluation, the following measurements were made:

1. Horizontal and vertical movement and strain of a point at the top of the pile upon cutting it free from the pile cap;
2. Horizontal and vertical movement of the point after release of the friction in the sand and gravel layers;
3. Horizontal and vertical movement of the point after release of the friction in the clay layer; and
4. The load required to jack the pile back to its original position.

Four Geonor vibrating wire strain gauges and four BLH weldable electrical resistance strain gauges were installed on the pile before it was cut, one each on both flanges and both sides of the web.

Vertical and horizontal deformations were monitored using the dial indicator system shown in Figure 7. The measuring platform and plates suspended from the abutment

Figure 1. Soil profile at Cutler Circle Bridge.

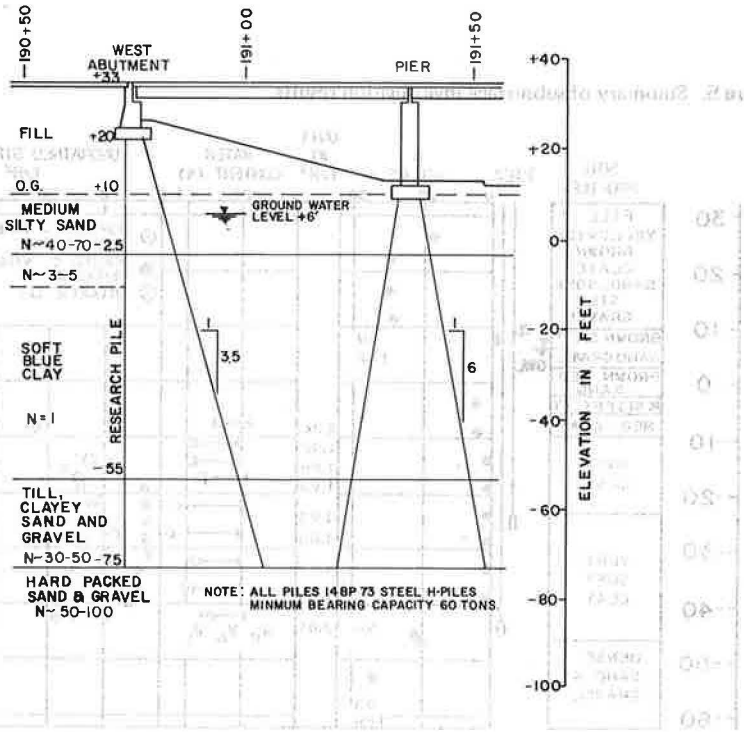

Figure 2. Settlement curves for bridge abutment and approach fill.

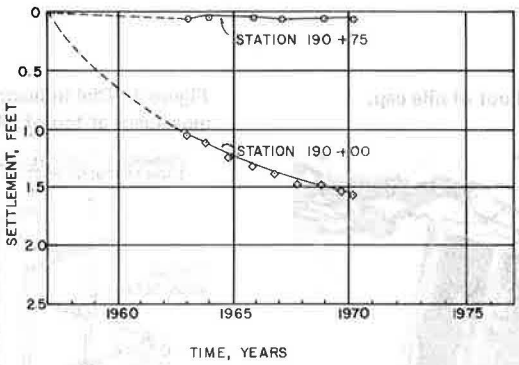

Figure 3. Differential settlement at wing wall.

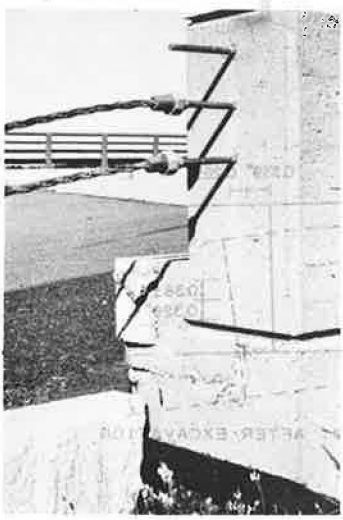

Figure 4. Breakup of slope protection beneath bridge deck.

Figure 5. Summary of subsurface investigation results.

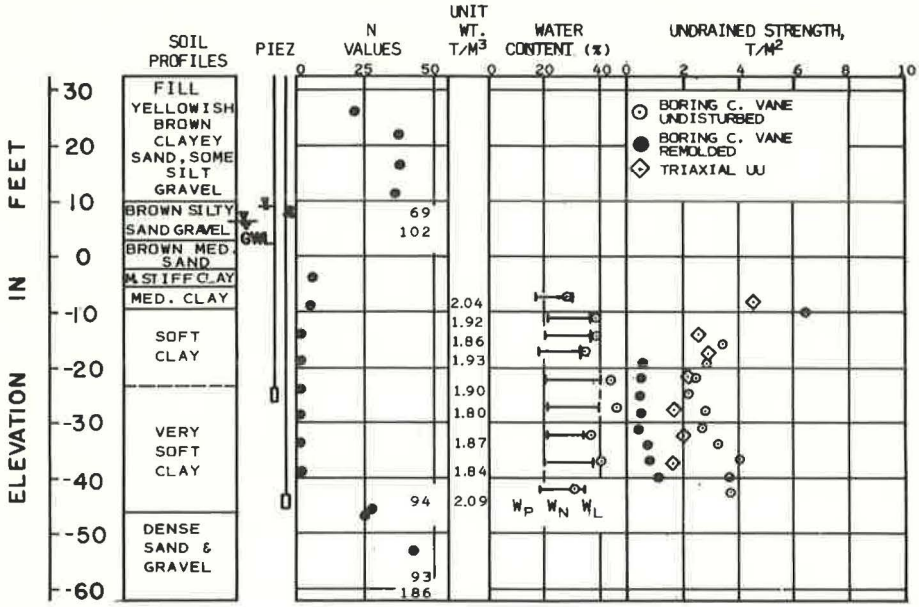

Figure 6. Batter piles pulled out of pile cap.

Figure 7. Dial indicator setup to measure movement at top of pile.

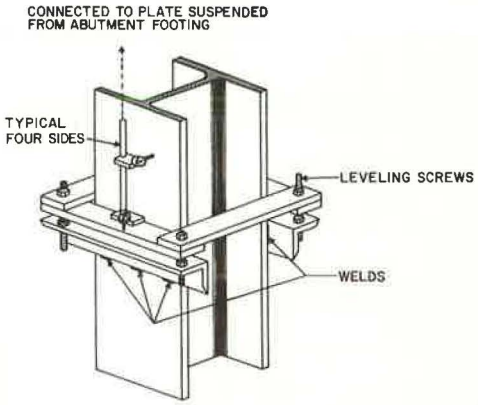

Figure 8. Movement of pile in horizontal plane after cutting and after excavating sand and gravel.

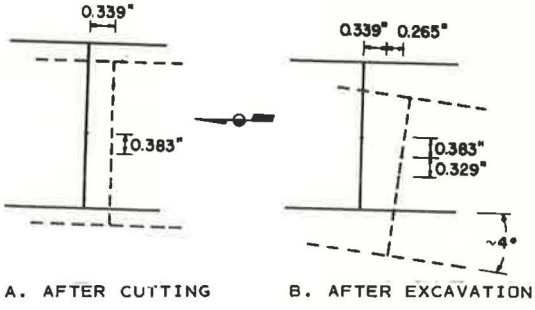

could be leveled so that initially the platform would be horizontal and the rods plumb. With this system, it was possible to correct the measured vertical movement for any false movements that might be introduced should the pile tilt, twist, or translate upon cutting. Thus the corrected vertical movement, provided that the pile was essentially vertical throughout its length, represents only the axial extension of the pile plus any rebound of the pile tip. If the pile was not vertical throughout its length, the corrected vertical movement would be less than the axial extension of the pile, and any pile loading deduced from that movement would be less than the actual loading.

As a precaution, the vertical movement was also obtained by measuring the distance between the two reference points on the pile, one above and one below the section that was cut out. In addition, the movement of the abutment during cutting was monitored.

MEASUREMENTS

Pile Cutting

To maintain a concentric load in the pile, cutting began with both flanges and then proceeded in toward the center of the web. The elastic deflection resulting from the release of bending moments in the pile after cutting is shown in Figure 8a. The vertical movement of the pile after cutting was 0.40 in. (10.2 mm) up.

The axial load and bending moment acting on the pile, computed from the strain gauge data (agreement between the two strain gauge systems was with 10 percent), were 114 tons (1015 kN) and 1,140 in.-kips (129 kN-m) respectively. The measured axial load is almost twice the design load, and the maximum fiber stress of 22 ksi (152 MPa) as a result of this bending moment is almost twice that allowed by the Boston building code.

Excavation of the Sand and Gravel

Above the water table, the sand and gravel were removed by hand in a 4 × 4-ft (1.2 × 1.2-m) caisson-type excavation. Below the water table, the sand was not removed but was placed in suspension by jetting down around the pile using a thick bentonite slurry. The deflected position of the pile after excavation of the sand and gravel is shown in Figure 8b. As shown in the figure, the horizontal movement of the pile was accompanied by a rotation of the pile about its own axis. The vertical movement of the pile plotted against depth of excavation is shown in Figure 9. Also shown are the corresponding N values at various depths. The total vertical movement was 0.097 in. (2.46 mm) up.

Electro-Osmosis

To remove the negative skin friction in the clay layer, a direct electric current was applied between the test pile (cathode) and a neighboring pile (anode) to induce large pore pressures at the face of the test pile. The results of the electro-osmosis are shown in Figure 10. The pile moved up a total of 0.157 in. (3.98 mm) during electro-osmosis.

Pile Reloading

With the electro-osmosis still applied, the pile was loaded with a hydraulic jack up to 220 tons (1958 kN) in 25-ton (222-kN) increments. The load at the top of the pile was measured with a calibrated electrical resistance load cell. The results of the reloading are shown in Figure 11. It was not possible to test load the pile to failure because of the danger of buckling the 20 ft (6 m) of unsupported pile left freestanding above the clay strata by the excavation of the sand and gravel.

Additional Measurements

During the research period the temperature in the work area remained around 30 F ±5 F, despite a fluctuation outside from 10 to 50 F. The temperature of the pile, as measured by a thermistor attached to the pile, varied even less.

Pore pressures at mid-depth of the clay were monitored throughout the research period. No significant pore pressure changes were noted, even during the electro-osmosis.

Figure 9. Vertical movement of pile during excavation of sand and gravel.

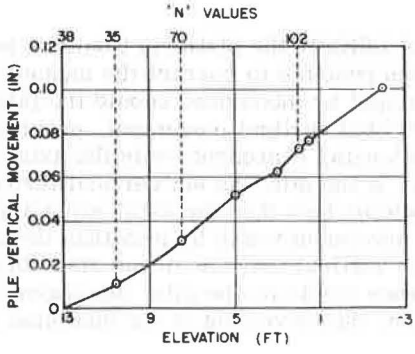

Figure 10. Vertical movement of pile during electro-osmosis.

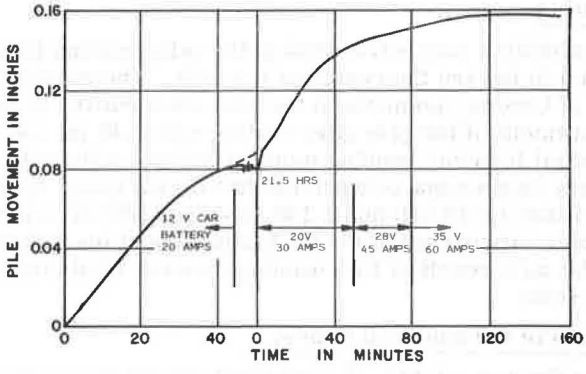

Figure 11. Results of pile load test.

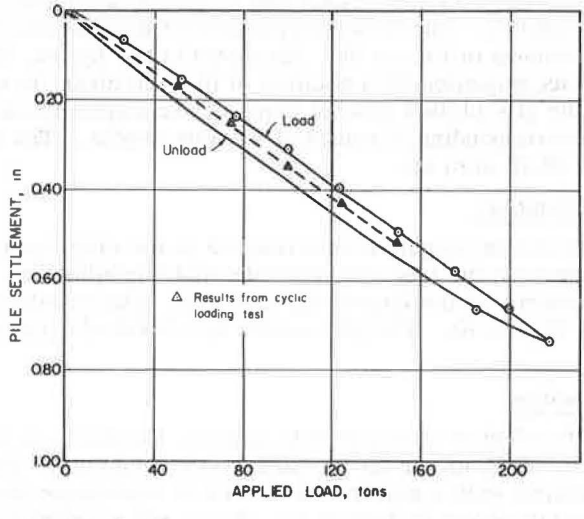

Table 1. Summary of vertical movement at various stages of load test.

	Movement of Top of Pile, in.	
Stage of Test	Predicted Range (average)	Measured
After cutting	0.060-0.755 (0.234)	0.401
After excavating sand	0.048-0.240 (0.112)	0.097
After electro-osmosis	0.080-0.180 (0.124)	0.157

ANALYSIS

Before the pile was exposed and the measurements taken, predictions were made of the movement of the pile during the various stages of the test by six foundation engineers practicing both in the United States and abroad (3). The range in predicted movement and the measured movements are given in Table 1. Although there was a fairly large range in the predicted movements, there was general agreement among the predictors on how the downdrag forces and the related movements could be computed. For example, all but one of the predictors calculated the negative skin friction acting along the soil-pile interface using some form of the equation $f_s = \beta \bar{p}_o$, where f_s is the negative skin friction, β is a constant depending on the soil conditions, and $\bar{p}_o$ is the effective overburden pressure.

Using the same procedures set forth by the six predictors, it was possible (5), by varying the parameter β and by selecting reasonable values for the positive skin friction, f_s, and the coefficient of subgrade reaction in the bearing layer, k_s, to back-figure a number of load-depth curves that fit the observed data. For example, the load-depth curves in Figure 12 yield movements that are within 3 percent of those measured during the field test.

These curves and the corresponding movements were obtained as follows: First, the effective overburden pressure-depth relationship ($\bar{p}_o$ - z) was obtained by subtracting the measured pore water pressures from the sum of the original geostatic stresses and the distributed stresses induced by the embankment loading (4, 7); second, using the assumed values of β given in the figure, the negative skin friction values were computed and plotted as a function of depth; third, the load-depth curves (P_z - z) for depths above the bearing stratum at various stages of the test were determined by integrating the skin friction-depth curves with a planimeter and multiplying the integral by the outer box perimeter of the pile, i.e.,

$$P_z = \text{perimeter} \int_0^z p_o dz$$

fourth, the load-depth curves for depths within the bearing stratum were obtained using the positive skin friction values given in the figure; fifth, the elastic extension of the pile for the various stages of the test was determined by dividing the planimetered area between the load-depth curves corresponding to those stages by the cross-sectional area and the modulus of elasticity of the pile, i.e.,

$$\delta_E = 1/AE \int_0^L P_z dz$$

and sixth, the rebound of the pile tip, computed by dividing the change in bearing pressure by the selected value of the coefficient of subgrade reaction, was added to the elastic extension of the pile to obtain the total movement, δ_T.

In all, a total of three solutions among the more than 20 trials analyzed gave movements close to those measured in the field test. In these three solutions β for the sand varied from 0.30 to 0.40, β for the clay varied from 0.20 to 0.25, the positive skin friction in the bearing stratum varied from 1.25 to 1.40 tsf (120 to 135 kPa), and the coefficient of subgrade reaction varied between 4,300 and 5,500 t/ft^3 (1370 and 1750 mN/m^3). The total load in the pile at the top of the bearing stratum varied from 215 to 245 tons (1900 to 2170 kN).

The values of β back-figured from the observed movements are in good agreement with data obtained by other investigators (1, 2), as are the positive skin friction values for the bearing stratum (6). The values of the coefficient of subgrade reaction are higher than those measured by Thompson and Brierly (8) for a compression pile in another glacial till in the Boston area, but a higher value would be expected for pile rebound because the plastic settlements that occur during compression do not occur during rebound.

Figure 12. Load-depth curves in pile at various stages of test.

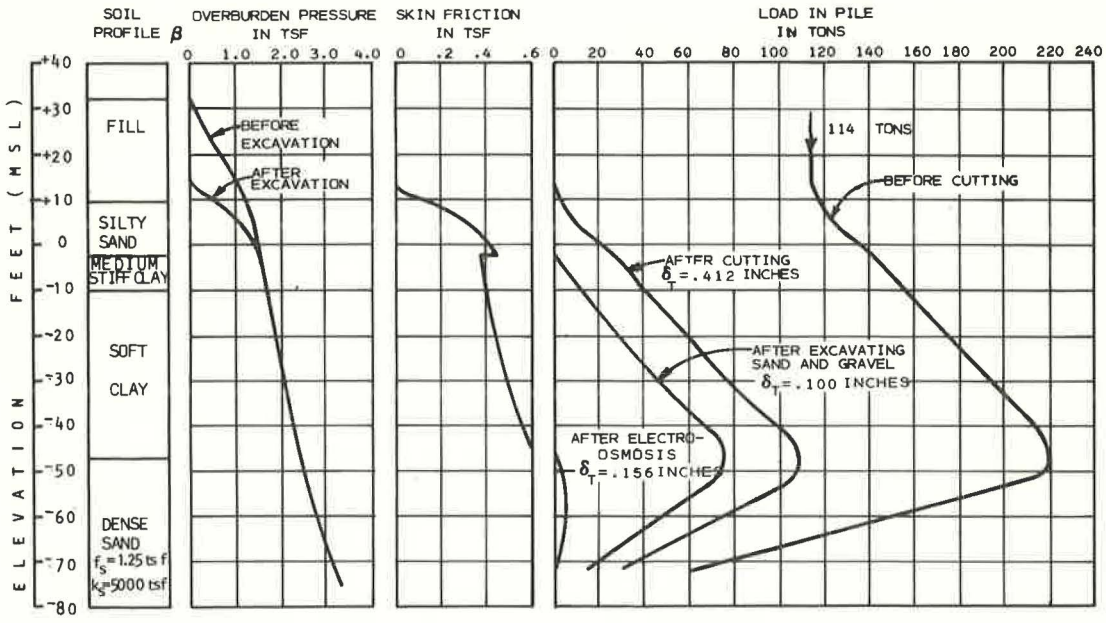

Figure 13. Procedure for determining downdrag load from pile load test.

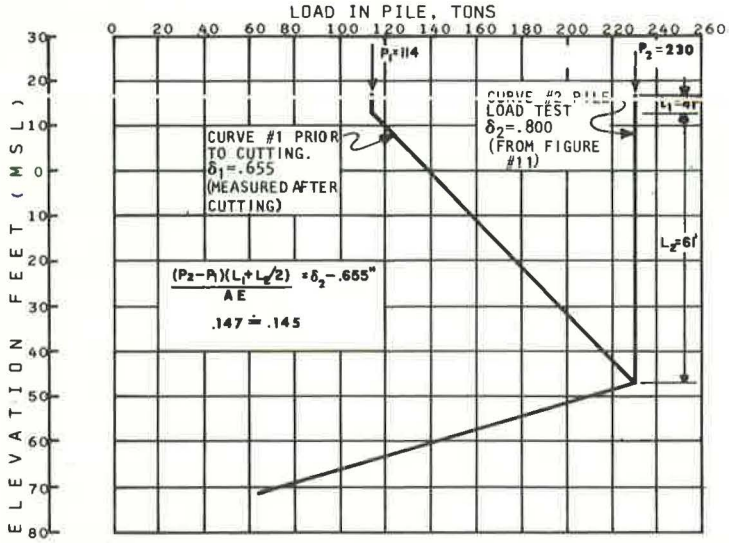

BY TRIAL AND ERROR
ELASTIC MOVEMENT CORRESPONDING TO AREA BETWEEN CURVES #1 AND #2 MUST EQUAL MEASURED MOVEMENT CORRESPONDING TO CURVE #2 MINUS MEASURED MOVEMENT CORRESPONDING TO CURVE #1

The total load in the pile at the top of the bearing stratum was also back-figured from the results of the pile load test (Figure 11). The procedure, which assumed only that the downdrag load in the pile increases linearly with depth, is shown in Figure 13. Using this procedure, the total load in the pile at the neutral point prior to cutting the pile was determined to be 230 tons (2050 kN). This value, along with the values determined using the previous analysis, indicate that the downdrag load in the pile was greater than 100 tons (890 kN).

CONCLUSIONS

1. The total downdrag load carried by the test pile was at least 100 tons (890 kN) and possibly as much as 130 tons (1160 kN).
2. The load and moment transmitted by the abutment to the top of the pile were 114 tons (1015 kN) and 1,140 in.-kips (129 kN-m) respectively.
3. Even though at least one of the piles was carrying almost four times the design load and several of the piles had pulled out of the pile cap, the abutment had settled less than ½ in. and appeared to be performing satisfactorily.
4. Downdrag loading can be predicted reasonably well using the equation $f_s = \beta\ p_o$ to determine the maximum negative skin friction and using empirically determined parameters for the soil constant β. Values of β equal to 0.20 to 0.25 for clay and 0.35 to 0.50 for sand appear to be reasonably conservative.
5. Not enough is known about the interaction between pile and pile cap to predict the load and movement transmitted from the pile cap to the pile. More field measurements in this area are needed.

ACKNOWLEDGMENTS

The research described in this paper was performed at the Massachusetts Institute of Technology under the general direction of T. W. Lambe. Other major participants in the research were L. A. Wolfskill and Samuel A. Leifer. The research project was sponsored by the Massachusetts Department of Public Works and the Federal Highway Administration. The author wishes to express his appreciation to those mentioned and to all of the other staff in the M.I.T. Department of Civil Engineering who contributed to the research. The opinions, findings, and conclusions expressed are those of the author and not necessarily those of the Massachusetts Department of Public Works or the Federal Highway Administration.

REFERENCES

1. Bjerrum, L., Johannessen, I. J., and Eide, O. Reduction of Negative Skin Friction on Steel Piles to Rock. Proc. 7th Int. Conf. on Soil Mechanics and Foundation Engineering, Mexico City, 1969, Vol. 2, pp. 27-34.
2. Endo, M., Minou, A., Kawasaki, T., and Shibata, T. Negative Skin Friction Acting on Steel Pipe Piles in Clay. Proc. 7th Int. Conf. on Soil Mechanics and Foundation Engineering, Mexico City, 1969, Vol. 2, pp. 85-92.
3. Garlanger, J. E., D'Appolonia, D. J., Davis, E. H., Esrig, M. I., Focht, J., and Perez-Guerra, G. Prediction of the Downdrag Load at Cutler Circle Bridge. Symposium on Downdrag of Piles, M.I.T. Department of Civil Engineering, 1973.
4. Gray, H., and Hooks, I. J. Charts Facilitate Determination of Stresses Under Loaded Areas. Civil Engineering, ASCE, June 1948.
5. Leifer, S. A. Field Evaluation of Negative Skin Friction Forces at a Bridge Abutment. Masters thesis, M.I.T. Department of Civil Engineering, 1973.
6. Mansur, C. J., and Kaufman, R. I. Pile Load Tests, Low Sill Structure, Old River, Louisiana. Trans. ASCE, Vol. 123, 1958, pp. 715-743.
7. Osterberg, J. O. Influence Values for Vertical Stresses in a Semi-Infinite Mass Due to an Embankment Loading. Proc. 4th Int. Conf. on Soil Mechanics and Foundation Engineering, London, 1957.
8. Thompson, D. E., and Brierly, G. S. Load Transfer in Long Pipe Piles in Clay. To be published.

FIELD PERFORMANCE OF DRIVEN ENLARGED-TIP PILES

Stanely Merjan, Underpinning and Foundation Associates, Inc., Long Island City, New York

Recent experience is presented on the performance of piles with a precast enlarged tip in a variety of soil profiles in the New York City area. The design, construction, and use of one version of enlarged-tip pile are described, along with the conditions under which it may be used to advantage. Although more costly than conventional piles, enlarged-tip piles are used economically where they are significantly shorter than conventional piles or of higher capacity, thus allowing pile substitutions of one for two or one for three. Wave equation analysis of pile driving has made it possible to predict very closely the appropriate hammer size, cushioning material, and driving resistance necessary to produce specific pile capacities with various combinations of pile tips and stems. Soil bearing capacity theory helps to explain why field performance of enlarged-tip piles is markedly superior to that of conventional piles, especially in loose granular soils. Case histories illustrate the range of conditions under which these piles have proved effective.

•CERTAIN precast concrete bulb piles have been shown to be advantageous in Europe, particularly in soil profiles where piles of conventional prismatic form must extend to great depths to reach bearing (3). Franki-type piles (labeled PIFs and bulb piles in the United States) are also enlarged-tip piles but are cast-in-place rather than precast. Precast enlarged-tip piles have heretofore been little used in the United States; however, during the past 3 years considerable experience has been obtained in the New York City area in a variety of soil profiles with a pile having a precast enlarged tip. The design, construction, and field performance of the TPT (tapered pile tip) pile (1) are described here along with the conditions under which it may be used to advantage.

IDEALIZED SOIL PROFILES

Three generalized soil profiles in which TPT piles are useful are shown in Figure 1. A deep deposit of loose sand is shown in Figure 1a. Such a deposit occurs in Brooklyn, where conventional piles of 50-ton capacity or more must be driven to depths of 50 to 100 ft or more to reach bearing. However, both TPT piles and Franki-type piles have been driven for capacities of 100 tons or more at less than half the depth of conventional piles.

A 3-layer soil system is shown in Figure 1b. The overlying fill may be strong and incompressible, but the underlying compressible layer dictates that foundations be carried to or through the third layer, the loose sand. Such a condition occurs in Rockaway (Queens), where a strong upper layer is predrilled. Conventional piles achieved 60-ton capacities at a depth of 70 ft, whereas TPT piles achieved capacities of 150 tons at a depth of 50 ft.

Another 3-layer soil system is shown in Figure 1c. The upper layer is too weak and compressible to function as a bearing layer; thus, bearing must be obtained in the underlying sand or stiff clay strata. Figure 1c shows conditions in a portion of Queens. In one case, 50-ton conventional piles drove through the sand layer to depths of 90 to 100 ft, whereas a TPT pile achieved 50-ton bearing in the sand at a depth of 58 ft.

The significant feature of these idealized conditions is that a TPT pile was able to achieve bearing in a suitable granular soil layer with relatively shallow penetration, whereas conventional piles were much deeper. Further, the bearing capacity achieved with a TPT pile can be double or triple that of normal conventional piles.

From the economic standpoint, the TPT pile is more costly per unit of length than conventional piles. As a consequence, the conditions under which TPT piles are economically used are where they are (a) significantly shorter than conventional piles; (b) of higher capacity, allowing pile substitutions of one for two or one for three; or (c) combinations of (a) and (b). Franki-type piles are a direct competitor for precast TPT piles. Experience to date has been that productivity, approximately double that of the Franki system, favors the TPT.

THE TPT PILE

Schematics of the TPT system are shown in Figure 2. For high load capacities, a steel pipe mandrel (Figure 2a) is used to drive a precast reinforced-concrete tip. The shaft is a corrugated shell, which is filled with concrete after driving. For low load capacities, a wood or steel pipe shaft (Figure 2b) is attached to the precast tip and then is top-driven rather than mandrel-driven. In both cases, conventional pile-driving rigs and hammers are used. TPT piles may be driven on batters and, where the shaft is to be concrete, may be internally reinforced. Thus, the only significant difference from conventional piles is the tip itself.

TPT piles are available in a variety of sizes. The sizes labeled A through E in Figure 3 have top diameters varying from 29 to 41 in. whereas the tip diameter is 6 in. smaller; the height is 60 in. Generally a 16-in. diameter socket is used for the A through E sizes, and the working load capacities have ranged to 150 tons. These piles have been driven with hammers ranging from the Vulcan 06 (19,500 ft-lb/blow) to the Vulcan 010 (32,500 ft-lb/blow).

The smaller TPTs, labeled Y, X, and W in Figure 3, have been used with creosoted timber pile stems with 8-in. tips. The timber piles are trimmed to 8 in. at the tips to fit into the socket. Pile working loads up to 30 tons have been proved to date. Hammers of up to 15,000 ft-lb/blow energy have been used for driving.

Analyses of the hammer-cushion-mandrel-TPT system have been made using the wave equation analysis of pile driving. M. T. Davisson, Professor of Civil Engineering, University of Illinois at Urbana-Champaign, has been consultant to the author on many applications of the TPT system. Dr. Davisson has been able to predict very closely the appropriate hammer size, cushioning material, and driving resistance necessary to produce specific pile capacities with various combinations of pile tips and stems. Further, the wave equation analysis provides the dynamic loads on the TPT system during driving; with this information, reinforcement for the tip can be designed on a rational basis. W. L. Gamble, Professor of Civil Engineering, University of Illinois at Urbana-Champaign, has been consultant to the author on design of reinforcement. Both conventional reinforcing steel and wire fiber reinforcement are in use; the wire fiber is presently used only in the Y and X sizes of TPT.

BEARING CAPACITY THEORY

The theoretical reasons for the effectiveness of enlarged-tip piles can be seen by inspection of the bearing capacity formula for shallow circular footings (4):

$$Q = \frac{\pi B^2}{4}(1.2\ c\ N_c) \quad \text{for cohesive soil}$$

and

$$Q = \frac{\pi B^2}{4}(\gamma\ D_f N_q + 0.3\ \gamma\ B N_\gamma) \quad \text{for granular soil}$$

where B = footing diameter. Note that for cohesive soil the ultimate load capacity Q increases directly with the bearing area ($\pi B^2/4$) and is a function of the square of tip diameter. For granular soil, however, Q increases with the square of tip diameter in the first term and the cube of tip diameter in the second term. On the assumption

Figure 1. Idealized soil profiles.

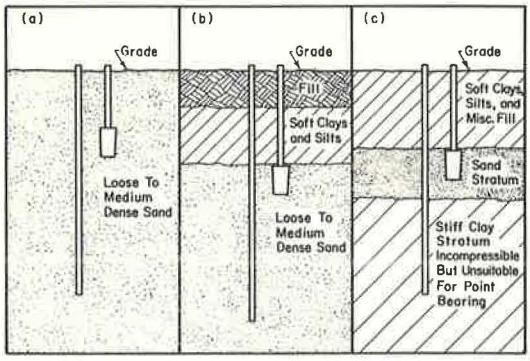

Figure 2. TPT system.

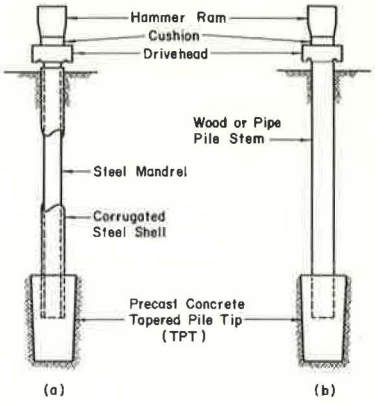

Figure 3. TPT sizes.

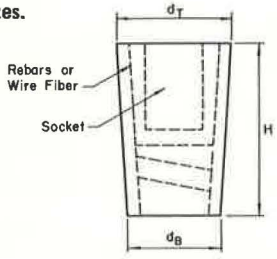

TPT Designation	d_T Inches	d_B Inches	H Inches
Y	17	13	30
X	19	15	30
W	21	17	34
A	29	23	60
B	32	26	60
C	35	29	60
D	38	32	60
E	41	35	60

Figure 4. Ultimate load versus depth, Queens.

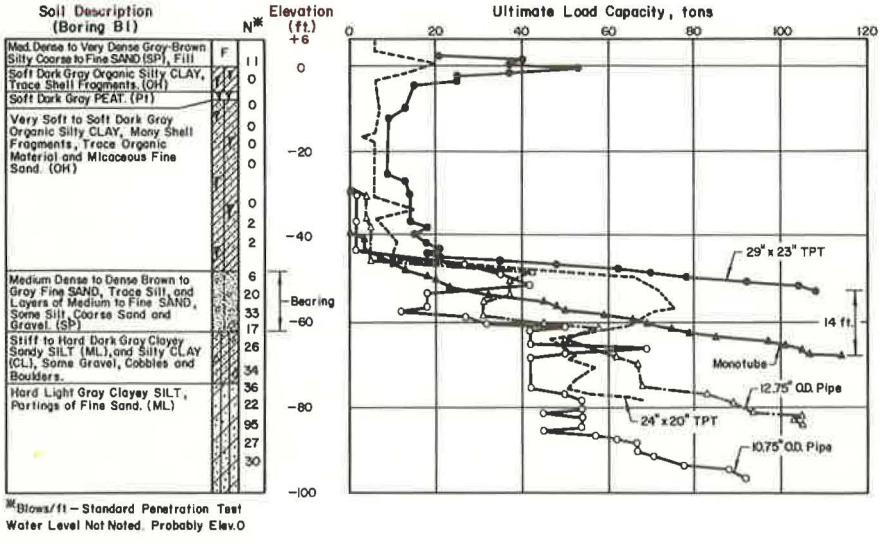

*Blows/ft – Standard Penetration Test
Water Level Not Noted. Probably Elev. 0

that deep foundations behave analogously to shallow footings, the fact that Q increases with B^3 is perhaps part of the reason for the excellent behavior of TPT piles in granular soil.

Another feature of the TPT that perhaps adds to its effectiveness is taper of the sides. Taper was shown (2) to increase the bearing capacity of conventional piles in granular soils. In addition, sand densification due to driving was shown to occur below and around enlarged pile tips (3); this raises the effective ϕ-value and the bearing capacity factors N_q and N_γ in the equation, resulting in increased load capacity. Thus, sand densification is another factor that may help explain the excellent behavior of TPT piles in granular soil. Whatever the reasons, the effectiveness of TPT piles is most pronounced in loose sands.

CASE HISTORIES

Three case histories are presented here that illustrate the range of conditions under which the TPT has proved effective.

Queens

Conventional piles of 60-ton capacity were called for in the design of a department store storage facility. The site was covered by a thin layer of fill over approximately 50 ft of peat and organic silty clay. Then a 10-ft strata of medium sand was encountered over a deep bed of hard clayey silt extending to depths beyond 100 ft. A typical boring log is shown in Figure 4.

Six piles were driven and load-tested to failure; in all cases the ultimate load agreed very closely with that predicted by the wave equation analysis of pile driving. This made it possible to convert the driving record for each pile into a plot of ultimate load capacity versus depth. Five different piles were driven in the vicinity of boring B1; their graphs of ultimate load versus depth are shown in Figure 4. Note that the 10.75-in. OD and 12.75-in. OD piles drove through the granular soil layer to depths of 103 ft and 90 ft respectively without reaching bearing of 120 tons (twice the 60-ton design load). However, an 8.5-in. OD by 16-in. OD by 20-ft monotube with a 12.75-in. OD pipe extension reached bearing at a depth of 74 ft. This illustrates the effect of pile taper in granular soils.

A W-size TPT (24 by 20 by 34 in.) also penetrated the granular soil layer but while the tip was in the granular soil achieved approximately twice the load capacity of the pipe piles. A larger A-size TPT (29 by 23 by 60 in.) was driven and achieved the required bearing at a depth of 58 ft. From Figure 4 it can be seen that the A-size TPT was the most effective of the five piles and achieved bearing approximately 14 ft shorter than the monotube pile. It is also obvious that continued driving of the A-size TPT would have produced an even higher bearing value in the granular soil.

Figure 4 shows a comparison of the five piles, illustrating the effectiveness of both pile taper and an enlarged tip.

Brooklyn

A small city (approximately 15,000 population) is under construction in Brooklyn, consisting of 54 apartment buildings varying from 11 to 20 stories each plus 20 parking garages of 5 stories each. Subsoil conditions consist of 15 ft of hydraulic and sanitary fill over 6 ft of loose organic sandy silt. Then a loose to medium deposit of sand is encountered that extends to depths of 100 ft or more. Conventional piles typically achieve 50-ton capacities at depths of approximately 50 ft in this soil deposit.

The first 19 buildings were supported by 120-ton Franki-type piles. Pile capacities were marginal and production was very low, on the order of 4 to 7 piles per day per pile-driving rig. The next 35 buildings were supported on 6,500 TPTs varying in capacity from 90 tons to 120 tons. Production was on the order of 12 to 20 piles per day per pile-driving rig, or more than double that of the Franki-type piles.

The New York City building code places very stringent requirements on high-capacity piles. Fifty-nine load tests on TPT piles were conducted under the New York code; each

test pile was loaded to twice design load and held for 96 hours. All tests were successful. The 90-ton piles were driven with the Vulcan "0" hammer (24,375 ft-lb/blow) to resistances varying from 66 to 100 blows/ft; for 100-ton piles the final driving resistance varied from 100 to 120 blows/ft. The Vulcan 010 hammer (32,500 ft-lb/blow) was used to drive the 120-ton piles to final resistances varying from 70 to 90 blows/ft. Penetrations into the granular bearing layer varied from 2 ft to 15 ft, and average pile length was approximately 26 ft.

Pile spacing varied from 54 in. to 60 in., depending on tip size. Pile cap sizes varied from 1 pile to 4 piles. Tip sizes driven within a pile cap varied in accordance with the densification produced by the driving of the initial piles in a cap. The maximum tip elevation difference permitted in any pile cap was 10 ft; where the tip difference was more than 5 ft, however, the pile was not stopped until the resistance criterion was doubled. When a pile penetrated more than 2 ft below other piles already installed in the pile cap, the short piles were redriven to assure no loss in bearing capacity. Also, an extensive redriving program was conducted to investigate the possibility of pile relaxation; redriving produced resistances generally equal to or somewhat greater than the original driving resistances, indicating no relaxation.

When the TPT pile is driven, an annular space may remain around the pile stem caused by the penetration of the larger base. Usually this space will be filled immediately with the soil below the water table while the driving is still in progress. Any remaining space is backfilled with granular soil at the completion of driving. To ascertain the lateral stability of the piles, a number of lateral load tests were conducted. Generally usable lateral capacities of 5 tons or more were indicated by these tests, which were conducted with 50 percent of design vertical load on the piles.

A typical soil boring, driving record, and load test result are shown in Figure 5. The B-size TPT (32 by 26 by 60 in.) was driven to 74 blows/ft with the Vulcan 010 hammer, resulting in 4 ft of penetration into the medium-dense sand bearing layer. The pile was intended for 120 tons capacity; therefore it was tested to 240 tons, resulting in gross and net tip settlements of 0.41 in. and 0.20 in. respectively. A retest to 300 tons resulted in gross and net tip settlements of 0.54 in. and 0.25 in. respectively. It is obvious that the pile is satisfactory for working loads up to 150 tons.

The underground utility system for this project is designed on approximately 9,000 20-ton piles. Conventional timber piles driven for 20 tons capacity average 35 ft in length. Currently, Y-size TPTs with timber stems are being driven with a Vulcan No. 1 hammer (15,000 ft-lb/blow) to average lengths of approximately 18 ft. A typical boring, driving record, and load test result are shown in Figure 6. For a final driving resistance of 4 blows/in., the gross and net butt settlements are 0.45 in. and 0.18 in. respectively. It is obvious that the allowable load capacity of the pile is at least 25 tons and probably 30 tons.

The Brooklyn project illustrates the technical effectiveness of enlarged-tip piles. Also, a direct comparison with the Franki-type pile system shows the TPT system to be economically competitive and to require less construction time by a factor or two.

Rockaway

Two 20-story apartment houses are under construction in Rockaway (Queens) at a site within a few hundred feet of the Atlantic Ocean. The soil profile consists of several feet of fill underlain by loose sand, organic silt, and peat to a depth of approximately 27 ft. Then a dense sand layer approximately 7 ft thick is encountered over a 19-ft-thick layer of compressible clayey silt and gravel. The bearing layer is sand, encountered at a depth of 53 ft. Conventional cast-in-place piles achieve a 60-ton capacity at depths of approximately 70 ft in this soil profile.

A total of 450 piles of 150-ton capacity were driven for this project. Three load tests were performed under the relatively severe requirements of the New York City code. All tests were satisfactory. A typical soil boring, driving record, and load test result are shown in Figure 7. Predrilling to a depth of 42 ft and a diameter of 30 in. was performed to assure penetration below the dense sand at a depth of 27 ft. Then, the A-size TPT (29 by 23 by 60 in.) was driven with the Vulcan 010 hammer to

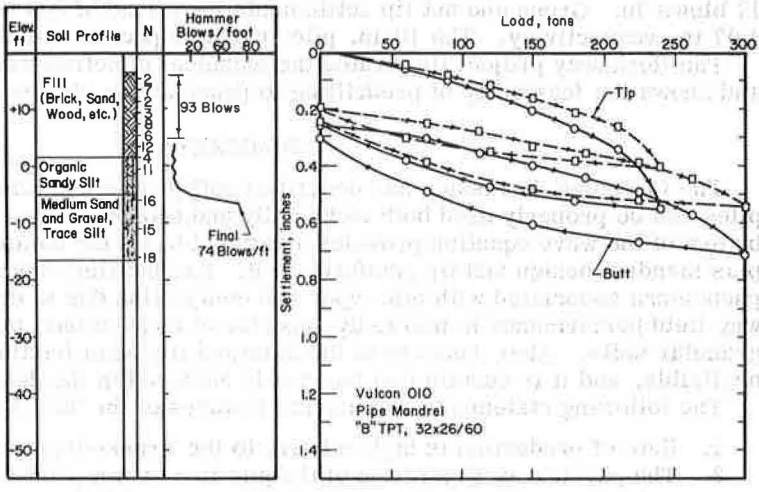

Figure 5. Load test data, B TPT, Brooklyn.

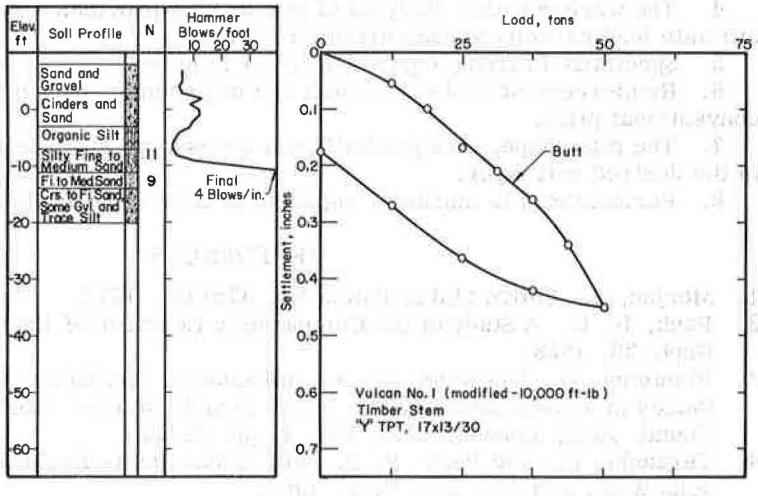

Figure 6. Load test data, Y TPT, Brooklyn.

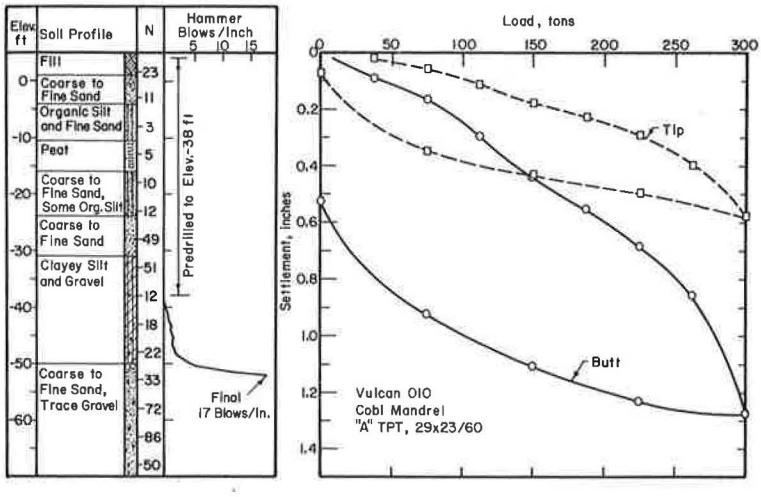

Figure 7. Load test data, A TPT, Rockaway.

17 blows/in. Gross and net tip settlements for a load of 300 tons were 0.58 in. and 0.07 in. respectively. The 16-in. pile shaft was poured with a 6,500-psi concrete.

The Rockaway project illustrates the technical effectiveness of enlarged-tip piles and shows the feasibility of predrilling to penetrate an obstructing soil layer.

SUMMARY

The foregoing discussion has described soil profile conditions in which enlarged-tip piles can be properly used both technically and economically. Analysis of pile driving by use of the wave equation provides a rational basis for hammer and cushion selection plus mandrel design and tip reinforcement. Soil bearing capacity theory, along with phenomena associated with pile taper and compaction due to driving, helps to explain why field performance is markedly superior to conventional piles, especially in loose granular soils. Also, because of the enlarged tip, skin friction on the pile stem is negligible, and it is certain that bearing is achieved in the desired soil layer.

The following statements summarize features of the TPT system described here:

1. Rate of production is high relative to the Franki-type pile.
2. The physical configuration of the pile is a known predetermined quantity, with structural integrity based on a rational design.
3. Field inspection involves the same techniques used for conventional piles.
4. The wave equation analysis of pile driving provides a reliable determination of ultimate load capacity versus driving resistance.
5. Specialized driving equipment is not required.
6. Reinforcement of the pile shaft can be accomplished in the same manner as for conventional piles.
7. The pile shape, plus predrilling if necessary, ensures that bearing is achieved in the desired soil layer.
8. Performance is markedly superior to conventional piles in loose granular soils.

REFERENCES

1. Merjan, S. United States Patent No. 3751931, 1973.
2. Peck, R. B. A Study of the Comparative Behavior of Friction Piles. HRB Spec. Rept. 36, 1958.
3. Plantema, G., and Nolet, C. A. Influence of Pile Driving on the Sounding Resistances in a Deep Sand Layer. Proc. Fourth Internat. Conf. on Soil Mech. and Found. Eng., London, 1957, Vol. 2, pp. 52-55.
4. Terzaghi, K., and Peck, R. B. Soil Mechanics in Engineering Practice, Second Ed. John Wiley and Son, New York, 1967.

LATERAL LOAD TESTS ON PILES IN BRIDGE EMBANKMENTS

Joseph A. Paduana, Department of Civil Engineering, California State University, Sacramento; and
Wilfred S. Yee, Transportation Laboratory, California Department of Transportation

Field lateral load tests were performed on embankment piles at three bridge sites in northern California. The investigation included determination of lateral load-deflection behavior of individual vertical embankment piles, correlation of test results with theoretical solutions, and determination of experimental values of n_h, the constant of horizontal subgrade reaction (or k, the subgrade modulus), for bridge embankment conditions. The pile tests showed that a linear variation of horizontal subgrade modulus with depth ($k = n_h x$) is a reasonable approximation; values of n_h varied from 10 to 65 lb/in.^{3} (2.7 to 17.6 N/cm^3), with higher values for the stiffer embankment; results suggest a simple rough approximation, $n_h \approx \overline{N}$, where $\overline{N}$ is the average blows per foot from standard penetration tests within the depth of the embankment; a fixed-head pile resists approximately twice the lateral load as a free-head pile at the same lateral deflection of 0.25 in. (0.64 cm); the computed effective length of the embankment test piles varied from 8 to 12 ft (2.4 to 3.7 m); a compacted fill of 12 ft (3.7 m) provides the major support for a laterally loaded pile and the influence of the underlying natural deposit is negligible.

•PILES in bridge foundations are often required to resist lateral forces resulting from post-tensioning of concrete superstructures, seasonal changes in length of superstructures without expansion joints, earth pressures, and earthquakes. It is important, therefore, to be able to predict the behavior of piles in bridge embankments subjected to lateral forces to ensure that both the deflections and stresses of the soil-pile-structure system are within tolerable limits.

Most analytical techniques for evaluating the behavior of a pile subjected to lateral loads are based on the theory of a beam on an elastic foundation (1) and require solutions of the differential equation

$$EI\frac{d^4y}{dx^4} + ky = 0 \qquad (1)$$

where EI is the flexural stiffness of the pile, y is the lateral deflection of the pile at depth x below the ground surface (Figure 1), and k is the subgrade modulus, a measure of the stiffness of the soil surrounding the pile. By definition, k is expressed in terms of y as

$$k = \frac{p}{y} \qquad (2)$$

where p is the soil reaction across the width of the pile that develops as a result of the pile deflection. As defined, k has units of force per unit length per unit of deflection.

The solution of Eq. 1 depends on the assumption regarding the variation of k with depth. Solutions are available (2) for any fixed variation of k with depth, but they generally require the use of a computer. For many practical problems, solutions are readily

Figure 1. Typical deflection and moment, laterally loaded pile.

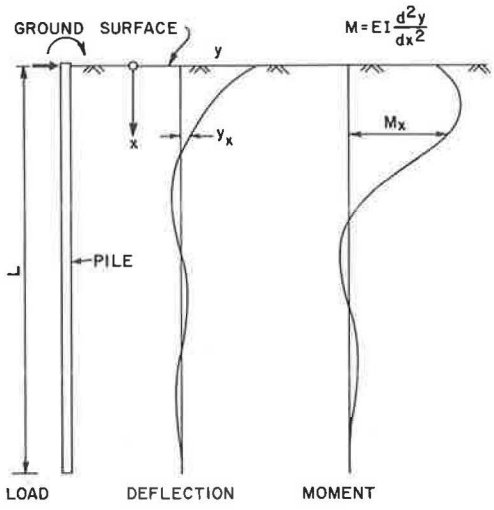

Figure 2. Laterally loaded pile in a bridge embankment.

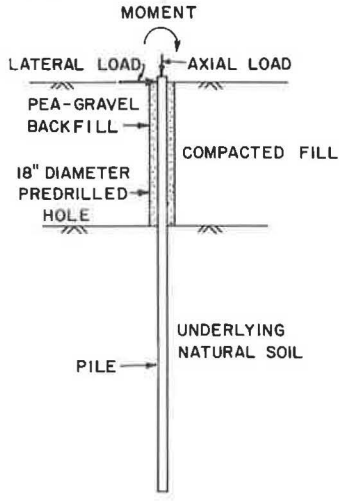

Table 1. Estimated values for k.

Soil Type	Value
Granular soils	n_h ranges from 1.5 to 200 lb/in.^{3}; is generally in the range from 10 to 100 lb/in.^{3}, and is approximately proportional to relative density
Normally loaded organic silt	n_h ranges from 0.4 to 3.0 lb/in.^{3}
Peat	n_h is approximately 0.2 lb/in.^{3}
Cohesive soils	k is approximately 67 c_u, where c_u is the undrained shear strength of the soil

Note: The effects of group action and repeated loading are not included in these estimates.

Figure 3. Occidental Drive test site.

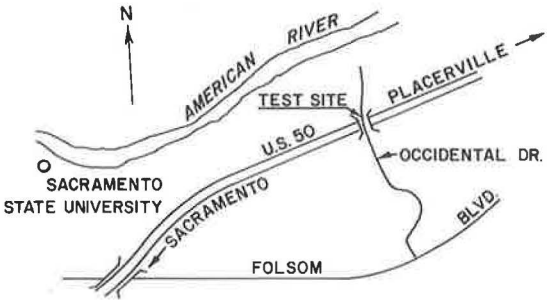

Figure 4. Linda Creek test site.

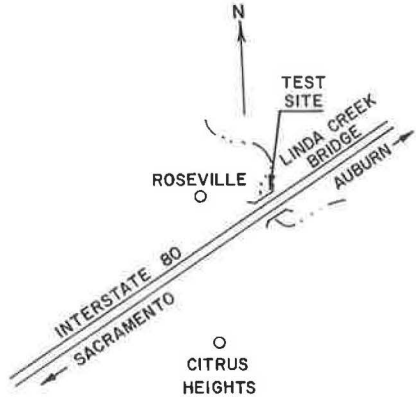

available for the cases where k is either constant with depth or increases linearly with depth in accordance with the expression

$$k = n_h x \tag{3}$$

where n_h is the constant of horizontal subgrade reaction. Terzaghi (3) suggested that, for preloaded cohesive soils, k may be assumed constant with depth. Davisson and Gill (4), however, showed that this assumption may lead to underestimates of moment and deflections by a factor of 2. Terzaghi further proposed that for sands k should vary linearly with depth from a value of zero at the surface, and the argument for such a variation was further developed by Reese and Matlock (5). Table 1 gives recommended values of k as summarized by Davisson (6), based on the literature and experience.

Solutions of Eq. 1 are readily available in nondimensional form. For the case where $k = n_h x$, Reese and Matlock (5) prepared a complete set of charts for determining deflections, moments, shears, and soil pressures. For the case of constant k or stepped variation in k, Davisson and Gill (4) prepared similar solutions for deflections and moments. The selection of appropriate magnitudes and distribution of k-values is basic to these solutions.

Although the preceding investigations have led to a good understanding of the behavior of laterally loaded piles, further experimental information is desirable for the conditions shown in Figure 2 of a typical laterally loaded pile in a bridge embankment. As shown, the embankment pile is inserted into an 18-in.-diameter (46-cm) predrilled hole in the compacted fill and driven into the underlying natural soil. The annular space between the pile and fill is backfilled with pea gravel to reduce negative skin friction resulting from future vertical settlements. Experimental evidence on the behavior of laterally loaded piles or on values of n_h or k for these soil conditions is very limited.

Full-scale lateral load tests on embankment piles were performed at three sites in northern California (Figures 3, 4, 5). The purposes of the testing program were (a) to determine the lateral load-deflection behavior of individual vertical embankment piles; (b) to correlate the results of full-scale tests on embankment piles with theoretical solutions; and (c) to determine experimental values of n_h (or k) for such embankment conditions. All test piles were used in the construction of bridge structures.

LATERAL LOAD TESTS AT OCCIDENTAL DRIVE OVERCROSSING

Test Layout and Soil Conditions

The location of test piles at the Occidental Drive overcrossing in Sacramento is shown in Figure 6. Lateral load tests were performed on 6 of the 12 vertical piles for bridge abutment 3. All piles were considered as single isolated piles not influenced by adjacent piles. The properties of the 10¾-in. (27.3-cm) OD steel pipe test piles are given in Table 2. The piles are embedded in approximately 28 ft (8.5 m) of the underlying natural sandy silt and in approximately 12 ft (3.7 m) of the annular pea gravel and surrounding compacted silty sand with gravel (Figure 7).

Figure 8 shows a general boring log for the site, including values of the standard penetration resistance. The fill was compacted to a minimum of 95 percent of maximum density based on California compaction test 231-E. No groundwater was encountered during the subsoil investigation. Properties of samples taken in the compacted fill and in the underlying natural soil are given in Table 3. Figure 9 shows the grain-size distribution of the pea-gravel backfill. More detailed descriptions of the soil profile are given elsewhere (7).

Instrumentation

Lateral loads perpendicular to the pile axis were applied at the ground surface with a calibrated hydraulic jack. The corresponding lateral deflections at the tops of the piles were measured with deflection transducers.

All test piles were equipped with SR-4 electrical resistance strain gauges along the embedded upper portion of the piles. Strain observations were recorded under lateral

Figure 5. North Maxwell test site.

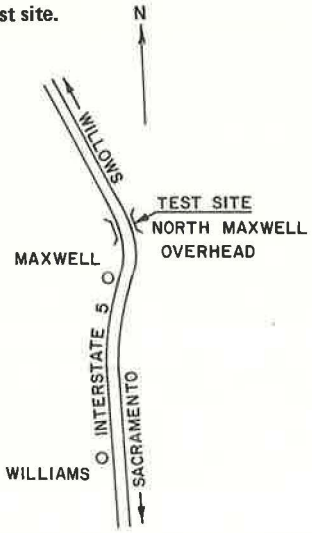

Figure 6. Plan of test piles, Occidental Drive site.

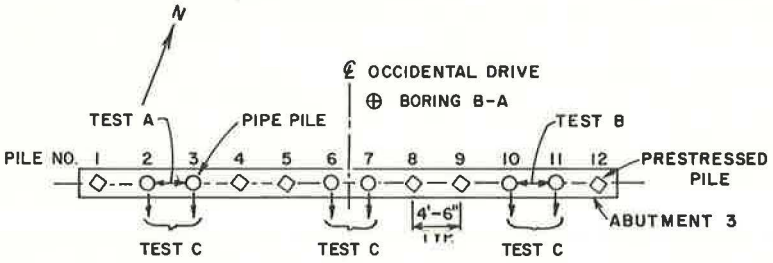

Table 2. Properties of test piles.

Test Site	Pipe Number	Pile Type	Moment of Inertia of Steel Pile or H-Pile ($in.^4$)	Moment of Inertia of Concrete in Pipe Pile ($in.^4$)	Modulus of Elasticity of Concrete $\times 10^3$ ($kips/in.^2$)	EI $\times 10^6$ of Pile ($kip\text{-}in.^2$)
Occidental Drive	2, 3, 6, 7, 10, and 11	$10^3/_4$-in. OD steel pipe[a] ($^1/_4$-in. wall) filled with reinforced concrete[b]	114	542	4.30 and 4.66[c]	6.00 and 6.19
Linda Creek	1 and 2	H-pile[a] (8 × 8 in., 40 lb/ft)	146	–	–	4.38
Linda Creek	3 and 4	H-pile[a] (10 × 8 in., 42 lb/ft)	205	–	–	6.15
North Maxwell		$10^3/_4$-in. OD steel pipe[a] ($^1/_4$-in. wall) filled with concrete	114	542	4.33 and 4.45[c]	5.76 and 5.82

[a]Modulus of elasticity of steel taken as 30×10^3 $kips/in.^2$.
[b]Concrete reinforced with 4 No. 6 vertical bars.
[c]Modulus of elasticity of concrete determined by California test method 522; lower value for pile tests A and B, upper value for subsequent pile test C.

Figure 7. Test pile, Occidental Drive site.

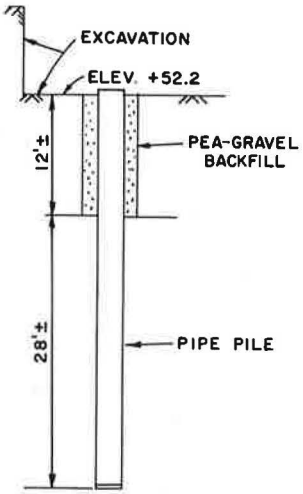

Figure 8. Boring log, Occidental Drive site.

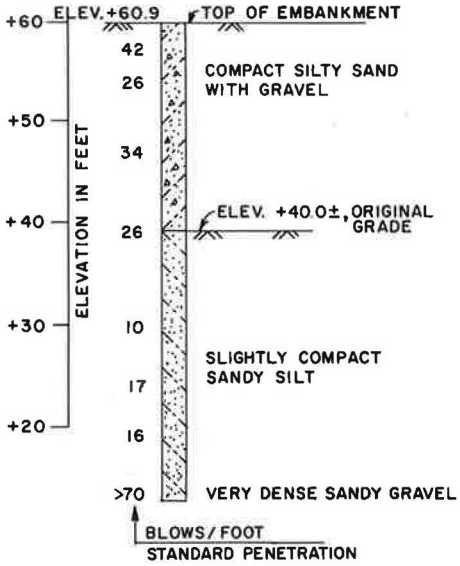

Table 3. Properties of sampled soil for test piles.

Soil Property	Occidental		Linda Creek		North Maxwell	
	Compacted Fill	Underlying Natural Soil	Compacted Fill	Underlying Natural Soil	Compacted Fill	Underlying Natural Soil
Depth below ground surface, ft	6 to 10	18 to 20	5 to 7	15 to 17	5.5 to 10.5	25.5 to 30.5
Unit weight, lb/ft^3	122	114	128	121	125	124
Grain size:						
Percentage gravel	8[a]	0[b]	5	2	0	1
Percentage sand	45[a]	39[b]	45	4	6	7
Percentage silt	35[a]	52[b]	29	41	31	33
Percentage clay	12[a]	9[b]	21	43	63	59
Average water content, percent	23	18	22	29	24	28
Liquid limit, percent	22[a]	24[b]	30	44	50	48
Plastic limit, percent	2[a]	2[b]	16	17	20	19
Shear strength parameters (UU triaxial compression):						
Range of confining pressures, tons/ft^2	Not available		¼ to 1	½ to 2	¼ to 1	½ to 2
ϕ_u, degrees			8.0	9.5	13.5	7.0
C_u, lb/ft^2			1,400	400	1,400	1,900

[a]Sample taken after construction, July 11, 1973, at a depth of 5 ft below ground surface.
[b]Sample taken after construction, July 11, 1973, at a depth of 17 ft below ground surface.

Figure 9. Gradation curves of pea gravel backfill.

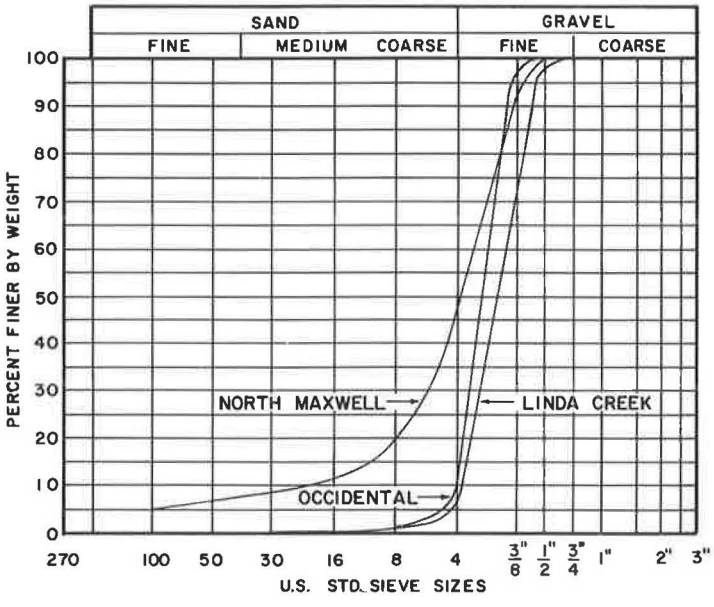

Figure 10. Free-head load versus deflection, Occidental Drive site.

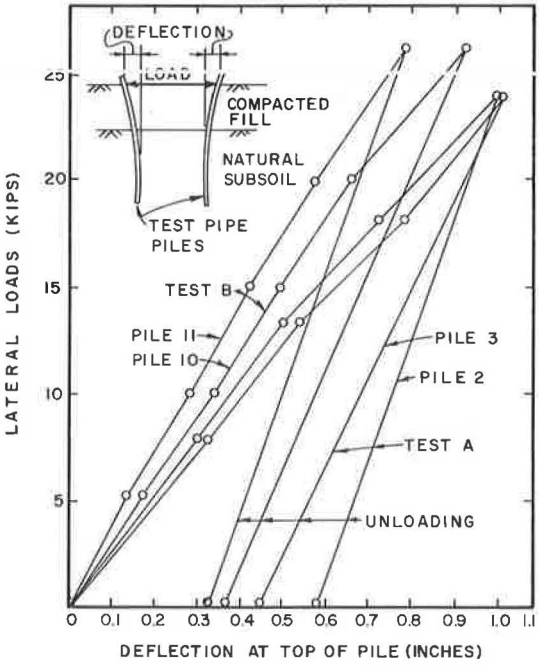

load to measure flexural stresses within the pile. The flexural stresses were then converted to bending moments. Complete details of the instrumentation are given elsewhere (7).

Test Procedure

Three types of lateral load tests were performed at the Occidental site (Figure 6): test A on piles 2 and 3, test B on piles 10 and 11, and test C on piles 2, 3, 6, 7, 10, and 11. Tests A and B were conducted before construction of the abutment, while test C was conducted after construction of the superstructure. Therefore, test piles were considered as free-head for tests A and B and fixed-head for test C.

The lateral load for tests A and B was applied at the ground line by jacking horizontally between a pair of test piles. During test A, a constant incremental lateral deflection was induced between the tops of piles 2 and 3, allowing the applied lateral load to vary in order to maintain a constant deflection. Constant total incremental deflections of ½, 1, 1½ and 2 in. (1.3, 2.5, 3.8, and 5.1 cm) were induced between the piles and maintained for 2 hours for each increment, in sequence. During test B, constant incremental lateral loads of 5, 10, 15, 20, and 25 kips (22, 44, 67, 89, and 111 kN) were applied, in sequence, between piles 10 and 11. Each load increment was held constant for a minimum period of 2 hours and until the pile head movement was less than 0.010 in. (0.025 cm) per hour. The test procedure for the after-construction test C is presented later.

Free-Head Test Results and Analysis

The free-head test results (tests A and B) are plotted in Figure 10 as lateral load applied at the ground line versus deflection at the top of the pile for piles 2, 3, 10, and 11. The corresponding strain gauge readings were converted to moments at the selected load levels, and these measured moments versus depth are plotted as solid lines in Figures 11, 12, 13, and 14 for the 4 test piles.

The results of the free-head tests were analyzed by means of the nondimensional solution (5), using theoretical expressions and nondimensional coefficients based on a linear variation of k with depth (Eq. 3). For this solution, a relative stiffness factor T is defined as

$$T = \sqrt[5]{EI/n_h} \tag{4}$$

For a free-head pile, the horizontal deflection produced by a lateral load P at the ground line is given as

$$y = A_y \frac{PT^3}{EI} \tag{5}$$

where A_y is the free-head depth coefficient. The corresponding bending moment is given as

$$M = A_M PT \tag{6}$$

where A_M is the free-head moment coefficient. Values of A_y and A_M are readily obtained from charts (5) for various depths along the pile.

Values of n_h were determined in the following manner: A trial value of n_h was assumed for an applied lateral load, and the corresponding deflection at the top of the pile was computed (Eq. 5) and compared with the measured deflection. When the computed and measured deflections agreed closely, the assumed value of n_h was considered satisfactory. Plots of n_h-values versus deflection at the top of the piles are shown in Figure 15. To verify the assumption regarding the distribution of subgrade modulus, theoretical moments were computed (Eq. 6) using values of n_h from Figure 15. The theoretical moments are shown in Figures 11 through 14 as dashed lines for comparison with the measured moments from strain gauge readings for the same lateral load. The agreement is reasonably good for practical purposes.

Figure 11. Free-head moment versus depth, test A, pile 2, Occidental Drive site.

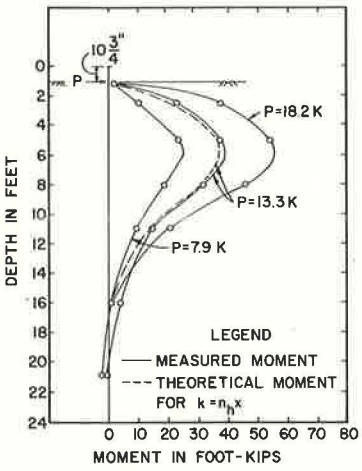

Figure 12. Free-head moment versus depth, test A, pile 3, Occidental Drive site.

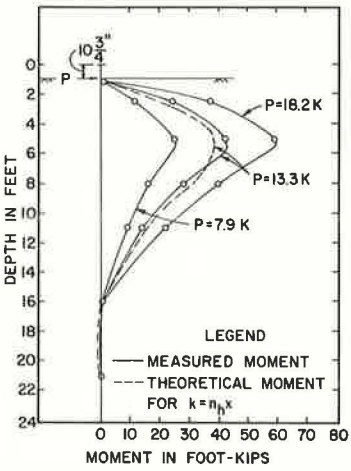

Figure 13. Free-head moment versus depth, test B, pile 10, Occidental Drive site.

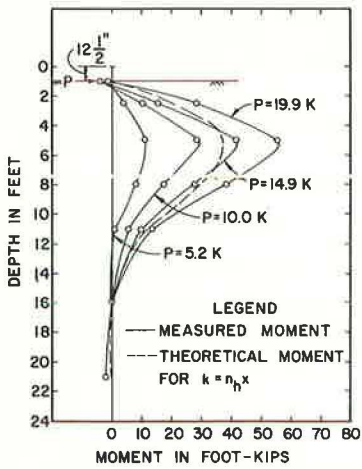

Figure 14. Free-head moment versus depth, test B, pile 11, Occidental Drive site.

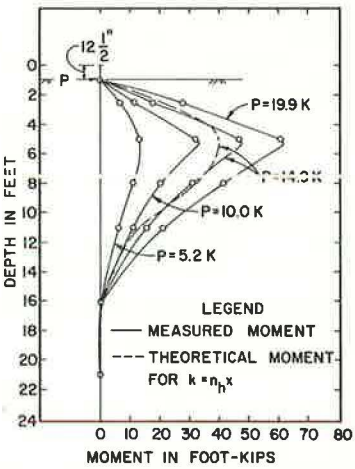

Figure 15. Free-head n_h versus deflection, Occidental Drive site.

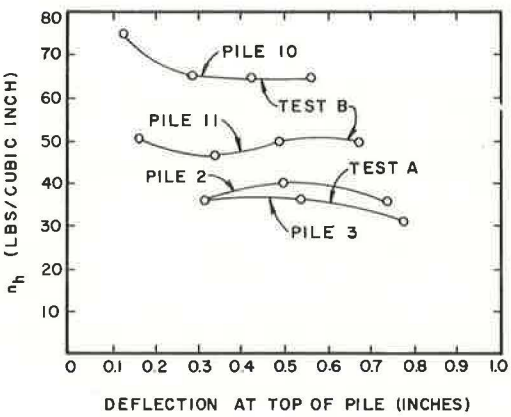

After-Construction Test Results and Analysis

For the after-construction test C (Figure 6), the effects of post-tensioning and dead load of the bridge superstructure were considered as loads for the test piles. The total prestress force for the concrete superstructure was 9,200 kips (41 000 kN).

The lateral deflections at the top of the test piles and the strains along the piles were measured after post-tensioning of the superstructure but with the falsework still in place. The measured deflections are shown in Figure 16. The strain gauge readings were converted to moments and plotted versus depth for piles 6 and 7, as shown in Figures 17 and 18. [It is noted that piles 2, 3, 10, and 11 were subjected to a reloading in test C in a direction normal to the initial loadings in tests A and B. The test results and analysis (7) for the reloading are not included, as only one-cycle loadings are considered here.] Construction operations did not permit measuring deflections after the falsework was removed, although the strains along the test piles were recorded. These strains were also converted to moments and plotted versus depth for piles 6 and 7 in Figures 17 and 18.

The results of the after-construction tests were also analyzed using the same nondimensional solution (5) but assuming fixed-head conditions. The deflection of a pile fixed against rotation at the ground line is given as

$$y_f = F_y \frac{PT^3}{EI} \tag{7}$$

where F_y is the fixed-head deflection coefficient and P is the shear force at the ground line. The corresponding bending moment is given as

$$M_f = F_M PT \tag{8}$$

where F_M is the fixed-head moment coefficient. Values of F_y and F_M are also readily obtained from charts (5) for various depths along the pile.

Values of n_h were determined as follows: Because of post-tensioning of the bridge superstructure with the falsework in place, a lateral force and a moment were induced at the top of each pile in the abutment. The lateral force was unknown, but the moments could be determined from strain gauge readings (Figures 16-18). A trial value of n_h was assumed, and a lateral force P corresponding to the measured moment at the pile top was computed from Eq. 8. By substituting this value of P in Eq. 7, a theoretical deflection at the top of the pile was computed and compared with the measured deflection (Figure 16). When the theoretical deflection agreed closely with the measured deflection, the assumed value of n_h was considered satisfactory. The value of n_h computed in this manner for piles 5 and 6 is 28 lb/in.^{3} (7.6 N/cm^3). The effect of the sloped embankment normal to the abutment was not considered and may account for the somewhat lower value of n_h compared to the free-head test values (Figure 15). Because construction procedures prevented the measurements of lateral deflections after the falsework was removed, it was not possible to compute theoretical moments for comparison with measured moments for this condition. However, it was possible to compute the lateral force and deflection at the pile tops (for the after-falsework-removed condition) using the corresponding measured moments (Figures 16-18), the value of n_h as 28 lb/in.^{3} (7.6 N/cm^3), and Eqs. 7 and 8. The values thus computed for pile 6 are equal to 11.2 kips (49.8 kN) and y_f equal to 0.170 in. (0.432 cm).

LATERAL LOAD TESTS AT LINDA CREEK OVERCROSSING

Test Layout and Soil Conditions

A plan of the test piles at abutment 4 of the Linda Creek overcrossing near Roseville, California, is shown in Figure 19. Lateral load tests were performed on 4 of the vertical H-piles; the properties are given in Table 2. The embedment of a typical test pile in the underlying natural silty clay to sandy silt and in the annular pea gravel surrounded by an existing compacted silty clayey sand embankment is shown in Figure 20.

Figure 16. Plan of lateral deflections, test C, Occidental Drive site.

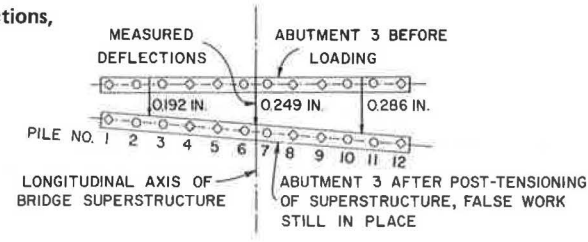

Figure 17. After-construction moment versus depth, test C, pile 6, Occidental Drive site.

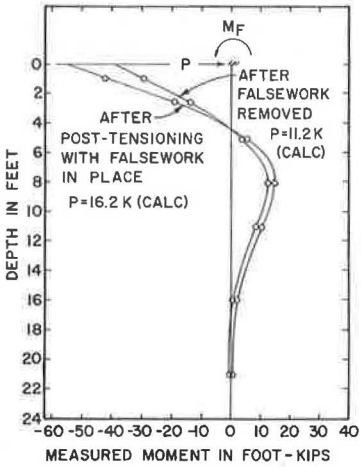

Figure 18. After-construction moment versus depth, test C, pile 7, Occidental Drive site.

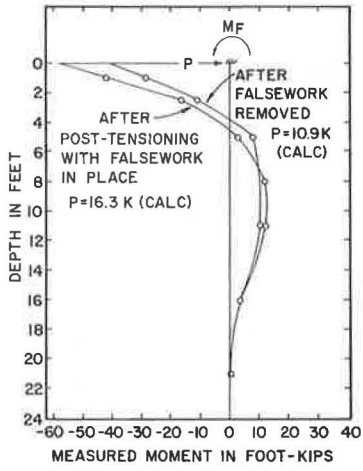

Figure 19. Plan of test piles, Linda Creek site.

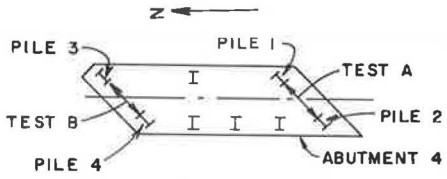

Figure 20. Test pile, Linda Creek site.

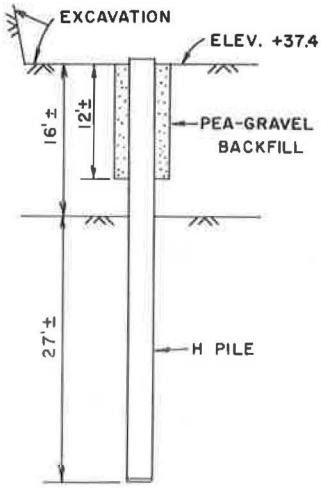

Figure 21. Boring log, Linda Creek site.

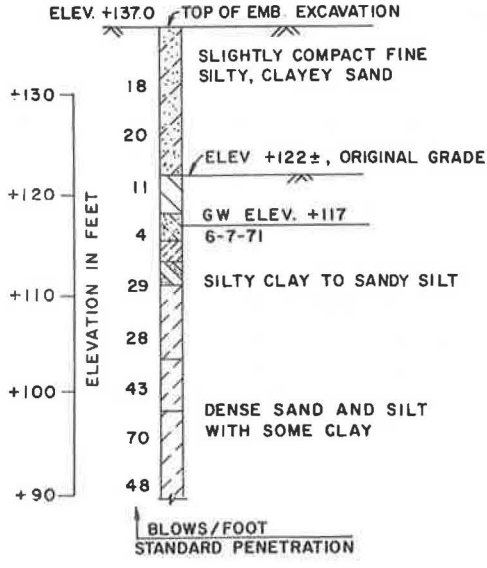

The embankment had been compacted to a minimum of 90 percent of maximum density based on California compaction test 231-E. A log of the nearest boring is shown in Figure 21. Table 3 gives the properties of samples taken in the compacted fill and in the underlying natural soil. A more detailed description of the soil profile is given elsewhere (8).

Instrumentation and Test Procedure

Lateral loads were applied by jacking horizontally between a pair of test piles before construction of the abutment. The instrumentation for measuring deflections, loads, and bending strains along the pile was similar to that described for the Occidental project. In addition, the slope at the top of the test piles was measured with an electronic level (8).

Only constant incremental lateral load tests (similar to the procedure described for test B at Occidental) were performed: Test A was on piles 1 and 2 and test B on piles 3 and 4 (Figure 19). Lateral loads were applied in increments of 5 kips (22 kN). It should be noted that H-pile 4 rotated slightly during driving. As a result, the lateral load was not applied in the plane of the principal axis of pile 4 (8).

Test Results and Analysis

A plot of lateral load applied at the ground line versus deflection at the top of the pile is shown in Figure 22 for piles 1, 2, 3, and 4. The results of the tests were evaluated using the same procedure described for the free-head tests at the Occidental site. A plot of n_h values versus deflection at the top of the piles is shown in Figure 23. Theoretical moments along the test piles and theoretical slopes at the pile tops were also computed (8) using these n_h values and the nondimensional solution (5). Maximum theoretical moments and maximum measured moments compared (8) within 15 percent for the same lateral load for piles 1, 2, and 3. However, the maximum theoretical moment for H-pile 4, which had rotated during driving, was about 30 percent greater than the maximum measured moment. Theoretical slopes at the top of the test piles also agreed reasonably well with the measured slopes (8), except for pile 4.

LATERAL LOAD TESTS AT NORTH MAXWELL OVERHEAD

Test Layout and Soil Conditions

The location of test piles 2, 3, 9, and 10 at the North Maxwell overhead near Maxwell, California, is shown in Figure 24. The properties of the 10¾-in. (27.3-cm) OD steel pipe piles are given in Table 2. As shown in Figure 25, a typical test pile is embedded in approximately 50 ft (15 m) of the underlying natural soft to stiff clay (with sand at deeper depths) and in approximately 20 ft (6 m) of the annular pea gravel and surrounding compacted silty sandy clay fill. The fill was compacted to a minimum of 90 percent of maximum density based on California compaction test 231-E. A log of the nearest boring is shown in Figure 26; it includes values of the standard penetration resistance. Properties of samples taken in the compacted fill and in the underlying natural soil are given in Table 3.

Instrumentation and Test Procedure

Lateral loads were applied by jacking between test piles before construction of the abutment. The instrumentation was similar to that described for the Occidental test piles and in addition included an electronic level for measuring the slope at the top of the test piles.

The test procedures for test A on piles 2 and 3 and test B on piles 9 and 10 are respectively similar to the constant-incremental lateral-deflection test and the constant-incremental lateral-load test described for the Occidental project.

Test Results and Analysis

Test results for piles 2, 3, 9, and 10 are shown in Figure 27 as lateral load applied

Figure 22. Load versus deflection, Linda Creek site.

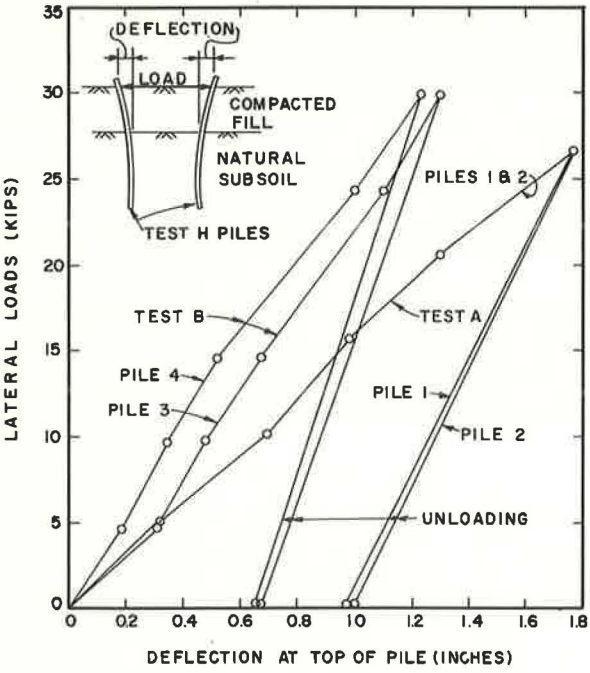

Figure 23. n_h versus deflection, Linda Creek site.

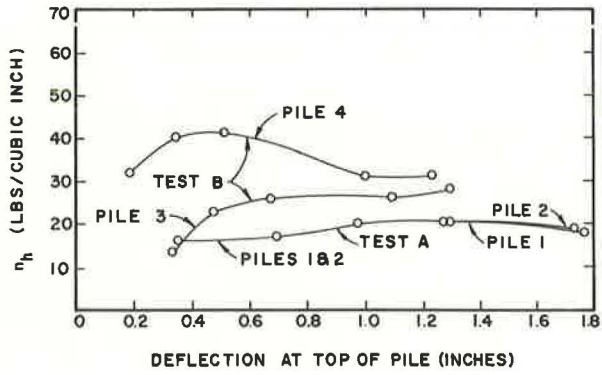

Figure 24. Plan of test piles, North Maxwell site.

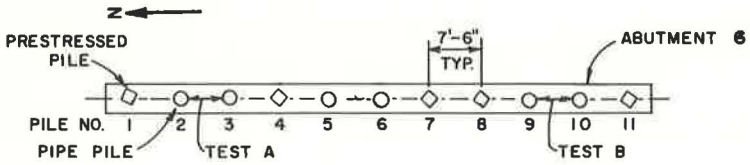

Figure 25. Test pile, North Maxwell site. .

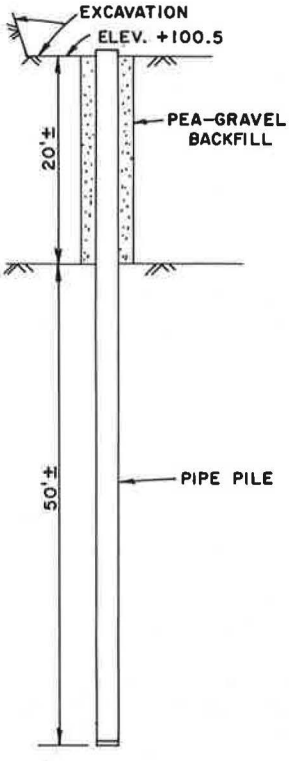

Figure 26. Boring log, North Maxwell site.

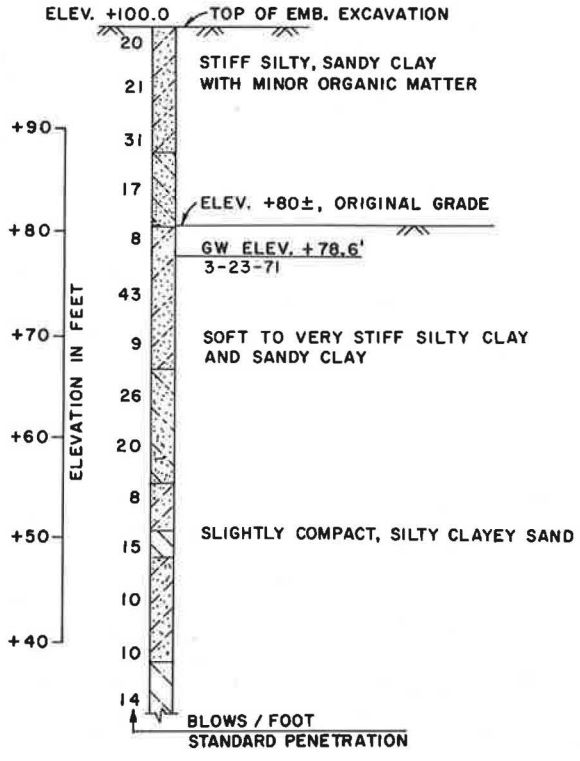

Figure 27. Load versus deflection, North Maxwell site.

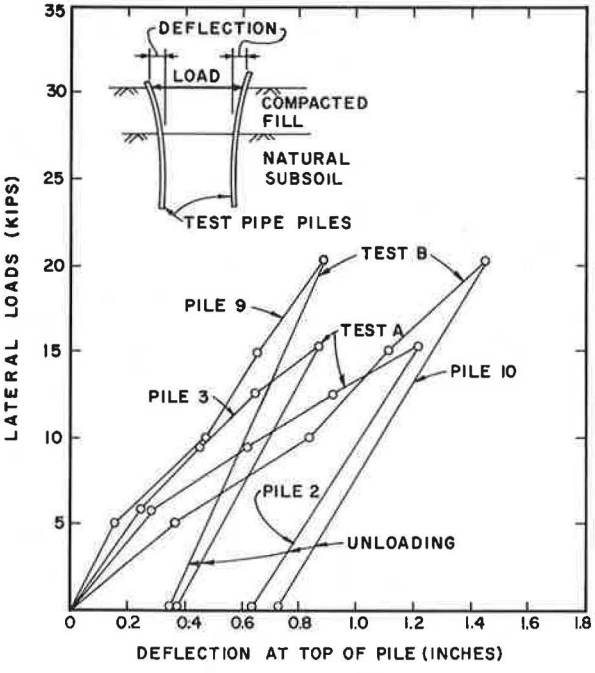

at the ground line versus deflection at the top of the pile. The results were analyzed using the same procedure described for the free-head tests at the Occidental site. Values of n_h determined by this procedure are plotted versus deflection in Figure 28. By using these values of n_h and the nondimensional solution (5), theoretical moments along the test piles and theoretical slopes at the top of the piles were also computed (8). A comparison (8) between maximum theoretical moments and maximum measured moments showed agreement within 8 percent. Similar good agreement resulted from a comparison (8) of theoretical and measured slopes at the pile tops.

SUMMARY AND USE OF TEST RESULTS IN DESIGN

n_h-Values

A summary of the test results for the three sites is given in Table 4 and includes n_h-values for a single cycle of loading. Values of n_h for the three embankments varied overall from 10 to 65 lb/in.^{3} (2.7 to 17.6 N/cm^3), with higher values for the stiffer embankment. The results suggest the following simple approximate relationship between values of n_h in pounds per cubic inch and the standard penetration resistance for the pile-soil conditions studied herein:

$$n_h \approx \overline{N} \tag{9}$$

where $\overline{N}$ is the average blows per foot from standard penetration tests within the depth of the compacted embankment.

It seems reasonable to expect some rough correlation between values of n_h and N values. Because the "pressure bulb" (seat of settlement) for lateral deflections of a pile includes both the pea-gravel backfill and the surrounding compacted fill, values of n_h should depend on the relative density of the pea gravel and the stiffness of the compacted fill. But for each test pile, the pea-gravel backfill was placed in the same manner by dumping from an extended chute of a truck. Therefore, differences in n_h-values would be accounted for primarily in differences in the stiffnesses of the compacted fill, as indicated by the N values.

Effect of End Restraint on Load-Deflection Behavior

Figures 10 and 16-18 show respectively lateral load versus lateral deflection relationships for the free-head and fixed-head pile conditions at the Occidental site. Because of the end restraint and base friction contributed by the pile abutment, the fixed-head pile resists approximately twice as much lateral load as the free-head pile at the same lateral deflection of 0.25 in. (0.64 cm).

Effective Length

The effective length of a laterally loaded pile is defined as the length of the embedded portion of a pile that is effective in transferring lateral load from the pile to the soil. The lower portion of a pile beyond the effective length shows no appreciable deflection and thus no appreciable soil reaction. For practical purposes, the effective length may also be considered as the depth to the first zero-deflection point of a pile.

The range of effective length for the test piles at the three sites was computed for lateral loads within a practical range and is given in Table 5. The effective length varied from 8 to 12 ft (2.4 to 3.7 m), which lies within the depth of the compacted fill. Thus, the compacted fill of a bridge embankment provides the major support for a laterally loaded pile, and the influence of the underlying natural deposit is practically negligible.

Use of Test Results

The tests reported here provided data that were used in the design of pile foundations for bridge embankments. The test results are in terms of the behavior of a single pile under a single cycle of loading. Cyclic loading and pile spacing in the direction of the

Figure 28. n_h versus deflection, North Maxwell site.

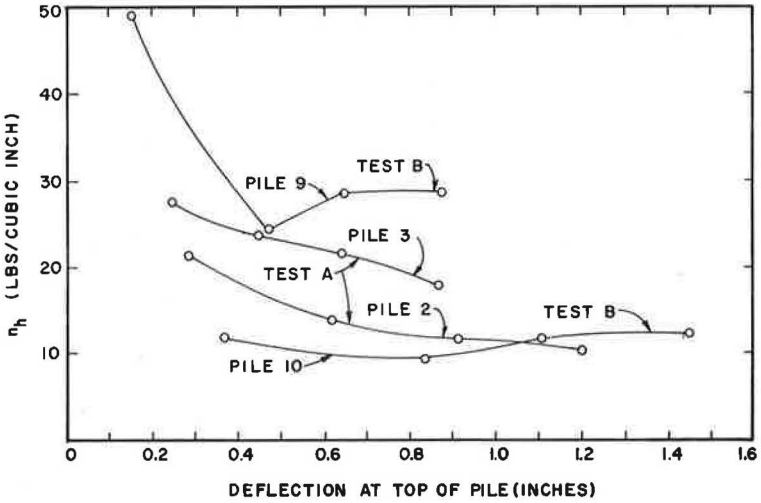

Table 4. Summary of test results.

Test Location	Test Pile	Pile Type	Restraint at Top of Pile	Depth of Pea-Gravel Backfill (ft)	Compacted Fill			Range[c] of n_h (lb/in.^{3})
					General Soil Type	Depth (ft)	$\bar{N}$[b] (blows/ft)	
Occidental	2, 3, 10, and 11	10¾-in. OD steel pipe filled with reinforced concrete	Free-head	12	Silty sand with gravel	12	30	30-65
Occidental	6 and 7	Ditto	Fixed-head[a]	12	Ditto	12	30	28
Linda Creek	1 and 2	H-pile (8 × 8 in., 40 lb/ft)	Free-head	12	Fine silty clayey sand	16	19	15-20
Linda Creek	3 and 4	H-pile (10 × 8 in., 42 lb/ft)	Free-head	12	Ditto	16	19	15-40
North Maxwell	2, 3, 9, and 10	10¾-in. OD steel pipe filled with concrete	Free-head	20	Silty sandy clay	20	22	10-30

[a]Assumed as fixed-head after construction of superstructure.
[b]Average blows/ft, standard penetration tests.
[c]For single cycle of loading.

Table 5. Effective length (depth to first zero-deflection point of pile).

Test Location	Test Pile	Restraint at Top of Pile	Depth of Compacted Fill (ft)	Range of Lateral Load at Top of Pile (kips)	Range of Depth to First Zero-Deflection Point of Pile (ft)
Occidental	2, 3, 10, and 11	Free-head	12	13-15	8-9
Occidental	6 and 7	Fixed-head	12	11	12
Linda Creek	1, 2, 3, and 4	Free-head	16	15-16	9-10
North Maxwell	2, 3, 9, and 10	Free-head	20	9-10	10-12

load must also be considered in selecting an appropriate value of the subgrade modulus k. Cyclic loading has the effect of reducing the value of k (9, 10). Pile spacing less than 8 pile diameters in the direction of the load also has the effect of reducing the value of k (11).

CONCLUSIONS

The following conclusions are considered valid from an analysis of full-scale lateral load tests on embankment piles at three bridge sites in northern California:

1. Comparisons of measured and theoretical bending moments versus depth for vertical piles in bridge embankments show that a linear variation of horizontal subgrade modulus with depth ($k = n_h x$) is a reasonable approximation.
2. Values of n_h for single-cycle loading at three embankment sites varied overall from 10 to 65 lb/in.^{3} (2.7 to 17.6 N/cm^3), with higher values for the stiffer embankment. Test results suggest a simple rough approximation, $n_h \approx \overline{N}$, for the soil-pile conditions studied.
3. Limited data indicate that a fixed-head pile resists approximately twice as much lateral load as a free-head pile at the same lateral deflection of 0.25 in. (0.64 cm).
4. The computed effective length (depth to first zero-deflection point) of the embankment piles varied from 8 to 12 ft (2.4 to 3.7 m) for lateral loads from 9 to 16 kips (40 to 71 kN).
5. A compacted fill of 12 ft (3.7 m) or more provides the major support for a laterally loaded pile, and the influence of the underlying natural deposit is practically negligible.

ACKNOWLEDGMENTS

The information contained in this paper was developed in cooperation with the Office of Structures of the California Division of Highways and the Federal Highway Administration. The contents of this paper reflect the views of the authors, who are responsible for the facts and the accuracy of the data presented. The contents do not necessarily reflect the official views or policies of the Federal Highway Administration. This paper does not constitute a standard, specification, or regulation.

REFERENCES

1. Hetenyi, M. Beams on Elastic Foundation. Univ. of Michigan Press, Ann Arbor, 1946.
2. Matlock, H., and Reese, L. C. Generalized Solutions for Laterally Loaded Piles. Proc. ASCE, Vol. 86, No. SM5, Oct. 1960, pp. 63-94.
3. Terzaghi, K. Evaluation of Coefficients of Subgrade Reaction. Geotechnique, Vol. 5, 1955, pp. 297-326.
4. Davisson, M. T., and Gill, H. L. Laterally Loaded Piles in a Layered Soil System. Proc. ASCE, Vol. 89, No. SM3, May 1963, pp. 63-94.
5. Reese, L. C., and Matlock, H. Non-Dimensional Solutions for Laterally Loaded Piles With Soil Modulus Assumed Proportional to Depth. Proc. 8th Texas Conf. on Soil Mechanics and Foundation Eng., Austin, 1956.
6. Davisson, M. T. Lateral Load Capacity of Piles. Highway Research Record 333, 1970, pp. 104-112.
7. Yee, W. S. Laterally Loaded Piles in a Bridge Embankment. MS thesis, California State University, Sacramento, 1971.
8. Lateral Resistance and Deflection of Vertical Piles. Bridge Department, California Division of Highways, Sacramento, Jan. 1973.
9. Alizadeh, M., and Davisson, M. T. Lateral Load Tests on Piles, Arkansas River Project. Proc. ASCE, Vol. 96, No. SM5, Sept. 1970, pp. 1583-1604.
10. Davisson, M. T., and Salley, J. R. Model Study of Laterally Loaded Piles. Proc. ASCE, Vol. 96, No. SM5, Sept. 1970, pp. 1605-1627.
11. Prakash, S. Behavior of Pile Groups Subjected to Lateral Load. PhD thesis, University of Illinois, 1962.

SPONSORSHIP OF THIS RECORD

GROUP 2—DESIGN AND CONSTRUCTION OF TRANSPORTATION FACILITIES
W. B. Drake, Kentucky Department of Transportation, chairman

SOIL MECHANICS SECTION
John A. Deacon, University of Kentucky, chairman

Committee on Foundations of Bridges and Other Structures
Melvin T. Davisson, University of Illinois, chairman
David R. Antes, Edwin C. Beethoven, William Bootz, Bernard E. Butler, Harry M. Coyle, Jacob Feld, Frank M. Fuller, David S. Gedney, Stanley Gordon, Bernard A. Grand, Robert J. Hallawell, T. J. Hirsch, Horace E. Hoy, Hal W. Hunt, Philip Keene, Richard E. Landau, Clyde N. Laughter, G. A. Leonards, R. M. Mattox, Thomas D. Moreland, A. Rutka

J. W. Guinnee, Transportation Research Board staff

The organizational units and the chairmen and members are as of December 31, 1973.